# Elucidating the Molecular Mechanisms of Developmental Timing in Mammals

---

Dissertation der Fakultät für Biologie

der Ludwig-Maximilians-Universität München


Alexandra de la Porte

München 2024

# Elucidating the Molecular Mechanisms of Developmental Timing in Mammals

Dissertation zur Erlangung des Akademischen Grades

**Doktor der Naturwissenschaften**

an der Fakultät für Biologie

der Ludwig-Maximilians-Universität München


Vorgelegt von

Alexandra de la Porte

geboren in

Surabaya, Indonesien


München 2024

Diese Dissertation wurde angefertigt
unter der Leitung von Prof. Dr. Wolfgang Enard
am Lehrstuhl für Anthropologie & Human Genetik an der Fakultät für Biologie
der Ludwig-Maximilians-Universität München

| | |
|---|---|
| Erstgutachter: | Prof. Dr. Wolfgang Enard |
| Zweitgutachter: | Prof. Dr. Micha Drukker |
| Tag der Abgabe: | 29.05.2024 |
| Tag der mündlichen Prüfung: | 18.12.2024 |

# Eidesstattliche Erklärung

Ich versichere hiermit an Eides statt, dass die vorgelegte Dissertation von mir selbständig und ohne unerlaubte Hilfe angefertigt ist.

München, den 20.12.2024 Alexandra de la Porte

(Unterschrift)

## Erklärung

Hiermit erkläre ich, *

- ☒ dass die Dissertation nicht ganz oder in wesentlichen Teilen einer anderen Prüfungskommission vorgelegt worden ist.

- ☒ dass ich mich anderweitig einer Doktorprüfung ohne Erfolg **nicht** unterzogen habe.

- ☐ dass ich mich mit Erfolg der Doktorprüfung im Hauptfach .....

  und in den Nebenfächern .....

  bei der Fakultät für ..... der .....

  (Hochschule/Universität)

  unterzogen habe.

- ☐ dass ich ohne Erfolg versucht habe, eine Dissertation einzureichen oder mich der Doktorprüfung zu unterziehen.

München, den 20.12.2024 Alexandra de la Porte

(Unterschrift)

*) Nichtzutreffendes streichen

# Table of Contents

# List of figures

# List of tables

# List of abbreviations

| Abbreviation | Explanation |
|---|---|
| α-KG | Alpha-Ketoglutarate |
| ATAC | Assay for transposase-accessible chromatin |
| CDM | Chemically defined media |
| cDNA | Complementary DNA |
| DGE | Differential gene expression |
| DMSO | Dimethyl sulfoxide |
| DNA | Deoxyribonucleic acid |
| DPBS | Dulbecco's Phosphate Buffered Saline |
| dSMADi | Dual SMAD-pathway inhibition |
| DTT | Dithiothreitol |
| E7 | Essential 7 |
| EDTA | Ethylenediaminetetraacetic acid |
| EpiLC | Epiblast-like stem cell |
| EpiSC | Epiblast stem cell |
| ESC | Embryonic stem cell |
| FACS | Fluorescence-activated cell sorting |
| FBS | Fetal bovine serum |
| GO | Gene ontology |
| HRP | Horseradish peroxidase |
| ICM | Inner cell mass |
| iPSC | Induced pluripotent stem cell |
| KO | Knockout |
| LIF | Leukemia inhibitory factor |
| mRNA | Messenger RNA |
| NAD | Nicotinamide adenine dinucleotide |
| NGS | Next generation sequencing |
| NPC | Neuroprogenitor cell |
| PCA | Principal component analysis |
| PCR | Polymerase chain reaction |
| PGC | Primordial germ cell |
| PSC | Pluripotent stem cell |
| PSM | Presomitic mesoderm |
| PTM | Post-translational modification |
| RNA | Ribonucleic acid |
| rpm | Revolutions per minute |

| | |
|---|---|
| RT | Room temperature |
| RT-qPCR | Reverse transcription quantitative PCR |
| scATAC seq | Single-cell ATAC using sequencing |
| SCNT | Somatic cell nuclear transfer |
| scRNA-seq | Single-cell RNA sequencing |
| SDS | Sodium Dodecyl Sulfate |
| TCA | Tricarboxylic acid cycle |
| TE | Trophectoderm |
| TSS | Transcription start sites |
| UPPS | Universal primed pluripotency media |
| UMAP | Uniform manifold approximation and projection |
| UMI | Unique molecular identifier |
| XCI | X-chromosome inactivation |

# Abstract

Embryonic development from a single cell to a fully grown organism in mammals adheres to a strict pattern, yet the speed of these events, the developmental timescale, is unique to each species and varies significantly. In this thesis, I explore the genetic, epigenetic, and extracellular factors orchestrating this transition. By leveraging *in vitro* models and single-cell sequencing techniques, I uncover the relationship between the properties of pluripotent stem cells (PSCs) and their developmental speed during neural differentiation, emphasizing the role of metabolic regulation in influencing differentiation potentials.

I demonstrated a robust, universal system by cultivating PSCs from mouse, human, cynomolgus, and orangutans under harmonized conditions. In addition, I employed a uniform protocol to differentiate PSCs into neural progenitor cells (NPCs), highlighting nuanced differences in developmental speed among mouse, cynomolgus, and human. This standardization provided a ground for comparative studies, free from the interfering effects of extrinsic factors.

Applying time-course single-cell multiome sequencing, I provided an in-depth view of transcriptional and chromatin changes during neural differentiation. This method revealed species-specific patterns, with mouse cells differentiating the fastest, followed by cynomolgus and human. Linear regression models showed that mouse cells differentiate approximately 2.4 times faster than human cells and 2.2 times faster than cynomolgus cells based on gene expression data. Single-cell ATAC sequencing data showed similar trends, with mouse cells differentiating 1.9 times faster than human cells and 1.7 times faster than cynomolgus cells. This analysis underscores how cells from different species resemble and differ in their differentiation trajectories.

Through single-cell RNA sequencing analysis, I identified UGP2 as a gene upregulated in slower-differentiating species and slower-differentiating cells within one species. Deleting UGP2 in human and cynomolgus PSCs using CRISPR/Cas9 technology depleted cells of glycogen and accelerated neural differentiation, indicating its role in regulating metabolic rates by controlling glucose availability.

In conclusion, my thesis enhances our understanding of the molecular mechanisms governing developmental speed across species, demonstrating the importance of UGP2 in regulating glycogen storage and influencing differentiation rates. This research lays the groundwork for future studies into species-specific developmental timing mechanisms, offering a robust framework for exploring developmental time scales across a broader array of species and developmental stages.

# Zusammenfassung

Die Embryonalentwicklung von einer einzelnen Zelle zu einem ausgewachsenen Organismus verläuft bei Säugetieren nach einem strengen Muster, doch die Geschwindigkeit dieser Ereignisse, die Entwicklungszeitskala, ist bei jeder Art einzigartig und variiert erheblich untereinander. In dieser Arbeit untersuche ich die genetischen, epigenetischen und extrazellulären Faktoren, die diese Entwicklung steuern. Durch den Einsatz von *In-vitro*-Modellen und Einzelzellsequenzierungstechniken decke ich die entscheidenden Beziehungen zwischen den Eigenschaften pluripotenter Stammzellen (PSCs) und ihrer Entwicklungsgeschwindigkeit während der neuralen Differenzierung auf, wobei ich die Rolle der Stoffwechselregulation bei der Beeinflussung des Differenzierungspotenzials hervorhebe.

Ich habe ein robustes, universelles System etabliert, indem ich PSCs von Maus, Mensch, Cynomolgus und Orang-Utan unter identischen Bedingungen kultiviert habe. Darüber hinaus verwendete ich ein einheitliches Protokoll zur Differenzierung von PSCs in neurale Vorläuferzellen (NPCs), wobei ich nuancierte Unterschiede in der Entwicklungsgeschwindigkeit zwischen Maus, Cynomolgus und Mensch herausstellte. Diese Standardisierung bot eine Grundlage für vergleichende Studien, die frei von eingreifenden Einflüssen äußerer Faktoren waren.

Durch die Anwendung von Einzelzell-Multiom-Sequenzierung im Zeitverlauf konnte ich einen detaillierten Einblick in die Transkriptions- und Chromatinveränderungen während der neuralen Differenzierung gewinnen. Diese Methode hob artspezifische Muster hervor, wobei sich Zellen der Maus am schnellsten differenzieren, gefolgt von Cynomolgus und Mensch. Lineare Regressionsmodelle zeigten, dass sich Mauszellen auf der Grundlage von Genexpressionsdaten etwa 2,4-mal schneller differenzieren als menschliche Zellen und 2,2-mal schneller als Cynomolgus-Zellen. Einzelzell-ATAC-Sequenzierungsdaten zeigten ähnliche Trends, wobei sich Mauszellen 1,9-mal schneller differenzieren als menschliche Zellen und 1,7-mal schneller als Cynomolgus-Zellen. Diese Analyse unterstreicht, wie sich Zellen verschiedener Spezies in ihrem Differenzierungsverlauf gleichen und unterscheiden.

Durch die Analyse der RNA-Sequenzierung einzelner Zellen konnte ich UGP2 als ein Gen identifizieren, das sowohl in langsamer differenzierenden Arten als auch in langsamer differenzierenden Zellen innerhalb einer Art hochreguliert ist. Durch die Deletion von UGP2 in menschlichen und Cynomolgus PSCs mit Hilfe der CRISPR/Cas9-Technologie wurde Glykogen von den Zellen nicht mehr gespeichert und die neurale Differenzierung

beschleunigt, was darauf hindeutet, dass UGP2 eine Rolle bei der Regulierung der Stoffwechselrate durch die Kontrolle der Glukoseverfügbarkeit spielt.

Zusammenfassend lässt sich sagen, dass diese Arbeit unser Verständnis der molekularen Mechanismen, die die Entwicklungsgeschwindigkeit bei verschiedenen Spezies steuern, verbessert und die Bedeutung von UGP2 bei der Regulierung der Glykogenspeicherung und der Beeinflussung der Differenzierungsraten zeigt. Diese Forschung legt den Grundstein für künftige Studien über artspezifische Mechanismen der Entwicklungszeitskala und bietet einen robusten Rahmen für die Erforschung der Entwicklungszeitskala bei einer breiteren Palette von Arten und Entwicklungsstadien.

# 1 Introduction

## 1.1 The meaning of time in early development

Timing is a critical aspect of developmental biology, encompassing the temporal regulation of key events essential for an organism's proper formation and function [1]. This regulation involves coordinating various processes such as cell division, differentiation, and organ formation, ensuring they occur sequentially and orderly [2], [3]. Both genetic and environmental factors influence the mechanisms controlling developmental timing, and disruptions to this timing can lead to developmental abnormalities or diseases, highlighting the significance of understanding and studying developmental timing [4], [5]. Moreover, understanding developmental timing is pivotal in various fields, including regenerative medicine. In stem cell therapies and tissue engineering, the precise timing of developmental events is crucial for successfully generating and integrating new tissues or organs [6]. However, despite the acknowledged significance of timing in development, the underlying mechanistic principles of these temporal patterns remain poorly understood.

### 1.1.1 Temporal dynamics in vertebrate development

Both spatial and temporal coordination characterize the development of a vertebrate egg [7]. Temporal coordination consists of two primary aspects: the sequential ordering of developmental decisions and the pace at which these processes unfold. Alterations in the sequence of developmental events can significantly impact the resulting morphology and may have been a critical factor in evolutionary transformations [8], [9]. The developmental rate, especially if it varies regionally within an embryo, can lead to uneven growth or differentiation in certain areas [5]. In the context of development, the concept of time is uniquely defined. Johnson and Day describe early developmental biological timers using the hourglass and clock models (**Figure 1**) [10]. Developmental timing depends on signaling cascades and chemical reactions sensitive to environmental variables such as temperature and pH [11], [12]. Biological timers lack the exactness of atomic clocks but compensate with adaptability and responsiveness to environmental changes, often regulated through

oscillatory feedback mechanisms. Examples include the cellular circadian rhythm and the cell cycle, closely linked to developmental processes [13], [14]. Alternatively, a different type of biological timer operates without oscillations, triggered by distinct events such as fertilization or describing the unidirectional terminal differentiation of cells. This type operates by accumulating or decaying molecular markers to a threshold, marking the elapsed time since an initiating event, akin to sand flowing through an hourglass. These hourglass timers can play roles within a clock system by signaling or monitoring phase transitions. Yet, they do not possess the cyclical and directional feedback that define biological clocks. By integrating mechanisms that buffer against environmental fluctuations, these timers gain enhanced stability, enabling developmental systems to adapt flexibly to changes in their surroundings [10].

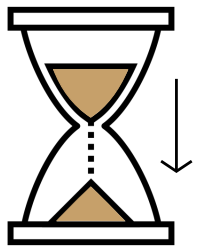

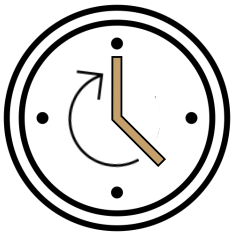

| | Hourglass model | Clock model |
|---|---|---|
| **Input energy** | Turning the hours glass | Winding the clock |
| **Timing mechanism** | Running of the sand | Turning of the hands |
| **Measure of time** | Emptying of top chamber and/or filling of lower chamber | Altered position of the hands |
| **Biological context** | Fertilization, cell differentiation | Cell cycle, circadian rhythm |

**Figure 1. Timing mechanisms in early development.** Two theoretical models for timing mechanisms in early development differentiate the actual timing mechanism. The clock model functions cyclically, whereas the hourglass model operates through a linear progression. Adapted from Johnson and Day, 2000 [10]).

### 1.1.2 Heterochronies: Genetic variations in developmental timing

Variations in the timing programs controlled by genetics in evolutionary developmental biology are defined as heterochronies [15]. Heterochronies categorize differences in the timing of developmental events and have significant implications. These variations can manifest as differences in when a developmental process starts, how long it lasts, or the speed at which it occurs compared to an organism's ancestors or different species. Changes in the onset or duration of these processes are often associated with genetic differences in regulatory sequences or how genes are expressed [16], [17]. On type is ordering heterochrony, which involves shifts in the initiation times of developmental processes, leading to the formation of new anatomical structures (**Figure 2A**). For instance, Darwin's finches, which exhibit a remarkable variety of beak shapes adapted to specific ecological niches, have differences in the expression of the *BMP4* gene. In particular, changes in the timing of *BMP4* expression affect beak width and depth, demonstrating how timing shifts in gene expression during critical developmental windows can lead to evolutionary adaptations [18]. Another type is interval heterochrony, which changes developmental phase duration and can alter cell type proportions and overall developmental timing (**Figure 2B**). In giraffes, interval heterochrony has resulted in an extended period of growth for the cervical vertebrae compared to their closest relatives, like the okapi, which do not have elongated necks. This extended growth period allows the cervical vertebrae in giraffes to become much longer, contributing to their distinctive long-necked profile [19].

Conversely, changes in the rate of a developmental process, known as allochrony, typically involve the same genetic programs but operate at varying speeds, impacting processes like the rate of biological reactions and the regulation of critical oscillatory genes like *HES7* (**Figure 2C**). These are usually not linked to differences in regulatory sequences and can be influenced by metabolic rates. [20], [21]. The underlying mechanisms that drive allochronies, however, still need to be understood.

In the upcoming sections, I will delve deeper into our current knowledge of developmental timing and the study of allochronies in mammalian organisms and provide a theoretical framework elucidating mammalian embryonic development, particularly emphasizing the pivotal role pluripotent stem cells (PSCs) play in developmental biology. I will introduce essential PSC properties, elucidating their remarkable potential for differentiation and how this distinctive attribute is harnessed in developmental investigations. Furthermore, I will introduce the utilization of single-cell sequencing methodologies, highlighting the application of these cutting-edge techniques in deciphering the intricacies of cellular dynamics and lineage determinations throughout embryonic development.

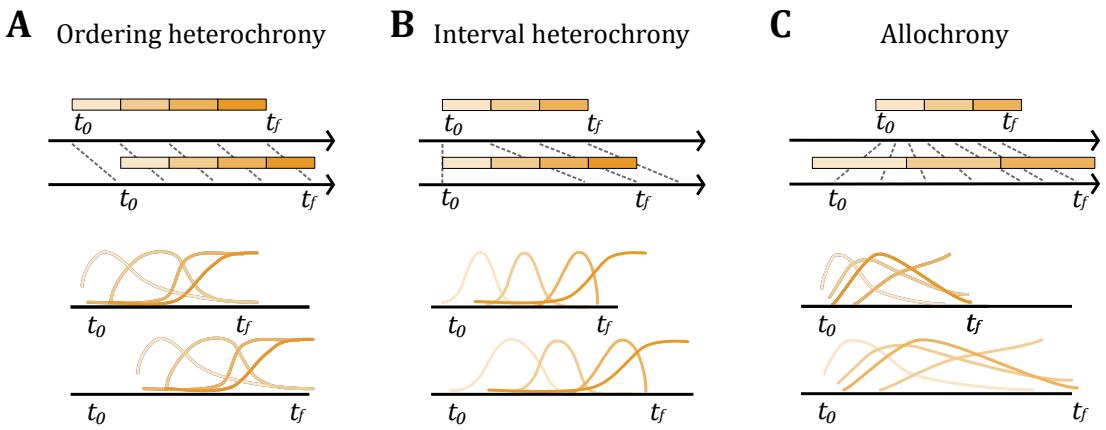


**Figure 2. Developmental heterochrony and their mechanisms. (A)** Ordering heterochrony: Alterations in the start time of a conserved process result in the development of new structures. **(B)** Interval heterochrony: Variations in the length of certain stages of a process can modify the mix of cell types and the general timing of the process. **(C)** Allochrony: Relative adjustments in the speed of the process. Adapted from Rayon, 2023 [15].

## 1.2 The role of PSCs in studying mammalian development

PSCs are an invaluable resource for exploring the mechanisms that govern species-specific differentiation schedules. With their capacity to self-renew and differentiate into progenitors of all germ layers and, ultimately, all adult body cells, PSCs are a potent tool for probing the intricacies of mammalian development. In this introduction I will first examine mammalian embryogenesis, as this process provides the foundation for the origin and potential of PSCs and offers insights into the natural occurrence of pluripotency. Following this, I will introduce the defining properties of PSCs, such as their self-renewal and differentiation capabilities, to highlight their significance and versatile applications in developmental biology research.

### 1.2.1 Mammalian embryogenesis

Mammalian embryonic development is a remarkable transformation from a single fertilized egg into a complex, multi-cellular organism. This process begins with the fusion of sperm and egg, setting off a series of developmental milestones that include cell division, differentiation, and tissue formation. Each step is finely tuned by genetic and molecular

mechanisms, ensuring the embryo forms correctly and functions properly as it prepares for the following stages.

At the beginning of embryogenesis, a zygote is formed with the fertilization of an oocyte by a sperm. This zygote then undergoes the maternal-to-zygotic transition, which includes gametic chromatin decompaction, global DNA demethylation, genomic reorganization, and chromatin remodeling, setting the foundational stage for subsequent embryonic development [22]. Initially, the zygote is transcriptionally inactive, relying on maternal mRNAs and proteins for early developmental processes [23]. Following the first cell division in mice, embryonic transcription commences with two bursts of activity after zygotic genome activation [24], [25]. This leads to a series of rapid mitotic divisions known as cleavage, proceeding to polarization by the 8-cell stage and culminating in morula formation at the 16-cell stage. In the morula stage, each cell, known as a blastomere, enhances its surface contact with adjacent cells through compaction [26], [27], [28]. Variations exist between mammalian species regarding the number of cells at the compaction stage, with bovine embryos showing differences already around 9 to 15 cells and in rabbits not until after 32 cells [29]. During this stage, cavitation occurs and ultimately forms a multicellular blastocyst by approximately 3.5 days post-fertilization in mice and 5 to 6 days in humans, consisting of the outer trophectoderm (TE), which contributes to the placenta, and the inner cell mass (ICM), which will develop into the embryo [30]. About 12 internal cells in mice form the new ICM, and 20-24 cells form the surrounding TE [31], [32].

TE cells form extraembryonic tissues as embryogenesis progresses and facilitate fluid influx into the blastocyst, creating a polarized structure with the ICM positioned at one end [33]. The distinct physical and functional segregation of the ICM from the TE is a defining feature of mammalian development, marking the first specification of cell lineages. The ICM evolves into a bilaminar disc consisting of the hypoblast and epiblast, containing progenitors to the three primary germ layers which are subsequently established during primitive streak formation and gastrulation: ectoderm, mesoderm, and endoderm [34]. The ectoderm differentiates into the skin, hair, nails, and nervous system, including the neural tube that forms the brain and spinal cord. The mesoderm develops into muscle, skeletal structures, the circulatory system, and organs like kidneys and gonads. The endoderm generates the linings of the digestive and respiratory tracts and associated organs such as the liver and pancreas [35]. After gastrulation, the embryo undergoes neurulation, which commences with forming the neural plate from the ectoderm, which then folds to create the neural tube. This tube will eventually differentiate into the brain and spinal cord, the principal components of the nervous system [36]. Additionally, somite formation from the paraxial

mesoderm occurs, producing structures contributing to the vertebral column, skeletal muscle, and dermis [37]. Throughout these stages, complex signaling pathways such as WNT, BMP, and FGF critically influence tissue differentiation and organ development, ensuring precise spatial and temporal embryonic development [38]. This meticulous coordination sets the foundation for the embryo's subsequent growth and functional maturation.

### 1.2.2 Foundations of pluripotency

Pluripotency refers to the capacity of cells to develop into cells from all three embryonic germ layers and potentially into primordial germ cells (PGCs), though not into extra-embryonic tissues [39]. While pluripotency naturally occurs only temporarily *in vivo*, pluripotent cells can be extracted from various stages of early embryonic development and perpetually sustained in a self-renewal state *in vitro* [40]. The nature of pluripotency is highly dynamic, evolving through different phases before and after implantation [41]. Nonetheless, the ability to maintain self-renewal *in vitro* has positioned pluripotent cells at the forefront of applications in tissue replacement, disease modeling, and animal engineering technologies [42], [43].

On a molecular level, research has shown pivotal transcriptional networks that underlie the maintenance of pluripotency, centrally involving the transcription factors OCT4 (also known as POU5F1), SOX2, and NANOG. These factors, integral to the network, synergistically stabilize the pluripotent state by co-localizing at specific sites on chromatin, where they regulate gene expression [44]. Furthermore, the expression levels of SOX2 and OCT4 are critically regulated. Deviations in their levels can initiate differentiation in mouse embryonic stem cells (ESCs), demonstrating their essential roles in maintaining stem cell identity [45], [46]. The regulation of pluripotency extends beyond these core factors. For instance, ESRRB is known to interact with OCT4 and NANOG to maintain pluripotency in ESCs [47]. REX1 is another crucial player in the pluripotency network, as it has been shown to regulate the expression of pluripotency markers and inhibit differentiation in mouse ESCs [48]. SALL4 is also essential for maintaining pluripotency, as it interacts with OCT4 and NANOG to regulate gene expression and prevent differentiation in ESCs [49]. The combined action of the OCT4/SOX2/NANOG complex with these additional factors leads to the regulation of roughly 600 genes, illustrating a vast and intricate network that controls pluripotent states [50]. In addition to these core factors and proteins, other transcriptional regulators have

been identified as essential players in maintaining pluripotency. For example, KLF4 has been shown to cooperate with OCT4, SOX2, and NANOG to induce pluripotency in somatic cells [51]. This extensive regulatory system ensures the fine-tuned balance required for pluripotency and highlights the complexity of the genetic and epigenetic mechanisms that govern cell fate decisions.

### 1.2.3 Types of pluripotent stem cells

#### *1.2.3.1 Embryonic and epiblast stem cells*

Evans and Martin's isolation of the first mouse ESCs from the ICM of mouse blastocysts in 1981 marked a pivotal advancement in stem cell research [52], [53]. The technique for isolating mouse ESCs typically involves mechanical or enzymatic separation of the ICM from the blastocyst around 3.5 days post-fertilization. This discovery laid the foundation for further investigations into the properties and applications of ESCs. Progress continued with extracting the first primate ESC line in 1995, broadening the spectrum of PSC research [54]. A significant leap was made in 1998 when Thomson established human ESC lines from surplus blastocysts from *in vitro* fertilization, enhancing opportunities for studying human development, disease modeling, and therapeutic possibilities [55]. Human ESCs are derived approximately 3-5 days post-fertilization, involving the meticulous extraction of the ICM [56]. Additional advances in stem cell research have led to the derivation of ESCs from various primate species, including rhesus monkeys and marmosets [57]. This expansion of diversity also includes, for example, the successful establishment of ESC lines from rats [58]. Furthermore, ESCs have also been successfully derived from domesticated farm animals such as pigs and sheep, broadening the applications of stem cell research in agriculture, biomedical studies, and xenotransplantation [59], [60]. These developments underscore the growing versatility and scope of ESC research across different mammalian species.

EpiSCs represent a distinct class of PSCs sourced from the post-implantation epiblast of the developing embryo, in contrast to ESCs, which are derived from the pre-implantation blastocyst [61], [62]. Research involving human equivalents of the post-implantation blastocyst has been limited due to ethical considerations, highlighting the complexities and challenges associated with this study area.

PSCs exist in two primary states known as ground, also referred to as naïve, pluripotency and primed pluripotency, each displaying unique molecular and functional characteristics corresponding to different phases of embryonic development [63], [64]. The ground state of

pluripotency is observed in pre-implantation epiblast stem cells in rodents. This state closely resembles the properties of mouse ESCs derived from the ICM of developing blastocysts (**Figure 3**). Key features of this state include the expression of specific ground marker genes, the absence of X chromosome inactivation, and a primary reliance on mitochondrial respiration for energy [63], [65], [66]. In culture, mouse ESCs are maintained in a ground state using LIF [67], [68], supplemented with inhibitors of MAPK-ERK and GSK3β (2i), which supports the maintenance of their undifferentiated state [69], [70], [71]. Conversely, primed pluripotency, corresponding to the post-implantation epiblast stem cells in rodents [61], [62], is characteristic of human ESCs (**Figure 3**). These cells undergo X chromosome inactivation, display a flatter morphology, and their transcriptional activities are similar to those of mouse EpiSCs. Ground mouse ESCs can be transitioned to a primed state by removing LIF and adding ACTIVIN and FGF [63].

Successfully capturing and maintaining the ground state in human PSCs has been challenging, indicating significant gaps in our understanding of the mechanisms governing state transitions [72]. This challenge is exacerbated by the variation in gene expression profiles and morphological characteristics seen in ground human ESCs across different studies, suggesting that the molecular identity remains controversial and inconsistent with that of mouse ESCs [73], [74]. Nevertheless, recent progress in studying both ground and primed states of pluripotency has illuminated that the observed differences between mouse and human ESCs stem from the distinct properties inherent to each state [75]. The primary stages of pluripotency are fundamentally linked by the Yamanaka factors, core pioneering transcription factors essential for establishing and sustaining pluripotency [76], [77], [78]. Studies have shown that the transitions between the ground and primed states are orchestrated by a sophisticated array of transcription factors, including NANOG and KLF4 [79], [80]. Experimentally manipulating these transitions, such as overexpressing NANOG or KLF4 in a 2i condition devoid of LIF, can revert primed PSCs to a ground state. The incorporation of LIF markedly enhances this reversion, indicating the essential supportive role of this signaling factor in the process [81].

The well-established primed pluripotent state, exhibited by human ESCs, mouse EpiSCs, and iPSCs from non-human and human primates, serves as a universal baseline for comparative research [61], [62], [82]. Previous studies have shown that this state allows for the consistent *in vitro* induction of differentiation across different species using standardized protocols and will therefore be utilized in this research [61], [83].

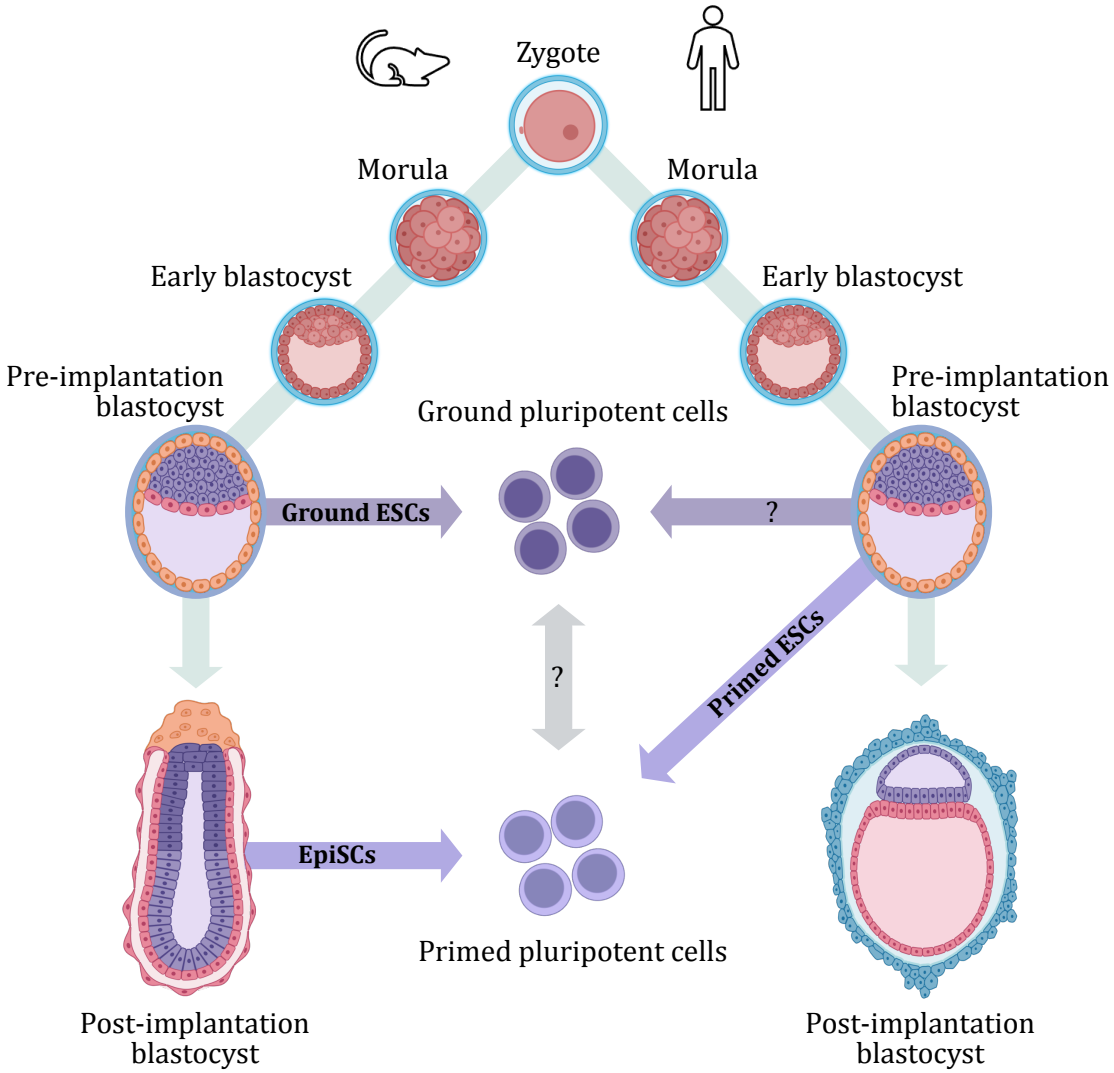


**Figure 3. PSC derivation across human and mouse.** Notable differences in embryo morphology become evident between mice and humans during the first stages of embryonic development. In mice (left path), naive ESC can be isolated from the ICM of pre-implantation blastocysts, and primed EpiSCs can be derived from post-implantation epiblasts. Conversely, in human (right path), primed pluripotent cells are isolated from the ICM of the pre-implantation blastocyst. However, due to ethical considerations, pluripotent cells are not derived from human post-implantation embryos. Adapted from Weinberger et al. [64]. Created with BioRender.com.

#### *1.2.3.2 Induced pluripotent stem cells*

A series of revolutionary experiments set the foundation of induced pluripotent stem cell (iPSC) technology, starting with Sir John Gurdon's work in the 1960s. Using the African clawed frog, *Xenopus laevis*, Gurdon demonstrated that a nucleus from a differentiated somatic cell, when transplanted into an enucleated oocyte, could develop into a fully functional organism [84]. This crucial experiment showed that cell differentiation did not permanently alter the genetic material, suggesting that mature cells could be reprogrammed back to an embryonic state. These findings significantly changed our understanding of cellular development and laid the conceptual groundwork for future cloning and cell reprogramming advances.

One of the most famous pre-iPSC experiments was the cloning of Dolly the sheep by Ian Wilmut and his team at the Roslin Institute in Scotland. This marked the first successful mammal cloning from an adult somatic cell through somatic cell nuclear transfer (SCNT), proving that adult cells could be reset to an embryonic state [85]. Subsequently, the field shifted towards therapeutic cloning, which involved using SCNT to create cloned embryos. Despite the ethical and technical challenges, these efforts aimed to generate patient-specific ESCs for transplantation and disease modeling [86]. Research also expanded into other methods of nuclear reprogramming, such as cell fusion techniques. Studies demonstrated that fusing somatic cells with ESCs could confer pluripotency to the somatic nuclei, further exploring the plasticity of cellular differentiation states [87]. These collective experiments deepened our understanding of cellular reprogramming and directly paved the way for developing iPSC technology.

iPSCs have emerged as a pivotal innovation in regenerative medicine and stem cell research. Introduced by Shinya Yamanaka and colleagues in 2006, these cells are transformed from adult somatic cells into a state similar to ESCs by introducing specific transcription factors, OCT4, SOX2, KLF4, and c-MYC [51], also referred to as ‘Yamanaka factors’. This transformation provides iPSCs with pluripotency and the ability to develop into any cell type from the three primary germ layers: ectoderm, mesoderm, and endoderm. The ability to reprogram somatic cells into iPSCs has revolutionized potential applications in regenerative medicine, providing avenues for advanced disease modeling and drug discovery [88]. However, they also retain some epigenetic memory of their tissue of origin, which can influence their differentiation potential [89]. iPSC technology facilitates the creation of patient-specific stem cells, which help explore genetic disease mechanisms, enhance drug testing, and formulate personalized treatments [90], [91].

Moreover, iPSCs present a solution to ethical issues associated with ESCs derived from non-embryonic sources. While groundbreaking, the process of reprogramming cells to iPSCs presents several challenges. Initially, integrating viral vectors was a significant concern due to the risk of mutagenesis and oncogenesis from insertional mutations. To mitigate these risks, newer techniques involving non-integrating vectors like adenoviruses, plasmids, and direct protein transduction have been developed, which help avoid alterations to the host genome [92], [93], [94].

In 2012, Shinya Yamanaka and John Gurdon were awarded the Nobel Prize in Physiology or Medicine for their pioneering work reprogramming mature cells to become pluripotent, fundamentally changing our understanding of how cells and organisms develop. iPSCs provide a scalable and ethically sustainable source of pluripotent cells that help study developmental biology, model diseases, and advance potential treatments across various medical conditions. As advancements continue, iPSC technology promises to fulfill the extensive potential of regenerative medicine, paving the way for personalized cell therapies in the foreseeable future.

### 1.2.4 Directed differentiation of PSCs

As previously highlighted, PSCs can be directly differentiated into cells of all three germ layers (**Figure 4**) and there have been considerable advancements in the directed differentiation of PSCs into specific cell types. One practical approach involves leveraging embryonic development signaling pathways to establish precise differentiation protocols for each cell type [95]. Another strategy employs small molecules to direct PSC differentiation, offering advantages over protein factors and genetic methods due to their cost-effectiveness, potency in modifying signaling pathways, and ability to provide precise temporal control by adjusting dosages and combinations [96], [97].

During embryonic development, mesoderm differentiation into tissues like hematopoietic, bone, vascular, cardiac, and skeletal muscle is driven by signaling pathways such as Wnt/β-Catenin and TGF-β, including Activin and BMPs [98], [99]. Initial activation and subsequent inhibition of Wnt/β-catenin are necessary for cardiac lineage specification. Researchers have developed monolayer-based differentiation using Activin A and BMP4 [100] and embryoid body-based differentiation involving complex signaling [101].

Organs derived from endoderm, such as the pancreas, liver, lung, and intestine, are key focus areas for regenerative therapies. In human and mouse ESC cultures, the induction of

definitive endoderm is highly promoted by robust activin/Nodal signaling [102], [103], [104]. In the embryonic development of both mice and humans, the induced endoderm forms an epithelial layer that differentiates into various sections termed foregut, midgut, and hindgut [105]. This process is influenced by signaling molecules from adjacent mesoderm-derived tissues. Induction methods often mirror these developmental stages for the *in vitro* generation of endoderm-derived lineages.

Neural ectoderm development in PSC cultures typically occurs without adding serum or external inducers but relies on endogenous FGF signaling from the differentiating PSCs [106]. In practical applications, researchers employ methods such as embryoid body formation, co-culture with neural-inducing feeders, and targeted neural induction to derive neural lineages from PSCs. A significant advancement was achieved by Lorenz Studer's lab, which developed the dual-SMAD inhibition (dSMADi) technique to enhance the differentiation of human PSCs into neural cells. This technique inhibits the TGF-β/Activin/Nodal pathway using SB431542 and the BMP pathway using Noggin, effectively suppressing mesoderm and endoderm differentiation to promote neuroectodermal outcomes [107]. The process yields early-stage neuroepithelial progenitors with over 80% purity in a monolayer culture, which are highly responsive to cues for regionalization, enabling the efficient generation of region-specific neuronal subtypes. Notably, inhibiting the Activin/Nodal pathway encouraged the differentiation of mouse EpiSCs and human ESCs into neural precursors, indicated by their transformation into rosette-like structures typical of such cells. In contrast, mouse ESCs retained their pluripotency even when blocking the Activin/Nodal pathway. However, using both JAK and ALK inhibitors directed these mouse ESCs toward a neuroectodermal fate, resembling EpiSCs treated with just the ALK inhibitor. Similarly, when exposed to the ALK inhibitor alone, human ESCs quickly ceased expressing pluripotency genes and developed neural traits. This suggests a functional similarity between primed mouse EpiSCs and human ESCs and highlights their developmental dynamics compared to mouse ESCs [62], [108].

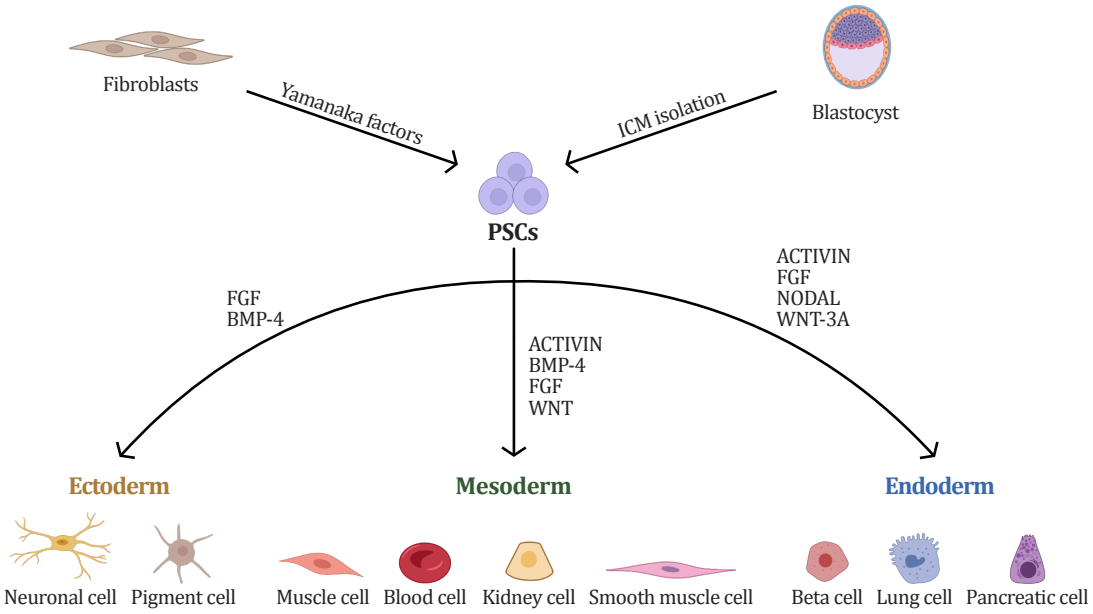


**Figure 4. PSCs can differentiate into cells of all three germ layers.** PSCs, whether ESCs isolated from the blastocyst or iPSCs generated by reprogramming somatic cells such as fibroblasts, can differentiate into cells from all three germ layers: ectoderm, mesoderm, and endoderm. The diagram illustrates representative cell types derived from each germ layer and highlights critical signaling pathways involved in their differentiation. Created with BioRender.com

### 1.2.5 The cell cycle of PSCs

The cell cycle of PSCs is a fundamental aspect of their biology, crucial for maintaining pluripotency and the ability to differentiate into various cell types. Unlike differentiated cells, ESCs are characterized by a unique cell cycle structure that supports their rapid proliferation and the maintenance of an undifferentiated state.

In general, ESCs exhibit a shortened G1 phase. This abbreviated G1 phase is critical because it minimizes the time during which differentiation signals might influence the fate of the cell, thus maintaining pluripotency. The high activity of cyclins and CDKs, typical ESC features, facilitates the rapid progression through the cell cycle [109], [110], [111]. Moreover, regulating the cell cycle in ESCs is tightly integrated with the core pluripotency network. Key pluripotency factors OCT4, SOX2, and NANOG regulate genes involved in maintaining pluripotency and interact with cell cycle regulators to promote the rapid cell division characteristic of ESCs [112]. These interactions highlight the complex interplay between the cell cycle machinery and the transcriptional network that maintains stem cell identity.

Disruptions in the pluripotent cell cycle program typically compromise pluripotency, leading to differentiation [113], [114], [115]. Therefore, maintaining pluripotency is dependent on precise cell cycle dynamics.

In mouse ESCs, the cell cycle is marked by an exceptionally short G1 phase, facilitating rapid proliferation. This characteristic is linked with the maintenance of ground pluripotency because it limits the exposure of cells to differentiation signals. Mouse ESCs depend less on checkpoint controls, allowing faster progression through the cell cycle [109]. However, this can also increase the risk of accumulating mutations [116], [117]. While mouse EpiSCs retain pluripotent properties and self-renewal ability, their pluripotency capacity is somewhat constrained compared to ESCs [118], [119].

Furthermore, changes in pluripotency states are linked to variations in the cell cycle duration [120]. Compared to mouse ESCs, primate ESCs, including those from humans, have a more extended G1 phase, similar to primed mouse EpiSCs, which is thought to provide a critical window during which developmental signals are integrated, thus influencing cell fate decisions. This extended G1 phase in primate ESCs indicates a greater control over cell cycle progression and a higher degree of scrutiny at checkpoints [121], [122]. These species-specific differences in cell cycle regulation highlight the evolutionary adaptations in embryonic development among mammals. The extended G1 phase of primate ESCs allows for more rigorous control of differentiation and may reflect adaptations to the complexity seen in primate embryogenesis. In contrast, the rapid cell cycle in mouse ESCs underscores a strategy focused on growth and speed, potentially reflecting the lesser developmental complexity relative to primates.

The unique characteristics of the ESC cell cycle are fundamental for their biology and have important implications for developmental biology research. Understanding how ESCs regulate their cell cycle and maintain pluripotency provides critical insights into early development processes. Besides the cell cycle, PSCs also exhibit distinct metabolic properties compared to somatic cells, which I will highlight in the following section.

### 1.2.6 The metabolism of PSCs

The metabolism of PSCs is intricately linked to their functional state, influencing their pluripotency and differentiation capabilities. Given the substantial energy and biosynthetic requirements of cellular division, metabolic processes are expected to vary between dividing and non-dividing cells.

In somatic cells, in general, glucose undergoes glycolysis, resulting in pyruvate, which can either be reduced to lactate or enter the mitochondria where it is converted to acetyl-CoA, feeding into the tricarboxylic acid (TCA) cycle (**Figure 5**) when sufficient oxygen is present. Under low oxygen conditions, acetyl-CoA production is limited, and pyruvate is more likely converted to lactate [123]. Growth and proliferation also dictate metabolic demands, as cells require both ATP and macromolecules for expansion [124].

PSCs exhibit a unique metabolic profile closely intertwined with their pluripotent state and self-renewal capabilities. In particular, in some fast-dividing cancer cells and PSCs, high rates of glycolysis are observed and occur even in the presence of sufficient oxygen, a phenomenon known as the Warburg effect. This effect results in the production of lactate from pyruvate. It allows glycolytic intermediates to be channeled into biosynthetic pathways instead of being fully oxidized in the TCA cycle, thereby supporting rapid cellular growth [123], [124], [125], [126], [127], [128]. Furthermore, ESCs are characterized by rapid division and a notably short G1 phase, as previously described. This rapid proliferation likely increases their reliance on glycolysis to meet the high energy and biosynthetic demands of cell growth and division. Furthermore, as ESCs differentiate into neurons, glycolysis diminishes as they terminally differentiate [129]. Similarly, during the reprogramming of fibroblasts to iPSCs, there is an uptick in glycolysis that precedes the emergence of pluripotency markers [130]. These observations underscore that PSCs exhibit higher glycolytic activity than their more differentiated counterparts.

Considerable research evidence indicating heightened glycolysis in stem cells highlights their elevated lactate production. In support of this, ESCs have been observed to produce lactate at a higher rate through glycolysis than differentiated cardiomyocytes [131], though they also engage in oxidative phosphorylation [132]. This lactate production, critical for maintaining glycolytic flux, allows the recycling of nicotinamide adenine dinucleotide (NAD+), essential for continuing glycolysis by converting pyruvate to lactate. This process facilitates the utilization of glycolytic intermediates in biosynthetic pathways by liberating resources. Key glycolytic intermediates, such as 3-phosphoglycerate, are diverted to synthesize serine and glycine, which are vital for producing amino acids, lipids, and nucleotides. Similarly, dihydroxyacetone phosphate is utilized for phospholipid synthesis, and glucose-6-phosphate may be channeled into the pentose phosphate pathway, further supporting cellular biosynthesis (**Figure 5**) [123].

This metabolic preference towards glycolysis is crucial for maintaining the pluripotent state of ESCs. It is regulated by core pluripotency factors such as OCT4, SOX2, and NANOG, highlighting the intricate connection between metabolism and pluripotency [133].

Inhibiting glycolysis in human ESCs leads to cell cycle arrest and apoptosis, further supporting the notion that glycolysis is crucial for cells that rapidly divide and have high anabolic needs [132], [134]. Similarly, suppressing glycolysis hinders the reprogramming of fibroblasts into iPSCs, although it does not impact fibroblast proliferation [130], [135]. While glycolysis plays a role in all cells to some extent, these findings indicate that it is especially critical for sustaining PSCs. The elevated glycolysis observed in PSCs may be due to the insufficient capacity of their mitochondria to support oxidative phosphorylation fully. It has been suggested that the mitochondria in mouse [131] and human ESCs [136] are less mature than those in more differentiated cells and exhibit reduced electron transport chain components transcription. While primed mouse EpiSCs possess more morphologically mature mitochondria than ground mouse ESCs, they rely heavily on glycolysis due to low cytochrome C expression [132]. Additionally, human ESCs utilize their mitochondria to consume rather than produce ATP despite having mitochondrial mass and oxygen consumption rates comparable to fibroblasts when adjusted for protein content.

In conclusion, PSCs rely heavily on glycolysis, even with sufficient oxygen, to meet their rapid growth and biosynthetic demands. This metabolic preference, regulated by pluripotency factors like OCT4, SOX2, and NANOG, is essential for maintaining their pluripotent state.

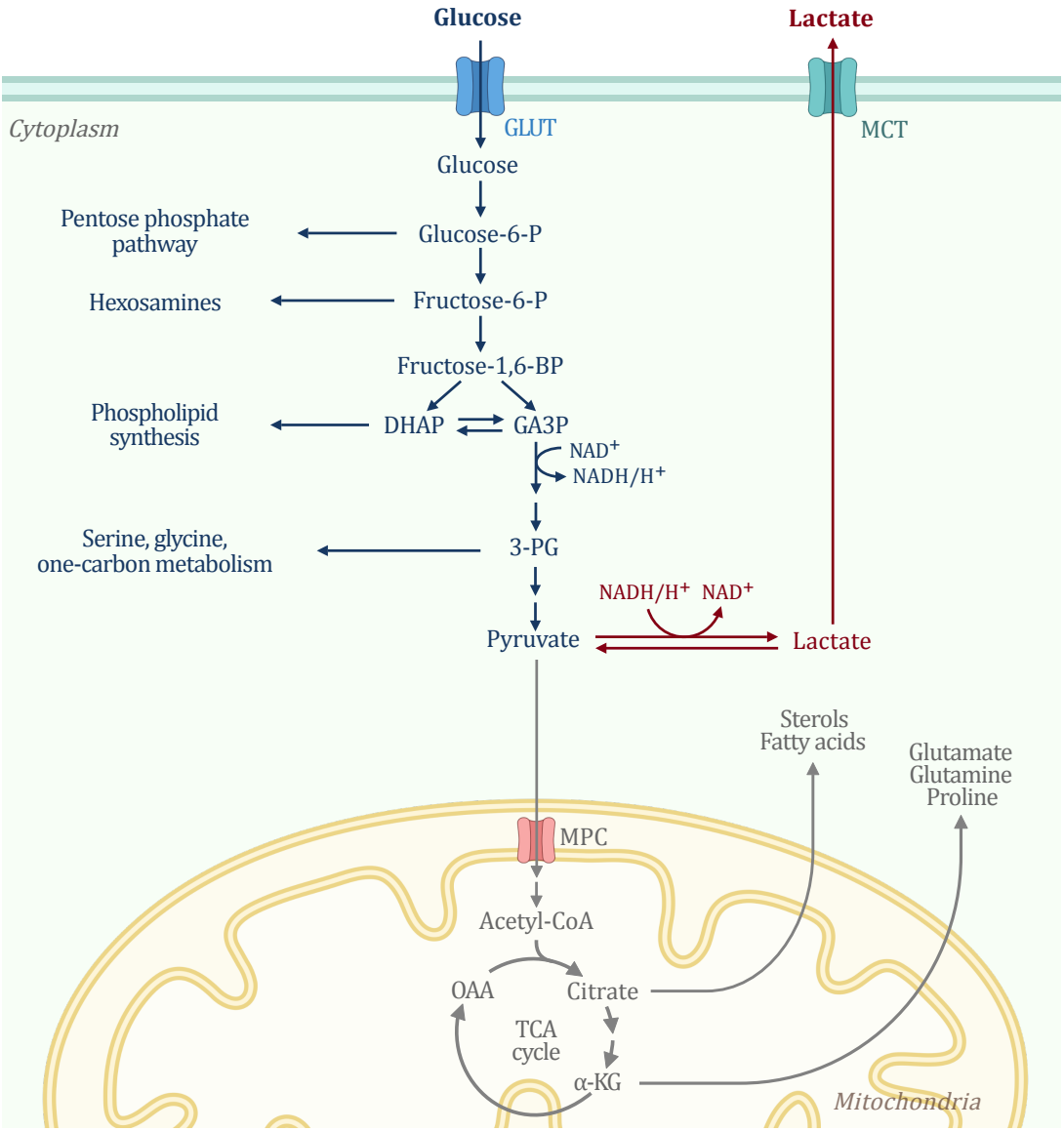


**Figure 5. Warburg-like metabolism of PSCs.** Schematic representation of metabolism in primed PSCs. Glycolysis is the primary energy source even in oxygen-rich environments, with cells converting pyruvate to lactate. GLUT = Glucosetransporter, MCT = Monocarboxylate transporter, P = Phosphate, BP = Bisphosphate, DHAP = Dihydroxyacetone phosphate, GA3P = Glyceraldehyde 3-phosphate, 3-PG = 3-Phosphoglycerate, TCA = Tricarboxylic acid, MPC = Mitochondrial pyruvate carrier, α-KG = α-Ketoglutarate, OAA = Oxaloacetic acid. Created with BioRender.com.

## 1.3 The regulation of developmental timing

### 1.3.1 Developmental timing is species-specific and intrinsically manifested

Time scales of life vary extensively, even within the same clade. The same absolute amount of time, for example, one year, amounts to more than half of a mouse's life span but only to a small fraction of a human life span. The difference is striking, given that the genetics and physiology are similar within the mammalian clade.

Delving deeper into development, these species-specific differences become even more apparent. While the sequence of events in mammalian embryonic development is similar across species, the timing varies significantly. Human embryos take approximately two weeks to progress from oocyte fertilization to gastrulation, but mice reach this developmental milestone in just six days [137]. This observation also further expands to organogenesis. For instance, brain vesicle formation during anterior brain development occurs around embryonic day ten in mice, but it takes up to five weeks in human embryonic development (**Figure 6**) [138], [139].

Historically, classic experiments, such as those by Harrison in 1924 [140] and Twitty and Schwind in 1931 [141], established foundational principles in developmental biology. These studies demonstrated that when amphibian tissues, like eye or limb buds, are transplanted, they continue to develop according to the inherent timelines and characteristics of their original species rather than conforming to the developmental schedule of the host species. More recent research corroborates this concept of developmental autonomy. For example, Saiz-Lopez et al. [142] used chick limb transplants to show that transplanted tissues maintain their species-specific developmental timing even when introduced to a different biological context. Additionally, research utilizing diverse animal models has investigated the differentiation of neural and glial precursors, cell fate decisions, and apoptosis and consistently demonstrated that such processes are specific to each species [143], [144], [145], [146], [147].

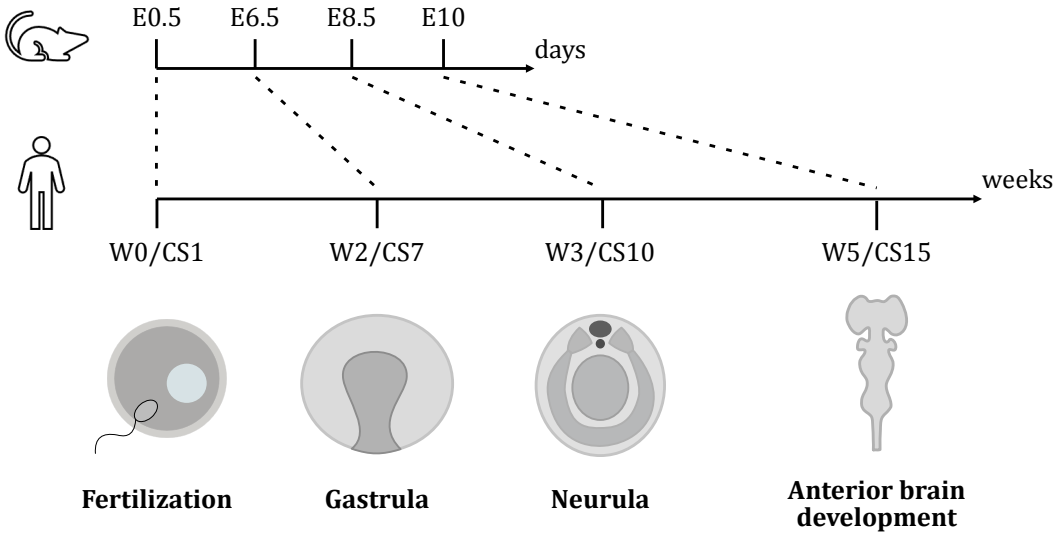


**Figure 6. Species-Specific time scales during organogenesis in anterior brain development.** Schematic illustration of the distinct developmental timelines for mice (top) and humans (bottom) during the formation of the anterior brain. The critical developmental milestones depicted from left to right are fertilization, gastrulation, neurulation, and brain vesicle formation. In mice, these milestones are marked in embryonic (E) days post-fertilization, while in humans, they are indicated by Carnegie stages (CS) and timed in weeks (W).

Notably, the rate of *in vivo* development is mirrored by the pace of *in vitro* differentiation in PSCs, which remains distinctly species-specific [83], [148], [149], [150], [151]. The duration of organogenesis and neuronal differentiation in the peripheral nervous system and midbrain is significantly longer in humans than in mice [152]. Additionally, human and non-human primate cortical neurons, derived from PSCs and xenotransplanted into the mouse cortex, continue to develop according to their species-specific developmental time frames [153], [154]. Furthermore, when human neural progenitors are transplanted into chick embryos, they keep differentiating according to the human developmental timeline, thus limiting the rate of differentiation [155]. Studies on directed differentiation *in vitro* demonstrate that human and non-human primate pluripotent cells strictly adhere to their species-specific cell cycle durations and maturation processes during neuronal differentiation [150], [156]. Other studies have highlighted that the segmentation clock, crucial for directing the differentiation of vertebral column precursors, exhibits oscillation periods of approximately 2.5 hours in mice and 5 hours in human presomitic mesoderm (PSM) models (**Figure 7**) [20], [21]. These observations highlight the profound role of

genetic and epigenetic intrinsic mechanisms in dictating species-specific developmental timelines, emphasizing the intricate evolutionary adaptations that govern the unique developmental trajectories of each species. In the following section, I will explore the current understanding of the intrinsic regulation of developmental timing in greater detail.

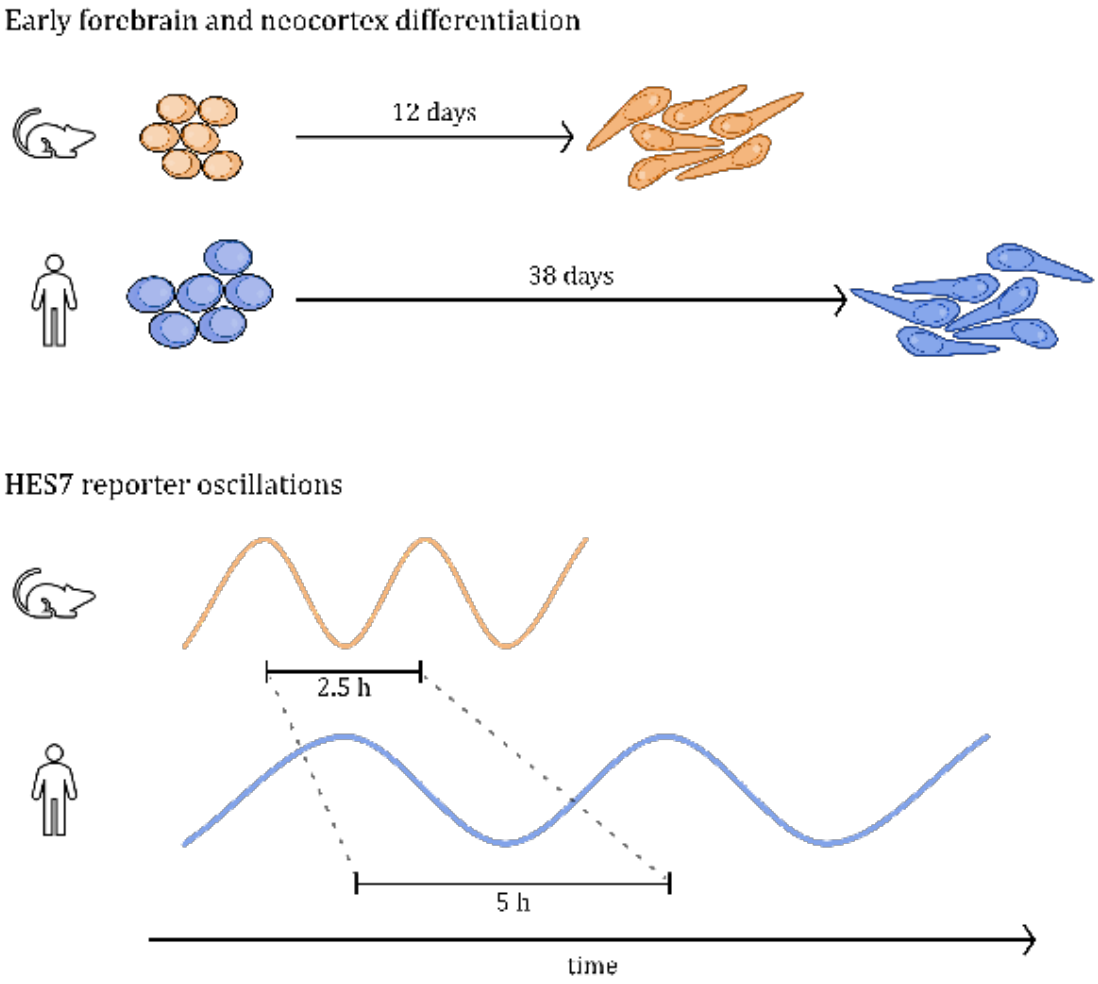


**Figure 7. *In vitro* PSM models reflect *in vivo* segmentation clock dynamics.** Schematic illustration of speed differences in *in vitro* models of early forebrain and neocortex differentiation in mouse versus human (top) and HES7 reporter oscillations in mouse and human PSM models (bottom). Differentiation into mature neurons takes 12 days in mice but 38 days in humans. The PSM mouse model displays an oscillation period of 2.5 hours, while the human model exhibits a more extended period of 5 hours.

### 1.3.2 Metabolic and biochemical regulation of developmental processes

#### *1.3.2.1 Biochemical reaction rates and protein stability*

One proposed mechanism for the differences in species-specific developmental speeds is the rate of biochemical reactions. Comparative *in vitro* differentiation studies of PSM cells, which develop into bones, muscles, and motor neurons, have been conducted to understand allochronic mechanisms between mice and humans. In one notable experiment, Matsuda et al. substituted the mouse *Hes7* gene with its human ortholog. This modification did not alter the oscillation period in mice, highlighting that the HES7 oscillation period is tightly linked to species-specific factors. Mathematical models of this feedback loop, which include analysis of the degradation rates of HES7 protein and mRNA, indicate that variations in transcription and translation kinetics drive these interspecies differences [20]. Additional research that involved inhibiting translation in human PSM cells demonstrated the critical role of protein turnover rates, as these interventions markedly reduced the pace of HES7 oscillations [21]. Notably, slower biochemical reaction rates, including protein turnover and transcription elongation speed, have been linked to increased longevity [157], [158], with species that have longer lifespans typically being more prominent in size and having extended gestational periods [159]. Furthermore, *in vitro* studies utilizing iPSCs differentiated into PSM cells have facilitated the examination of the segmentation clock across multiple mammalian species, including mice, rabbits, cattle, pigs, rhinoceroses, humans, and marmosets. These findings demonstrate that the segmentation clock period correlates with the rate of HES7 biochemical reactions, such as protein degradation and intron delay, rather than the body weight of the animal, indicating a fundamental mechanism for tempo regulation independent of size-related scaling. Furthermore, the rates of HES7 biochemical reactions are not proportional to cellular metabolic rates across species, suggesting that energy production alone does not account for the variations in species-specific biochemical kinetics [160].

In a study focusing on motor neuron differentiation from mouse and human stem cells *in vitro*, researchers noted similar trends in regulating developmental speed as in the PSM model. The differences in the rate of development between the two species are not attributed to changes in sensitivity to external signals or alterations in the DNA sequences of essential genes. Instead, the prolonged developmental timeline observed in humans correlates with increased protein stability. This finding suggests that differences in protein stability across species could be a key factor explaining the variations in developmental timing observed between humans and mice [148].

#### *1.3.2.2 Metabolic pathways and their influence on early cell fate decisions*

Constitutive protein turnover, including protein synthesis and degradation, accounts for as much as 25% of the metabolic expenditure, surpassing the energy required for other cellular activities like DNA replication or transcription. Research comparing protein turnover across varying-sized mammals indicates that larger animals typically exhibit a more stable proteome, with slower protein turnover rates associated with reduced ATP production [158]. This variation in basal metabolic rates and energy production among species may be a key factor explaining the discrepancies in developmental timelines.

Increasing evidence supports that metabolism is crucial in early cell fate decisions [128]. This influence is mediated through key metabolic signal transduction pathways such as AMPK/mTOR and critical metabolites like α-KG, S-adenosylmethionine, and acetyl-CoA, which are integral to regulating cell fate [161], [162]. For instance, ADP/ATP ratio fluctuations can inactivate the AMPK/mTOR pathway, mirroring the metabolic suppression observed during the physiological diapause in rodents, thereby halting development [161]. The AMPK/mTOR signaling is also essential for the proliferation of embryonic and extraembryonic cells post-implantation [163].

In PSM *in vitro* models, human cells are notably larger than mouse cells, with size-adjusted mass-specific metabolic rates corresponding to developmental speeds. The correlation between intermediary metabolism and physiological traits such as body size, lifespan, and embryonic development rates has been extensively explored. Research has demonstrated that lifespan often corresponds with the pace of embryonic development. Notably, metabolic rates exhibit an inverse relationship with body mass, where smaller animals display a higher mass-specific resting metabolic rate, the energy expended per gram of tissue per unit of time, compared to their larger counterparts, a phenomenon referred to as Kleiber's law [164]. Mouse PSM cells exhibit higher metabolic rates and quicker HES7 oscillations than their human counterparts. When the electron transport chain in human PSM cells is pharmacologically inhibited, the HES7 oscillation period lengthens.

In contrast, overexpression of NADH oxidase lbNOX enhances the translation rate and speeds up the segmentation clock. Experiments involving protein translation inhibitors show that these do not affect the metabolic rate, suggesting that the translation rate does not directly influence the metabolic rate to control the HES7 period in human PSM cells [21].

#### *1.3.2.3 Mitochondrial activity as a regulator of developmental timing*

The interplay between mitochondrial metabolism and developmental timing has been highlighted through various studies, underscoring its potential as a universal regulator of cellular maturation across different species and cell types. One prominent study utilized a novel system for timing neuronal birth and mitochondrial dynamics to explore this relationship in human and mouse cortical neurons, both *in vitro* and *in vivo* [165]. Initial observations noted smaller, less complex mitochondria in newly formed neurons, which mature over time, enhancing both size and function, a markedly slower process in humans than mice. Intriguingly, mitochondrial activity, particularly oxidative processes within the electron transport chain, matured more rapidly in mice, correlating with faster developmental rates observed in these species. Further experiments manipulating mitochondrial function through metabolic interventions confirmed a direct correlation between enhanced mitochondrial activity and accelerated neuronal maturation in humans. These interventions, which included modulation of pyruvate metabolism and fatty acid utilization, significantly expedited developmental milestones in human neurons, such as dendritic growth and synaptic functionality. These outcomes were replicated *in vivo* following xenotransplantation into mouse models [165].

This mitochondrial influence is not restricted to neurons but extends to other cellular contexts, such as the segmentation clock in PSM cells. Here, too, mitochondrial metabolism has been implicated in dictating the pace of developmental oscillations, with faster rates in mouse cells than human cells, highlighting a broader applicability of mitochondrial function in developmental timing [21]. However, contrasting findings in other studies suggest that while mitochondrial metabolism plays a crucial role, it is likely part of a more complex network of factors influencing developmental tempo [160].

In general, variations in metabolic rates may influence the pace of biochemical reactions by modulating energy availability. Similarly, specific mitochondrial metabolites that participate in posttranslational modifications might also play a role in determining developmental speeds.

### 1.3.3 Epigenetic control of developmental timing

Epigenetic mechanisms play a crucial role in the precise timing of gene expression. Inhibiting chromatin modifications at specific gene sites adjusts gene activation timing, introducing delays in gene expression. For example, during the development of the mouse

cortex, inhibiting PRC2 in radial glia accelerates the emergence of later-born neural cell types [166]. This epigenetic control over the timing of cortical progenitor differentiation might be connected to protein turnover rates. Comparative single-cell RNA sequencing (scRNA-seq) of cortical neural progenitors in the developing mouse brain has pinpointed a set of genes involved in translational regulation, which could influence timing transitions. Notably, the rRNA methyltransferase Fibrillarin reduces the translation of epigenetic modifiers like the H3K27me3 EZH2 methyltransferase and KDM6b demethylase, thereby postponing the differentiation of cortical neural progenitors [167]. In human cortical development, a reduction in epigenetic factors correlates with increased maturity in neurons differentiated from pluripotent stem cells. Temporary suppression of epigenetic regulators such as EZH2, EHMT1/2, or DOT1L in progenitor cells can expedite the maturation of neurons derived from human stem cells [168]. It is crucial to understand how such barriers are established in progenitors before neurogenesis begins and how they are maintained in differentiated neurons.

Epigenetic regulation may be closely connected with metabolism to influence developmental tempo through post-translational modifications (PTMs), which are influenced by metabolic byproducts [169]. Variations in nutrient absorption, along with fluctuations in glycolytic and lipolytic activities, the TCA cycle, and oxidative phosphorylation, can alter metabolite concentrations and affect physicochemical parameters such as pH, redox balance, and reactive oxygen species levels. These metabolites often act as substrates or modulators for PTMs, including processes like methylation and demethylation, acetylation and deacetylation, o-glycosylation, and DNA methylation [169], [170]. Such PTMs, particularly on histones, can significantly impact gene expression through the epigenetic modification of the chromatin structure. For instance, recent studies have causally linked histone PTM alterations to neuronal development in mouse cerebellar and human cortical neurons, highlighting the role of methylation dynamics in these processes [171], [172]. Furthermore, the metabolite α-KG, a co-factor for dioxygenase enzymes involved in demethylation processes, affects histone modifications like H3K9me3 and H3K27me3, pivotal in determining cell fate between different states of PSC pluripotency [173], [174]. Similarly, α-KG can drive the differentiation of PSCs by altering histone and DNA methylation during spontaneous differentiation of the mouse ESC [175] and human neuroectodermal differentiation [176].

The detailed mechanisms behind the epigenetic regulation of developmental timing require further exploration. This is especially significant given that epigenetic complexes comprise

function-specific subunits. Additionally, it remains to be explored how epigenetic factors influence developmental timelines differently across species.

### 1.3.4 The influence of the environment on developmental timing

While intrinsic timescales and genetically determined factors primarily govern developmental processes and dictate species-specific developmental speeds, external influences can modify them.

For example, experimental reductions in cell numbers in mouse embryos, through pharmacological or mechanical interventions, significantly slow down the differentiation process relative to cell proliferation during critical stages such as gastrulation [177], [178]. This alteration of the cellular environment showcases its impact on developmental dynamics, revealing how even subtle changes in cellular composition can influence the timing and efficiency of developmental milestones.

Another significant response to external influences is diapause, a natural adaptation in which development illustrates the flexibility of developmental systems to environmental cues, ensuring survival under adverse conditions by pausing the developmental clock.

On a cellular level, experiments involving *in vivo* mouse/rat chimeras have demonstrated that development is predominantly influenced by the host, as evidenced by body size and species-specific organogenesis [179], [180]. These studies highlight the dominant role of the host environment in guiding the developmental trajectory of implanted cells, underscoring the importance of external biological contexts in developmental outcomes. This was further supported by Brown et al. [181]. They created *in vitro* chimeric conditions by mixing human PSCs with a surplus of mouse PSCs and differentiating them into neurons together. Bulk RNA sequencing results indicated that human neural genes were upregulated earlier in these human/mouse co-cultures during neurodifferentiation compared to pure cultures. This suggests that the presence of cells from different species can alter the developmental programming of each cell type.

These examples emphasize the dynamic interaction between genetically programmed developmental pathways and the need for adaptability to environmental and experimental conditions. Such flexibility is crucial for developing developmental strategies that optimize survival and reproduction in diverse environments. These findings highlight the multifaceted nature of development, where intrinsic genetic programs are constantly exposed to and modulated by extrinsic factors, dictating developmental timing.

## 1.4 Single-cell sequencing as a tool to study developmental biology

### 1.4.1 The impact of single-cell technologies

Single-cell technologies have revolutionized biological research by providing detailed gene expression measurements, DNA accessibility, and other cellular features at the individual cell level. Previously, sequencing assays on a bulk scale averaged the data, obscuring individual cellular differences and specific molecular processes [182], [183]. This advancement enables granular analysis of cellular identity, diversity, development, and disease processes with unparalleled detail [184]. Recent progress has dramatically expanded the capabilities of these technologies, allowing for genome-wide profiling of RNA, DNA, and proteins across thousands or even millions of individual cells [185], [186]. In developmental biology, single-cell technologies enable scientists to observe cell development and differentiation dynamics in unprecedented detail, tracing lineage decisions in real time and dissecting the molecular underpinnings of developmental processes. This is essential for identifying how specific cells evolve from their precursors, how cellular diversities emerge during embryogenesis, and how errors in these processes might lead to developmental abnormalities.

Additionally, in cellular therapies, single-cell analyses identify and optimize regenerative mechanisms, helping to tailor cell-based treatments that closely mimic natural developmental pathways. This can significantly enhance the efficacy and safety of therapies by ensuring that engineered cells behave similarly to their healthy, tissue-derived counterparts in the human body [183].

Creating comprehensive cellular atlases and accumulating extensive single-cell datasets have revolutionized our understanding of cellular identities and functions. Historically, the classification of cell types was based on phenotypic attributes such as gene or protein expression or morphological characteristics. Recent advances in sequencing, imaging, and mass spectrometry have expanded our ability to assess cellular characteristics across multiple dimensions, including genomic, transcriptomic, epigenomic, and proteomic variations. These dimensions encompass a wide range of cellular markers, from single nucleotide variations to broader epigenetic modifications such as DNA methylation and histone modifications, which govern gene accessibility and expression levels [187]. Integrating these diverse data streams through multi-omics technologies provides a holistic view of cellular processes, allowing for a more nuanced understanding of cellular

development, differentiation, and function. This is crucial in developmental biology, where understanding the precise cellular mechanisms and their temporal dynamics can elucidate how complex organisms develop from a single cell. Such detailed insights are essential for identifying critical developmental pathways. Moreover, the shift from static to dynamic models of cell classification reflects a more profound comprehension of cellular states as fluid rather than fixed, facilitating a continuum model of development and cellular differentiation [188], [189]. This approach is valuable for developmental biology for mapping out the lineage decisions and differentiation pathways that shape the development of tissues and organs from embryonic stem cells.

In the following section, scRNA-seq and single-cell assay for transposase-accessible chromatin sequencing (scATAC-seq) will be explained in further detail. These technologies are at the forefront of my research on developmental timing, offering unprecedented resolution in understanding gene expression and chromatin accessibility on a cellular basis.

### 1.4.2 Single-cell RNA sequencing

As all cells within an organism possess nearly the same DNA, simply knowing the DNA sequence and the location of regulatory elements offers only a basic understanding of the complex and dynamic processes occurring within cells. This has led researchers to increasingly explore the transcriptome of cells, which reveals more about the proteins being actively transcribed. The groundbreaking first sequencing of a single-cell transcriptome occurred in 2009 [190]. Since then, advancements in technology have dramatically lowered the volume of sample needed while enhancing the sensitivity and the number of cells that can be analyzed. Various scRNA-seq platforms and methodologies exist today, but the core steps remain consistent. These steps include isolating and lysing the cells, capturing mRNA, and converting it into double-stranded cDNA with a unique identifier for each cell. Some protocols also tag each mRNA molecule with a unique molecular identifier (UMI) to track individual molecules [191], [192]. The cDNA is then amplified, and the labeled molecules are combined to form a library for next-generation sequencing [193], [194]. The droplet-based scRNA-seq platform by 10x Genomics is widely used. It utilizes microfluidic systems to isolate individual cells into nanoliter-sized droplets (**Figure 8A**). Each droplet captures a single cell and a bead coated with oligonucleotides. These oligonucleotides include a unique cell barcode, UMI, and a poly(T) sequence to complementary bind the poly(A)-tails of mRNA molecules. Once the cells are lysed within the droplets (**Figure 8B**), their mRNA adheres to

the poly(T) sequences on the beads (**Figure 8C**). The mRNA is then reverse-transcribed into cDNA (**Figure 8D**). Following amplification, cDNA from each cell are combined and sequenced using next-generation sequencing techniques (**Figure 8E**). Applying unique cell barcodes and UMIs allows for accurate identification and quantification of gene expression in individual cells, facilitating analysis even at low sequencing depths.

However, to fully understand cellular dynamics, it is essential to integrate additional omics techniques. While scRNA-seq provides detailed insights into gene expression, it does not capture all the regulatory mechanisms that control cellular behavior. For this reason, scATAC-seq has become a widely regarded method for profiling chromatin accessibility at the single-cell level, which will be described in the following section.

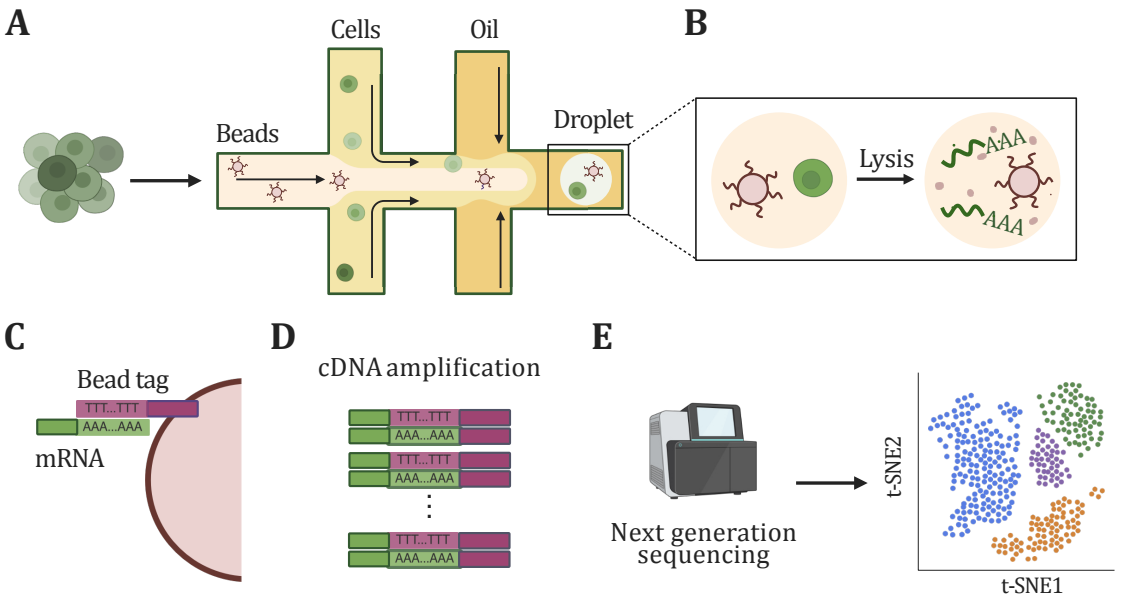


**Figure 8. Droplet-based scRNA-seq technique by 10x Genomics. (A)** Dissociated single-cells and tagged beads are input for droplet-based scRNA-seq and captured in oil droplets. **(B)** During cell lysis, mRNA is released within the droplets, and **(C)** subsequently binds with the poly(A) tail to oligonucleotides on the beads containing the PCR handle, cell barcode, UMI, and a poly(T) sequence. **(D)** cDNA is synthesized from the mRNA and then amplified. Sequencing libraries are constructed, pooled, and **(E)** subjected to next-generation sequencing after amplification. The resulting sequencing data is subjected to bioinformatic processing, which includes clustering and visualization techniques. Created with BioRender.com.

### 1.4.3 Single-cell ATAC sequencing

Cellular diversity is not only a product of variations in gene expression but also a consequence of how genes are regulated through epigenetic modifications. Given that all cells share an identical genetic foundation, the chromatin structure must be dynamic enough to allow for alterations in DNA accessibility, enabling adaptable transcriptional activity. The accessibility of specific genomic sequences indicates genomic activity, signifying gene expression or the openness of particular sequences like enhancers or transcription factor binding sites [195], [196]. In recent years, the activity of the transposase enzyme has been harnessed to map chromatin accessibility at the single-cell level. This enzyme randomly fragments and tags accessible chromatin DNA, subsequently integrating sequencing adapters. Since DNA regions wrapped around histone proteins are physically inaccessible, they remain unfragmented. Thus, the fragments generated represent the accessible areas of the chromatin (**Figure 9A**). Since the introduction of this technique [197], several variations have been developed. Similar to scRNA-seq, the scATAC-seq technique developed by 10x Genomics will be described. The procedure starts with the nuclei isolation of single cells. It is crucial to isolate nuclei accurately to capture chromatin DNA while excluding other DNA sources like mitochondrial DNA. The nuclei are then treated with Tn5 transposase and loaded with sequencing adapters (**Figure 9B**). This enzyme cuts the chromatin DNA at accessible sites and inserts sequencing adapters into these regions. The resulting nuclei with tagged chromatin fragments are encapsulated into droplets containing barcoded oligonucleotides that assign a unique cell barcode and a UMI. Like in scRNA-seq, each droplet captures a unique set of chromatin fragments from a specific cell. These droplets are then pooled, and the DNA is amplified by PCR to construct a sequencing library for next-generation sequencing (**Figure 9C**).

The advancement of single-cell sequencing technologies, including scRNA-seq and scATAC-seq, has transformed our ability to dissect cellular heterogeneity. The innovative single-cell multiome sequencing technology by 10x Genomics allows simultaneous profiling of gene expression and chromatin accessibility within the same cells. This technology enables a detailed characterization of molecular mechanisms and significantly enriches our fundamental understanding of cellular biology.

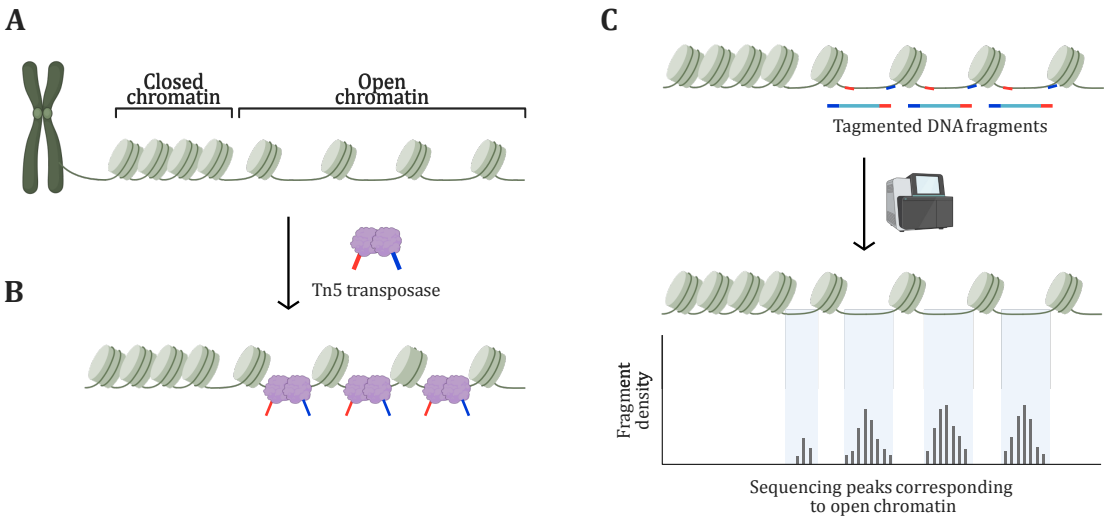


**Figure 9. Methodology behind ATAC sequencing. (A)** Chromatin is either accessible in open regions or inaccessible in closed areas. **(B)** In the scATAC-seq approach by 10x Genomics, reactions occur within oil droplets. Hyperactivated Tn5 transposase equipped with sequencing adaptors (blue and red) targets open chromatin regions. **(C)** The genomic DNA is subjected to tagmentation, forming tagged DNA fragments in areas of open chromatin. These fragments are then processed through next-generation sequencing. Bioinformatic analysis identifies peaks that indicate regions of open chromatin. Created with BioRender.com.

## 1.5 Aim and impact of the study

This study aims to thoroughly investigate the regulation of developmental timing across various mammalian species, focusing on the complex interactions among genetic, epigenetic, and extracellular factors that influence the progression from a fertilized oocyte to a mature organism. Recent research has highlighted the significance of developmental timing, yet the precise molecular mechanisms that dictate developmental rates remain largely undefined. This research seeks to enhance our understanding of the complex nature of developmental processes by utilizing advanced genetic and epigenetic analysis techniques. These include comparative single-cell multiome sequencing to identify critical genes that significantly impact the rate of development. Through this approach, I aim to uncover the molecular underpinnings that regulate species-specific developmental timing.
I refined and harmonized *in vitro* model systems by standardizing PSC culture conditions and neural progenitor differentiation for mouse, cynomolgus and human. This aspect of the research was designed to enhance the reliability, making it possible to conduct more

controlled and reproducible experiments across different laboratory settings. These standardized models facilitate a more systematic analysis of developmental processes and enable a more straightforward comparison of developmental dynamics across species, without the influence of external factors.

The ultimate goal of this study was to gain molecular insights with advanced technologies in genomics and bioinformatics to understand the complex mechanisms that regulate developmental timing. By combining detailed molecular analyses with computational tools, I elucidated species-specific rates of neural differentiation at both the transcriptomic and chromatin levels across various mammalian species. This integrative approach aimed to quantify and comprehend the species-specific developmental dynamics.

Furthermore, through this innovative approach, my research identified UGP2 as the first single candidate to influence species-specific developmental speed. I employed CRISPR/Cas9 gene-editing technology and conducted a functional analysis of UGP2 to delineate its role within the genetic network that governs developmental timing. By comparing wildtype and UGP2 Knockout (KO) models, I evaluated the influence of UGP2 KO on neural differentiation speeds in humans and cynomolgus. Such insights into the metabolic mechanisms could lead to new strategies for controlling developmental processes by highlighting potential targets for modifying how energy metabolism influences cellular development.

In conclusion, this study paves the way for understanding the regulation of developmental timing in mammals by identifying key genes like UGP2 through bioinformatic analysis. Future research could build on these findings to develop refined models for species-specific development, enhancing our knowledge and research in developmental timing.

# 2 Materials and Methods

## 2.1 Materials

The materials utilized in this study are listed in **Table 1 - Table 9** and are subsequently detailed in the experimental procedures according to their respective applications.

### 2.1.1 Cell lines

**Table 1.** Cell lines routinely used in this study.

| Cell line | Species | Source |
|---|---|---|
| *129S2C1a* mEpiSC | Mouse (*Mus musculus*) | Donated by Prof. Vallier (Cambridge) |
| *56A1* iPSC | Cynomolgus (*Macaca fascicularis*) | Donated by Prof. Enard (LMU) |
| *56A1* iPSC UGP2 KO 29cl6 | Cynomolgus (*Macaca fascicularis*) | Generated in lab |
| *70Af1* iPSC | Orangutan (*Pongo abelii*) | Donated by Prof. Enard (LMU) |
| *H9* hESC | Human (*Homo sapiens*) | WiCELL Research Institute |
| *H9* hESC UGP2 KO 3-2/35 | Human (*Homo sapiens*) | Donated by Dr. Barakat (Erasmus MC) |
| *HMGU1* iPSC | Human (*Homo sapiens*) | iPSC Core Facility, HMGU |
| *Sengi cl.1* iPSC | Elephant shrew (*Macroscelides proboscideus*) | Generated in lab |

### 2.1.2 Cell culture media, chemicals and solutions

**Table 2.** Cell culture media, supplements, chemicals and solutions routinely used in this study.

| Reagent | Manufacturer | Cat. No. |
|---|---|---|
| β-Mercaptoethanol | Thermo Fisher Scientific | 31350-010 |
| Accutase® solution | Sigma-Aldrich | A6964 |
| Agarose | Biozym | 840004 |
| Ascorbic acid | Sigma-Aldrich | A8960 |
| B-27 Supplement (50x) | Thermo Fisher Scientific | 17504044 |

| | | |
|---|---|---|
| Bovine Albumin Fraction V, 7.5% solution | Thermo Fisher Scientific | 15260037 |
| CHIR99021 | Tocris | 4953/10 |
| Clarity Western ECL Substrate | BioRad | 1705060S |
| CryoStor® cell cryopreservation media | Sigma-Aldrich | C2874 |
| CutSmart® Buffer | New England Biolabs | B7204 |
| Digitonin (5%) | Thermo Fisher Scientific | BN2006 |
| DMEM/F12 | PAN Biotech | P04-41250 |
| DMEM, high glucose | Thermo Fisher Scientific | 11965092 |
| Dimethyl sulfoxide, DMSO | Honeywell | D5879 |
| DNA Gel loading dye, 6x | Thermo Fisher Scientific | R0611 |
| Dorsomorphin | Miltenyi Biotech | 130-104-466 |
| DPBS | Thermo Fisher Scientific | 14190094 |
| DPBS with $Ca^{2+}$/$Mg^{+}$ | Thermo Fisher Scientific | 14040091 |
| DTT | Thermo Fisher Scientific | 18080044 |
| EDTA, 0.5 M | Promega | V4231 |
| Fetal Bovine Serum (FBS) | HyClone | SH30071.03 |
| Formaldehyde 16% (w/v), Methanol-free | Thermo Fisher Scientific | 10321714 |
| Gelatin powdered, pure Ph. Eur., NF | AppliChem GmbH | A1693 |
| Geltrex Basement Membrane Matrix | Thermo Fisher Scientific | A1413302 |
| GeneRuler 1kb Plus | Thermo Fisher Scientific | SM1331 |
| GlutaMAX (100x) | Thermo Fisher Scientific | 35050-038 |
| Human Recombinant Insulin (4 mg/mL) | Thermo Fisher Scientific | 12585014 |
| HyClone Fetal Bovine Serum | GE Healthcare | SV30160.03HI |
| INK128 | Cell Signaling | 30690 |
| IWP-2 | Santa Cruz | sc-252928 |
| IWR-1 | Sigma-Aldrich | I0161 |
| LDN-193189 HCl | Peprotech | 1066208 |
| Laemmli Buffer, 2x | BioRad | 1610737EDU |
| Magnesium Chloride solution, 1 M | Sigma-Aldrich | M1028 |
| Matrigel® Matrix | Corning | 354234 |
| MEM Non-Essential Amino Acids Solution (100x) | Thermo Fisher Scientific | 11140-035 |
| Methanol | Serva Electrophoresis | 45631.02 |
| Mini PROTEAN® TGX stain-free gel | BioRad | 4568023 |
| mTeSR1 | Stem Cell Technologies | 05850 |
| N2 Supplement (100x) | Thermo Fisher Scientific | 17502048 |
| NaCl (Sodium chloride) | Carl Roth | P029.2 |
| Neuropan | PAN Biotech | P04-00900 |
| Nuclease-Free Water | Thermo Fisher Scientific | AM9932 |

| | | |
|---|---|---|
| PageRuler Prestained Protein Ladder | Thermo Fisher Scientific | 26616 |
| Penicillin/Streptomycin (100x) | Thermo Fisher Scientific | 15070063 |
| Polyethylene glycol 1500 | Roche | 10783641001 |
| Powdered milk, blotting grade | Sigma Aldrich | T145.1 |
| ProLong™ Glass Antifade Mountant with DAPI | Thermo Fisher Scientific | P36935 |
| Protector RNase inhibitor | Sigma-Aldrich | 3335402001 |
| Recombinant Human FGF-basic (bFGF) | Peprotech | 100-18B |
| Recombinant Human/Murine/Rat Activin A (E.coli derived) | Peprotech | 120-14E |
| RIPA Lysis and Extraction Buffer | Thermo Fisher Scientific | 89900 |
| ROCK inhibitor Y-27632 | R&D Systems | 1254/10 |
| SB431542 | Peprotech | 3014193 |
| Sodium Butyrate | Sigma-Aldrich | B5887 |
| Sodium Chloride solution, 5 M | Sigma-Aldrich | 59222C |
| Sodium Dodecyl Sulfate | Serva Electrophoresis | 20768.02 |
| StemFit Basic 02 | Ajinomoto | Basic02 |
| StemMACS iPS Brew XF | Miltenyi Biotech | 130-104-368 |
| StemMACS™ Passaging Solution XF | Miltenyi Biotech | 130-104-688 |
| SYTOX Blue Dead Cell Stain | Thermo Fisher Scientific | S34857 |
| TERGITOL™-Solution, Type NP-40 | Sigma-Aldrich | NP40S |
| TRIS base | Carl Roth | 5429.3 |
| Tris/Glycine Buffer (10x) | BioRad | 1610734 |
| Triton™ X-100 | Sigma-Aldrich | X100-500ML |
| Trizma Hydrochloride solution, pH 7.4 | Sigma-Aldrich | T2194 |
| TrueCut™ Cas9 Protein v2 | Thermo Fisher Scientific | A36496 |
| Trypan Blue Stain (0.4%) | Thermo Fisher Scientific | T10282 |
| Tween-20 | Sigma-Aldrich | P9416 |

### 2.1.3 Consumables

**Table 3.** Consumables routinely used in this study.

| **Consumables** | **Manufacturer** | **Cat. No.** |
|---|---|---|
| 10/20 µL XL TipOne® filter tips | Starlab | S1120-3810-C |
| 1000 µL TipOne® filter tips | Starlab | S1126-7810-C |
| 20 µL TipOne® filter tips | Starlab | S1120-1710-C |
| 200 µL TipOne® filter tips | Starlab | S1120-8810-C |
| 12-well cell culture plate | Corning | 353043 |

| | | |
|---|---|---|
| 24-well cell culture plate | Corning | 353047 |
| 6-well cell culture plate | Thermo Fisher Scientific | 140685 |
| 384-well PCR plates | Kisker | G034-ABI |
| CELLSTAR® Serological pipette, 10 mL | Greiner Bio-One | 607180 |
| CELLSTAR® Serological pipette, 25 mL | Greiner Bio-One | 760180 |
| CELLSTAR® Serological pipette, 5 mL | Greiner Bio-One | 606180 |
| CELLSTAR® Serological pipette, 50 mL | Greiner Bio-One | 768180 |
| Conical tube, 15 mL | Sarstedt | 62554502 |
| Conical tube, 50 mL | Sarstedt | 62547254 |
| Countess Cell Counting Chamber Slides | Thermo Fisher Scientific | C10228 |
| CryoPure Tube 1.6 mL | Sarstedt | 72380 |
| DNA LoBind® Tubes, 1.5 mL | Eppendorf | 0030108051 |
| DNA LoBind® Tubes, 2 mL | Eppendorf | 0030108078 |
| Falcon® 5 mL Tubes with Cell Strainer Cap | Corning | 352235 |
| MicroAmp™ Optical Adhesive Film | Thermo Fisher Scientific | 4311971 |
| Safe-Lock Tubes, 1.5 mL | Eppendorf | 0030123328 |
| Safe-Lock Tubes, 2 mL | Eppendorf | 0030123344 |
| Superfrost® Plus Microscope Slides | Thermo Fisher Scientific | J1800AMNZ |

### 2.1.4 Antibodies

**Table 4.** Primary and secondary antibodies and isotype controls routinely used in this study.

| Target | Host | Dilution | Manufacturer | Cat. No. |
|---|---|---|---|---|
| **Primary Antibodies** | | | | |
| GAPDH | Mouse | 1:1000 | Thermo Fisher Scientific | MA1-16757 |
| NANOG | Rabbit | 1:100 | Cell Signaling Technology | 4903 |
| NANOG (mouse specific) | Rabbit | 1:100 | Cell Signaling Technology | 8822 |
| OCT4 | Rabbit | 1:100 | GeneTex | GTX101497 |
| OCT4 (mouse specific) | Rabbit | 1:100 | Cell Signaling Technology | 83932 |
| PAX6 | Rabbit | 1:200 | BioLegend | 901301 |
| SOX1 | Goat | 1:200 | R&D Systems | AF3369 |
| SOX2 | Mouse | 1:100 | R&D Systems | MAB2018 |
| SSEA1 | Mouse | 1:20 | Santa Cruz | sc-21702 |

| | | | | |
|---|---|---|---|---|
| TRA-1-60 | Mouse | 1:100 | abcam | ab16288 |
| UGP2 | Mouse | 1:1000 | Santa Cruz | sc-514174 |
| **Secondary Antibodies** | | | | |
| Anti-Goat IgG (H+L) Cross-Adsorbed Secondary Antibody, Alexa Fluor™ 594 | Donkey | 1:800 | Thermo Fisher Scientific | A-11058 |
| Anti-Mouse IgG (H+L) Highly Cross-Adsorbed Secondary Antibody, Alexa Fluor™ 488 | Donkey | 1:800 | Thermo Fisher Scientific | A-21202 |
| Anti-Mouse IgG & IgM Antibody, HRP conjugate | Goat | 1:10.000 | Sigma Aldrich | AP130P |
| Anti-Rabbit IgG (H+L) Highly Cross-Adsorbed Secondary Antibody, Alexa Fluor™ 647 | Donkey | 1:800 | Thermo Fisher Scientific | A-31573 |
| **Isotype controls** | | | | |
| Goat IgG | Goat | variable | R&D Systems | AB-108-C |
| Mouse IgG | Mouse | variable | Thermo Fisher Scientific | 14471485 |
| Mouse IgM | Mouse | variable | Santa Cruz | sc-3881 |
| Rabbit IgG | Rabbit | variable | GeneTex | GTX35035 |

### 2.1.5 Commercial Kits

**Table 5.** Commercial kits and sets routinely used in this study.

| Kit name | Manufacturer | Cat. No. |
|---|---|---|
| Chromium Next GEM Chip J Single-cell Kit, 16 rxns | 10x Genomics | 1000230 |
| Chromium Next GEM Chip J Single-cell Kit, 48 rxns | 10x Genomics | 1000234 |
| Chromium Next GEM Single-cell Multiome ATAC + Gene Expression Reagent Bundle, 4 rxns | 10x Genomics | 1000285 |
| DreamTaq Green DNA Polymerase (5 U/µL) | Thermo Fisher Scientific | EP0712 |
| GeneJET Plasmid Miniprep Kit | Fermentas | K0502 |
| Inside Stain Kit | Miltenyi Biotech | 130-090-477 |
| NovaSeq 6000 S1 Reagent Kit (100 cycles) | Illumina | 20028319 |
| NovaSeq 6000 SP Reagent Kit (100 cycles) | Illumina | 20028401 |
| P2 Primary Cell 4D-Nucleofector® X Kit | Lonza | V4XP-2024 |
| P3 Primary Cell 4D-Nucleofector® X Kit | Lonza | V4XP-3024 |

| | | |
|---|---|---|
| PureLink HiPure Plasmid Filter Maxiprep Kit | Thermo Fisher Scientific | K210017 |
| QIAamp DNA Mini Kit | Qiagen | 51304 |
| QIAquick PCR Purification Kit | Qiagen | 28104 |
| RNeasy Mini Kit | Qiagen | 5001329 |
| SYBR Green qPCR Master Mix | Thermo Fisher Scientific | 4367659 |
| Verso cDNA Synthesis Kit | Thermo Fisher Scientific | AB1453A |

### 2.1.6 Enzymes

**Table 6.** Enzymes routinely used in this study.

| Enzyme | Manufacturer | Cat. No. |
|---|---|---|
| Collagenase, Type IV | Thermo Fisher Scientific | 17104019 |
| SalI-HF | New England Biolabs | R3138 |
| EcoRI-HF | New England Biolabs | R3101 |
| HindIII-HF | New England Biolabs | R3104 |
| SacI-HF | New England Biolabs | R3156 |
| RNase-Free DNase Set | Qiagen | 5000650 |

### 2.1.7 Plasmids

**Table 7.** Plasmids routinely used in this study.

| Plasmid | Manufacturer | Cat. No. |
|---|---|---|
| MIP 247 CoMiP 4in1 with shRNA p53 | Addgene | #63726 |
| pCLXE-hMLN | Addgene | #27079 |

### 2.1.8 Oligonucleotides for RT-qPCR

**Table 8.** Sequences of oligonucleotides routinely used for RT-qPCR.

| Target Gene | Target Species | Sequence |
|---|---|---|
| *ASCL1* | Human | F – CCAAGCAAGTCAAGCGACAG<br>R – TTGTGCGATCACCCTGCTTC |

| | | |
|---|---|---|
| *ASCL1* | Orangutan, Gorilla | F – GAGCGCAGCCTTAGTAGGAG<br>R – TAGCCAAAGCCGCTGAAGTT |
| *ASCL1* | Mouse | F – TGGACTTTGGAAGCAGGATG<br>R – TGCATCTTAGTGAAGGTGCCC |
| *ASCL1* | Cynomolgus | F – AGGACTTTGAAAGCAGGGTGA<br>R – GACCCGAGCAAGAGCTTTCA |
| *FOXG1* | Human, Orangutan, Gorilla | F – GGCAAGGGCAACTACTGGAT<br>R – CTGAGTCAACACGGAGCTGT |
| *FOXG1* | Mouse | F – CTGATTGGTTCGGCAGTAGGA<br>R – TAGCAAAAGCTGCAACCACC |
| *FOXG1* | Cynomolgus | F – GGCAAGGGCAACTACTGGAT<br>R – CTGAGTCAACACGGAGCTGT |
| *GAPDH* | Primates, mouse | F – CATCACTGCCACCCAGAAGACTG<br>R – ATGCCAGTGAGCTTCCCGTTCAG |
| *NANOG* | Primates | F – GATTTGTGGGCCTGAAGAAA<br>R – CAGATCCATGGAGGAAGGAA |
| *NANOG* | Mouse | F – GAAATCCCTTCCCTCGCCAT<br>R – CAGGCATTGATGAGGCGTTC |
| *OCT4* | Primates | F – GACAGGGGGAGGGGAGGAGCTAGG<br>R – CTTCCCTCCAACCAGTTGCCCCAAAC |
| *OCT4* | Mouse | F – CCTGGGCGTTCTCTTTGGAA<br>R – ACCATACTCGAACCACATCCTTC |
| *PAX6* | Human, Orangutan, Gorilla | F – CTAGCCAGGTTGCGAAGAAC<br>R – CTTGGGAAATCCGAGACAGA |
| *PAX6* | Mouse | F – CTGAGGAACCAGAGAAGACAGG<br>R – CATGGAACCTGATGTGAAGGAGG |
| *PAX6* | Cynomolgus | F – CCAAACAGAACTCTTGACAGGAA<br>R – TTCACTCCGCTGTGACTGTTC |
| *SOX1* | Human, Orangutan, Gorilla | F – CATCTAGCGCCTTCGGGAC<br>R – AGTGCTTGGACCTGCCTTAC |
| *SOX1* | Mouse | F – CGGATCTCTGGTCAAGTCGG<br>R – GGGACCTCGGTACAAAGTCG |
| *SOX1* | Cynomolgus | F – CTGACGCATATCTAGCGCCT<br>R – GTGCTTGGACCTGCCTTACT |
| *SOX2* | Human | F – AACCAGCGCATGGACAGTTA<br>R – GACTTGACCACCGAACCCAT |
| *SOX2* | Orangutan, Gorilla | F – TTTGTCGGAGACGGAGAAGC<br>R – TAACTGTCCATGCGCTGGTT |
| *SOX2* | Mouse | F – CAAAAACCGTGATGCCGACT<br>R – CGCCCTCAGGTTTTCTCTGT |
| *SOX2* | Cynomolgus | F – TTTGTCGGAGACGGAGAAGC<br>R – TAACTGTCCATGCGCTGGTT |

### 2.1.9 Oligonucleotides for CRISPR Editing

**Table 9.** Guide RNA sequences used for the generation of KO cell lines.

| Gene | Target Species | Label | Thermo ID | Sequence |
|---|---|---|---|---|
| *UGP2* | Cynomolgus | sgRNA_2 | GRWCZCZ | AAACUCAUGUGACGAUGCUG |
| *UGP2* | Cynomolgus | sgRNA_3 | GRXGUWX | CGUCACAUGAGUUUGAGGUA |
| *UGP2* | Cynomolgus | sgRNA_9 | GRYMNGV | AGCAAAGCAAUGUCUCAAGA |

## 2.2 Experimental procedures

### 2.2.1 Cell culture

#### *2.2.1.1 Original PSC maintenance conditions*

The original maintenance conditions are listed in **Table 10**. Human ESCs (H9) and iPSCs (HMGU1) were cultured in feeder-free conditions on Matrigel diluted 1:100 in DMEM/F12 using StemMACS iPS Brew XF. For routine passaging, cells were washed with DPBS and incubated with StemMACS Passaging Solution XF at 37°C for 10 minutes. The detached cells were collected in a 15 mL conical tube and centrifuged for 2 minutes at 300 x *g*. They were then resuspended in culture media before being distributed.

Orangutan, gorilla, and cynomolgus iPSCs (70Af1, 55D1, and 56A1, respectively) were cultured in feeder-free conditions on Geltrex Matrix diluted 1:100 in DMEM/F12 using in StemFit Basic02 media supplemented with 100 ng/mL bFGF and 1x Penicillin/Streptomycin. For passaging, cells were washed with DPBS and incubated with 0.5 mM EDTA for 3-7 minutes at RT until the edges of the colonies started to lift. Cells were then carefully washed with DPBS and detached by pipetting culture media directly on top. Subsequently, cells were resuspended three to five times and transferred as aggregates.

Mouse EpiSCs (129S2C1a) were maintained in EpiSC media which consisted of a 1:1 mixture of DMEM/F12 and Neuropan supplemented with 0.5x N2, 0.5x B27, 0.033% BSA 7.5%, 50 µM β-Mercaptoethanol, 1x GlutaMAX, 1x Penicillin/Streptomycin, 20 ng/mL Activin A, 12 ng/mL bFGF and 2 µM IWP-2. The cells were grown in feeder-free conditions on Gelatin with 1:100 FBS. For passaging, cells were washed with DPBS and incubated with 0.5 mg/mL

collagenase IV for 5 minutes at 37°C. After carefully washing with DPBS, cells were resuspended in culture media, collected in a 15 mL conical tube, and centrifuged for 2 minutes at 300 x *g*. The supernatant was removed, and the cells were triturated into small clumps in culture media.

All cells were maintained in a HERAcell 240i incubator at 37°C and 5% $CO_2$. These maintenance conditions were consistent for all subsequent cell culture applications and differentiations.

**Table 10.** Original conditions of the different cell lines assessed in this study.

| **Cell Type** | **Media** | **Coating** | **Passaging** | **Reference** |
|---|---|---|---|---|
| Mouse EpiSC | EpiSC media | Gelatin | Collagenase | Kurek et al. 2015 |
| Primate iPSC | StemFit | Geltrex | EDTA | Geuder et al. 2021 |
| Human ESC | iPS Brew | Matrigel | StemMACS | Grosch et al. 2020 |

#### *2.2.1.2 Adaptation to common cell culture conditions*

Universal compatibility of defined cell culture conditions (coating, media, passaging) for maintaining primed PSCs was tested. Successful adaptation to a new coating or passaging method was assessed by observing the formation of characteristic stem cell colony morphology. For media adaptation, PSCs were initially split into their respective original media as previously described. Subsequently, a stepwise exchange to the new tested media was performed: 2:1 original media to new media on the first day, followed by 1:2 original media to new media on the second day, and finally, a complete switch to the new media after an additional 24 hours. The efficacy of a stem cell media in maintaining pluripotency was, in addition to evaluating colony morphology, analyzed by immunofluorescence staining and FACS after several passages under the new conditions. All media compositions tested are listed in **Table 11.** Compositions of media tested for cell culture harmonization.

**Table 11.** Compositions of media tested for cell culture harmonization.

| **EpiSC media** | **StemFit** | **CDM** | **UPPS media** |
|---|---|---|---|
| 1:1 Neurobasal & DMEM/F12 | StemFit Basic02 | 1:1 IMDM & F12 | StemMACS iPS Brew XF |
| + 0.5x N2 + B27<br>+ 0.033% BSA 7.5%<br>+ 50 µM ß-ME<br>+ 2 mM GlutaMAX<br>+ 1x Pen/Strep<br>+ 20 ng/ml Activin A<br>+ 12 ng/ml bFGF<br>+ 2 µM IWP2 | + 100 ng/mL bFGF<br>+ 1x Pen/Strep | + 10 ng/mL Activin A<br>+ 12 ng/mL bFGF<br>+ 1x ITS<br>+ 450 µM MTG<br>+ 0.033% BSA 7.5% | + 1 µM IWR-1<br>+ 0.5 µM CHIR |

#### *2.2.1.3 Harmonized media conditions and cell passaging*

Eventually, all PSC lines were maintained in feeder-free conditions on Matrigel diluted 1:100 in DMEM/F12 using UPPS media [198] consisting of StemMACS iPS Brew XF supplemented with 1µM IWR-1 and 0.5 µM CHIR99021. Culture media was exchanged daily. For passaging, cells were washed with DPBS and incubated with 0.5 mM EDTA for 5-10 minutes at RT until the edges of the colonies started to lift. EDTA was removed, and cells were detached by pipetting UPPS media directly on top. Subsequently, cells were carefully resuspended three to five times and transferred as aggregates in a dilution of 1:10-1:20 for all primate PSCs and 1:20-1:40 for mouse EpiSC.

#### *2.2.1.4 Freezing and thawing*

For cryopreservation, PSCs were grown to 80-90% confluency in a 6-well plate. The cells were then triturated into small clumps using 0.5 mM EDTA, as described previously. After removing EDTA, the cells were resuspended in 5-8 mL of CryoStor® cell cryopreservation media. Subsequently, 1 mL of cell suspension was distributed per cryotube. The cryotubes were placed in freezing containers at -80°C and later transferred to liquid nitrogen tanks for long-term storage. To thaw the cells, they were placed in a 37°C water bath, resuspended in culture media supplemented with 10 µM ROCK inhibitor Y-27632, and transferred to 15mL

conical tubes for centrifugation at 300 x *g*. Afterward, the cells were resuspended in fresh culture media supplemented with ROCK inhibitor. The contents of one cryotube were distributed onto two Matrigel-coated plates of a 6-well plate.

### 2.2.2 Generation of elephant shrew iPSCs

#### *2.2.2.1 Isolation of fibroblast and cell culture*

Fibroblasts were obtained from a 4.5-year-old male *Macroscelides proboscideus* from the Salzburg Zoo. First, the tail and ears were carefully cleaned, employing 70% EtOH for sterilization and precisely cut with scissors. Subsequently, the cleaned specimens were placed in PBS supplemented with 3x Penicillin/Streptomycin. The ears underwent further preparation, each being transferred to a 100 mm dish and cut into smaller pieces. These ear fragments were transferred into cryogenic tubes filled with 1.8 mL of CryoStor CS10. The tail preparation involved several steps, including making a lengthwise incision along the tail and meticulously removing the outer layer of skin and hair. Subsequently, the tail was halved, each half subjected to culture in distinct media. The tail was further divided into smaller pieces, and these tail fragments were placed in a 15 mL conical tube containing a sterile Collagenase VI solution with a concentration of 2 mg/mL, followed by incubation at 37°C for 1 hour. After the incubation period, two 6-well plates were prepared by coating them with a solution of 2% FBS in 0.1% Gelatin for 30 minutes at 37°C. The falcon tubes were then centrifuged at 300 *x g* for 2 minutes, and under laminar flow conditions, the supernatant was removed, and the contents of each tube were resuspended in 1.5 mL of the respective medium, either EF medium (DMEM, 10% FBS, 1x GlutaMAX, 1x NEAA, 1X Penicillin/Streptomycin) or RPMI medium (RPMI, 10% FBS, 1x GlutaMAX, 1x NEAA, 1x HEPES, 1x 2-ME, 1x Penicillin/Streptomycin). The tissue suspension was transferred into one well within a 6-well plate, with each well receiving one to two tissue pieces and being filled with 0.5 mL of the corresponding medium. Finally, the biopsy samples were incubated under controlled conditions at 37°C, with 5% $O_2$ and 5% $CO_2$.

#### *2.2.2.2 Plasmid based reprogramming*

Reprogramming of elephant shrew fibroblasts was performed using a non-integrating plasmid-based approach as outlined by Diecke et. Al [92]. This technique utilizes the 4-in-1 CoMiP vector, which incorporates codon-optimized versions of the Yamanaka factors (*Oct4, Sox2, Klf4, c-Myc*) and an shRNA targeting p53, alongside the pCXLE-hMLN plasmid, which

codes for human C-MYC, LIN28, and NANOG. For the transfection process, 1 x $10^6$ fibroblasts were nucleofected with 12 µg of the combined DNA from these plasmids using the P2 Primary Cell 4D-Nucleofector™ Kit, following the protocol provided by the manufacturer and employing the DN100 program on the Amaxa 4-D Nucleofector (Lonza). After nucleofection, cells were spread onto Matrigel-coated 10 cm dishes. The cells were maintained in a fibroblast medium consisting of DMEM high glucose with 10% HyClone Fetal Bovine Serum, supplemented with 0.1 mM sodium butyrate and 64 µg/mL ascorbic acid. On the third day post-nucleofection, the medium was replaced with either naïve medium containing LIF or Essential 7 media for primed conditions. At around day 10, the first iPSC-like colonies emerged, and the medium was switched to mTeSR for further cultivation. By day 21, the cultures were expanded under feeder-free conditions, with the initial plate being split 1:3 onto new Matrigel/mTeSR-coated 10 cm dishes, allowing for the continued analysis and characterization of the iPSC colonies.

#### *2.2.2.3 Cultivation of elephant shrew iPSCs*

After initial reprogramming in mTeSR, sengi iPSCs were transferred to EpiSC media. Media was exchanged daily, and cells were maintained under feeder-free conditions in 1:100 Matrigel in DMEM/F12. Cells were passaged in clumps as previously described in **2.2.1.3**.

### 2.2.3 Flow cytometry

For sample preparation for flow cytometric analysis, cells were washed with DPBS, dissociated into single cells using Accutase, collected in 15 mL conical tubes, and centrifuged for 2 minutes at 300 x *g*. For surface marker staining, cells were once washed with FACS buffer (0.5% BSA and 2 mM EDTA in DPBS), followed by centrifugation at 300 x *g* for 5 minutes and removal of the supernatant. Cells were incubated with primary antibodies for 30 minutes on ice. Then, after another centrifugation and removal of supernatant, cells were incubated with secondary antibodies for 30 minutes on ice, then washed and resuspended in FACS buffer. The Inside Stain Kit was used according to the manufacturer's protocol for intracellular staining. Cells were incubated with primary antibodies for 1 hour at room temperature and with secondary antibodies for 30 minutes on ice. After an additional wash with Inside Perm solution, cells were resuspended in FACS buffer for further analysis on a BD FACSAria III cell sorter (BD Biosciences). Flow cytometry data was analyzed using the FlowJo software. Antibodies and their respective dilutions are listed in **Table 4**.

### 2.2.4 Immunofluorescence staining

For immunofluorescence staining, the cells were seeded onto Matrigel-coated coverslips in a 24-well plate and allowed to grow until the desired confluency or differentiation state was achieved. DPBS with $Ca^{2+}$/$Mg^{+}$ was used for all subsequent washing steps and dilutions. The cells were washed three times with DPBS, and fixation was performed by adding 4% formaldehyde and incubating for 15 minutes at RT. After fixation, the cells were rinsed with DPBS. The cells were kept in fresh DPBS at 4°C for time-course experiments until further processing. First, the cells were rinsed three times with DPBS, followed by three rounds of washing with PBT-BSA solution (1% BSA and 0.1% Triton X-100 in DPBS) for 15 minutes each. The primary antibody was diluted in PBT-BSA and incubated overnight at 4°C. Subsequently, the cells were rinsed three times with PBT-BSA and washed three times for 15 minutes each in PBT-BSA. From this step onward, the samples were constantly protected from light. The secondary antibody was diluted in PBT-BSA and incubated for 2 hours at RT. After incubation, the cells were rinsed twice with PBT-BSA and washed twice for 15 minutes each in PBT-BSA. The cells were washed twice for 10 minutes each in DPBS. The coverslips were mounted onto microscopy slides using ProLong™ Glass Antifade Mountant with DAPI. Antibodies and their respective dilutions are listed in **Table 4**.

### 2.2.5 NPC differentiation

All NPC differentiation media compositions tested are listed in **Table 12**. Only the chosen '3N' protocol will be explained in detail in the following. PSCs were dissociated into single cells using Accutase as described previously to prepare for NPC differentiation. After counting the cells with the Countess II FL Automated Cell Counter, primate iPSCs were seeded at a density of 1.25 x $10^5$ cells/$cm^2$, and mouse EpiSCs were seeded at a density of 6.25 x $10^4$ cells/$cm^2$ on Matrigel-coated plates in UPPS media supplemented with 10 µM ROCK inhibitor Y-27632. Within 24 hours of incubation, the cultures reached confluence for each species. For neural induction, the media was switched to NPC differentiation and maintenance media consisting of 1:1 DMEM/F12 and Neuropan supplemented with 0.5x N2 and B27 supplements, 1x MEM Non-Essential Amino Acids Solution, 1x GlutaMAX, 0.1 mM β-Mercaptoethanol, 5 µg/mL human recombinant Insulin, 10 µM SB431542 and 100 nM LDN193189. The differentiation was carried out up to 14 days, with daily media exchanges after washing the cells with DPBS.

**Table 12.** Overview of the NPC differentiation protocols tested.

| **Protocol** | **'8GMK'** | **'3N'** | **'NMM'** |
|---|---|---|---|
| **Source** | Enard lab | Götz lab | Schröter lab |
| **Media composition** | GMEM<br>+ 8% KSR<br>+ 1x MEM-NEAA<br>+ 0.1 mM β-ME<br>+ 1 mM Pyruvate | 1:1 DMEM/F12 & Neuropan<br>+ 0.5x N2<br>+ 0.5x B27<br>+ 1x MEM-NEAA<br>+ 1x GlutaMAX<br>+ 0.1 mM β-ME<br>+ 5 µg/mL Insulin | 1:1 DMEM/F12 & Neuropan<br>+ 0.5x N2<br>+ 0.5x B27<br>+ 1x MEM-NEAA<br>+ 1x GlutaMAX<br>+ 0.1 mM β-ME |
| **SMAD inhibitors** | 100 nM LDN-193189<br>500 nM A-83-01 | 100 nM LDN-193189<br>10 µM SB-431542 | 1 µM Dorsomorphin<br>10 µM SB-431542 |
| **Splitting solution** | Accutase: single-cells | Accutase: single-cells | EDTA: clumps |
| **Seeding density** | $1.25*10^4/cm^2$ | Primate: $1.25*10^5/cm^2$<br>Mouse: $6.25*10^4/cm^2$ | ~1:15 from 1 confluent 6 well/$cm^2$ |

### 2.2.6 RNA extraction and RT-qPCR

RNA was extracted using the RNeasy Mini Kit following the manufacturer's protocol. Cells were lysed with RLT buffer at defined time points in time-course experiments. The lysates were immediately frozen at -20°C and stored for concurrent RNA extraction. The concentration of the isolated RNA samples was measured using a Nanodrop ND-1000 system. Subsequently, cDNA was synthesized from 500 ng of RNA using the Verso cDNA Synthesis Kit, following the manufacturer's instructions. For RT-qPCR, a total reaction volume of 10 µL was prepared by combining SYBR Green PCR Master Mix, cDNA, and 5 µM of each forward and reverse primer. RT-qPCR was performed in 384-well-plates on a QuantStudio 12K Flex qPCR machine. The cycling conditions consisted of an initial

denaturation at 50°C for 2 minutes, followed by 40 cycles of 15 seconds at 95°C and 1 minute at 60°C. Technical and biological triplicates were included for each sample. To calculate relative normalized expressions, the $\Delta\Delta C_T$ method was employed, utilizing the $C_T$ values of the housekeeping gene *GAPDH* for normalization. The primers used in the experiments are listed in **Table 8**.

### 2.2.7 Generation of cynomolgus iPSC UPG2 KO cell lines

#### *2.2.7.1 CRISPR/Cas9 gene editing*

CRISPR editing of cynomolgus iPSCs was conducted using a plasmid-free method, employing TrueCut Cas9 protein and Invitrogen TrueGuide sgRNAs. The guide RNAs, targeting the UGP2 gene locus in *Macaca fascicularis*, were designed using the Synthego CRISPR design tool and are listed in **Table 9**. To generate KO cell lines, ribonucleoprotein (RNP) complexes were formed by combining individual guide RNAs with TrueCut Cas9 protein, followed by a 10-minute incubation at RT and subsequent storage on ice for later use. Subsequently, 5 x $10^5$ cells were suspended in 100 µl of P3 Nucleofector™ solution per reaction per the manufacturer's protocol, and the prepared RNP complexes were combined as needed. The nucleofection was executed using the DN100 program on the Amaxa 4-D Nucleofector (Lonza). Post-transfection, the cells were seeded onto 6-well plates coated with 1:100 Matrigel in UPPS media with 10 µM ROCK inhibitor Y-27632 and incubated for 24 hours. Once the cells reached 80% confluency, they were dissociated into single cells using Accutase as described previously. Then, 10,000 single cells were plated onto 10 cm polystyrene dishes coated with 1:100 Matrigel in UPPS media containing 10 µM ROCK inhibitor Y-27632 for 24 hours. The culture was maintained until visible colonies formed, and individual colonies were carefully selected and transferred to 12-well plates, where they were kept in UPPS media for further analysis and evaluation.

#### *2.2.7.2 Genomic DNA isolation*

To assess successful homogenous deletion, genomic DNA was extracted from KO clones post-nucleofection of RNPs using the QIAamp DNA Mini Kit, following the manufacturer's guidelines.

#### *2.2.7.3 PCR and PCR clean-up*

PCR amplification was conducted utilizing the DreamTaq Green DNA Polymerase (5 U/µL), adhering to the manufacturer's protocol. The resulting PCR product was then extracted using the QIAquick PCR purification kit.

#### *2.2.7.4 Gel electrophoresis*

PCR products were analyzed using 1% agarose gels in 1x TAE buffer consisting of 40 mM TRIS base, 20 mM acetic acid, and 1 mM EDTA. SYBR Safe DNA Gel Stain was added to the gel in a dilution of 1:10,000. Electrophoresis was conducted at a voltage of 100 V in TAE buffer. The separated DNA fragments were then visualized using the ChemiDoc MP Imaging System (BioRad).

#### *2.2.7.5 Sanger Sequencing*

PCR fragments were sent for Sanger Sequencing at Eurofins Scientific. The resulting sequences were then analyzed using the SnapGene viewer software (version 7.1.1) to confirm the accuracy of the intended deletions.

#### *2.2.7.6 Western Blot*

Western Blot was performed to assess successful KO cell line generation on a protein level. Total protein was extracted using RIPA buffer supplemented with 1x protease inhibitor. Lysed cells were then incubated on ice for 5 minutes, followed by centrifugation at 14,000 *x g* for 15 minutes. The resulting supernatant was transferred to a fresh tube. For analysis, 2x Laemmli buffer was added in equal parts and then incubated at 95°C for 5 minutes. The prepared protein sample was then applied to a 7.5% Mini PROTEAN® TGX stain-free gel for electrophoresis, using SDS running buffer with 1x Tris/glycine and 3.5 mM SDS. Wet blotting onto a nitrocellulose membrane was conducted for 1 hour at 100 V using a blotting buffer with 1x Tris/glycine and 20% methanol. The membrane was then blocked for 1 hour at RT in TBST buffer, containing 20 mM TRIS base, 150 mM NaCl, 0.1% Tween-20, and 5% skim milk powder. The primary antibody was diluted 1:1000 in blocking buffer, applied to the membrane, and incubated overnight at 4°C. Following three TBST buffer washes, the membrane was incubated with a secondary antibody conjugated to horse radish peroxidase (HRP) at a 1:10,000 dilution in blocking buffer for 2 hours at RT. After another three 15-minute washes in TBST buffer, the membrane was stained with Clarity Western ECL

Substrate and visualized after a 2-minute incubation using the ChemiDoc MP Imaging System.

### 2.2.8 Sample preparation for single-cell multiome sequencing

#### *2.2.8.1 Nuclei isolation*

For the pilot experiment, human ESCs, mouse EpiSCs, cynomolgus iPSCs, and elephant shrew iPSCs were individually dissociated into single cells using Accutase. Subsequently, 2.5 x $10^5$ cells per species were collected in a 2 mL DNA LoBind Tube and combined into a single sample for further processing. Human ESC, mouse EpiSC, and cynomolgus iPSCs were used for time course NPC differentiation. Nuclei isolation was carried out following the 'Nuclei Isolation for Single-cell Multiome ATAC + Gene Expression Sequencing' protocol provided by 10x Genomics with some modifications. Briefly, the cells were centrifuged at 300 x *g* for 5 minutes, and the supernatant was removed. The cell pellet was gently resuspended in 100 µL lysis buffer (10 mM Tris-HCl pH 7.4, 10 mM NaCl, 3 mM $MgCl_2$, 0.05% Tween-20, 0.05% NP40, 0.01% Digitonin, 1% BSA, 1 mM DTT and 1 U/µL RNase inhibitor in RNase free water), and then incubated for 3 minutes on ice. After incubation, the sample underwent washing steps with wash buffer (10 mM Tris-HCl pH 7.4, 10 mM NaCl, 3 mM $MgCl_2$, 0.1% Tween-20, 1% BSA, 1 mM DTT and 1 U/µL RNase inhibitor in RNase free water), followed by centrifugation at 1000 x *g* for 5 minutes and removal of the supernatant. The nuclei pellet was resuspended in Diluted Nuclei buffer (1x Nuclei Buffer, 1mM DTT, and 1 U/µL RNase inhibitor in RNase-free water). The concentration of nuclei was determined with the Countess II FL Automated Cell Counter, and successful nuclei isolation was confirmed by visual examination under the microscope using Trypan Blue. The aimed target recovery was 10,000 single nuclei for sequencing.

#### *2.2.8.2 Library preparation*

To create single-cell ATAC and gene expression libraries, the Chromium Next GEM Single-cell Multiome ATAC + Gene Expression Reagent Bundle from 10x Genomics was utilized, following the manufacturer's instructions. The resulting libraries were then sequenced on an Illumina NovaSeq 6000 platform, with the following read length specifications: for RNA sequencing: R1/28 | i7/10 | i5/10 | R2/90 and for ATAC sequencing: R1/50 | i7/8 | i5/24 | R2/49. Michael Sterr of the Single-cell Genomics Unit at Helmholtz Munich conducted the

library preparation using the 10x Genomics Chromium Next GEM Single-cell Multiome ATAC + Gene Expression kit in these experiments. Sequencing and the bioinformatic pre-processing of the multiome data were performed by the Sequencing and Bioinformatics Core Facilities at Helmholtz Munich.

### 2.2.9 Bioinformatic analysis of single-cell gene expression data

The bioinformatic analysis was carried out with the help of Moritz Thomas from the Marr group at the Institute of AI for Health, Helmholtz Munich.

#### *2.2.9.1 Species assignment*

A dual strategy was employed for demultiplexing species from sequencing data. First, the max count assignment method was used, where each sequence read was assigned to a species based on the most frequently occurring barcode among the reads. In addition, the souporcell [199] tool was utilized with a 'k=3' parameter setting, which efficiently separated mixed-species sequencing data into three distinct groups. This combined approach ensured accurate sorting and identification of the sequencing data.

#### *2.2.9.2 Pre-processing and quality control*

Barcodes representing an excessive percentage of mitochondrial gene content, surpassing 30%, were excluded as they likely indicated cells dying or under stress. Cells identified as doublets by souporcell and scrublet [200] were removed from the dataset. Cells were selectively filtered for each species based on the overall distributions of UMI counts and gene expressions, following a detailed visual review of each sample. Genes detected in fewer than 20 cells were not included in subsequent analysis. The UMI counts for each cell were normalized using the SCRAN algorithm, as implemented in an R-based package [201], [202]. This process involved estimating size factors correlating with the counts of the captured cells, which were then utilized for normalization before log-transforming the data.

#### *2.2.9.3 Feature selection and visualization in a low-dimensional embedding*

Each species' top 4,000 highly variable genes were identified based on a normalized dispersion [203] and as implemented in Scanpy (pp.highly_variable_genes). Briefly, genes were ranked by mean expression, and those with the highest variance-to-mean ratio were

selected. Principal Component Analysis (PCA) for dimension reduction was then carried out on these highly variable genes, with 15 principal components computed using Scanpy's pp.pca. Subsequently, a neighborhood graph was calculated on the first 50 principal components using Scanpy's pp.neighbors with a parameter of 15 neighbors. Finally, this neighborhood graph was embedded using UMAP [204], running Scanpy's tl.umap with default parameters, and focusing on lineage driver genes identified from Waddington OT.

#### *2.2.9.4 Differential gene expression and enrichment analysis*

Differential gene expression analysis and enrichment are critical to identifying and understanding the functional differences between various cell populations. DESeq2 was applied to compare gene expression levels between previously defined clusters, aiming to identify significantly upregulated or downregulated genes in one cluster compared to others. After identifying differentially expressed genes, enrichment analysis was conducted to understand their biological significance. Differentially expressed genes (DEG) were analyzed using Gene Ontology (GO), indicating potential biological processes or active pathways in one cell population over another.

#### *2.2.9.5 Clustering*

The Leiden algorithm was utilized for unsupervised clustering, maintaining a consistent resolution of 0.2 for all species. Subsequently, the tl.rank_genes_groups method was applied within the Leiden clusters, employing the Wilcoxon test to identify DEGs. The resulting DEG lists were generated and exported for each species. To refine the analysis, an intersection of these gene lists was performed, retaining only those common genes across all three species and displaying a p-value < 0.01. These genes were used as marker genes to define clusters within the dataset. Further subdivision of these clusters was carried out, and smaller subclusters were analyzed for overlap with the marker genes. Ultimately, each subcluster was assigned to the larger cluster with the most significant overlap, resulting in a comprehensive and integrated approach to cluster analysis in this study.

#### *2.2.9.6 Cell cycle inference*

For cell cycle assessment, datasets from Macosko [205] and Tirosh [206] were utilized. Scanpy allows for the scoring of cell cycle phases by assigning scores to genes associated with specific cell cycle stages. This scoring system is based on the expression levels of a

predefined set of marker genes for each phase. The cells in the dataset were then classified into different cell cycle stages based on their respective scores.

#### *2.2.9.7 Combining UMAP projections of different species*

Using annotated reference datasets to annotate new scRNA-seq data can simplify further analysis and interpretation despite challenges like technical variations and biological noise. The accuracy of annotation transfer hinges on the reference data quality, the chosen model, and their compatibility with the new dataset [207]. Scanpy's ingest method offers a straightforward solution for merging query data annotations with those from a reference dataset. It achieves this by projecting query data onto pre-defined UMAP spaces based on the reference, here mouse, then applying a k-NN classifier to map cell labels onto the embedding, here cynomolgus and human datasets. This resulted in the 'mouse mapped time' for humans and cynomolgus.

#### *2.2.9.8 Linear regression modeling*

To examine the relationship between the mapped time resulting from ingest mapping and corresponding sampling time points across the human and cynomolgus datasets, linear regression was employed. Mean values measured over the mapped time were utilized for each dataset, facilitating a comparative analysis. The regression models were constrained to intersect the origin, indicative of a presumed proportional relationship between time and the measured means, effectively negating any inherent offset. The fit of each model was assessed using the R-squared statistic, which quantified the variance in the measured means that could be explained by the model based on time. In addition, relative differentiation speeds were calculated using the slope of the linear fits compared to the mouse. This approach facilitated a coherent quantitative and visual comparison of the linear relationships between mouse and human and mouse and cynomolgus within a unified analytical framework.

#### *2.2.9.9 Intra-species analysis of fast versus slow differentiating cells*

To explore the underpinnings of developmental speed differences within and between species, a methodological approach focused on the analysis of cells sharing closely matched gene expression profiles at specific developmental milestones. The goal was to unravel the complexities of developmental progression. This analytical strategy was structured around a three-phase process: The first phase involved a cross-species comparative analysis to

pinpoint common developmental divergences. Following this, attention was directed towards genes implicated in these divergent processes, specifically those exhibiting species-specific expression patterns. This aimed at identifying essential genes driving the variability in developmental pacing. The final phase honed in on single-cell trajectory analyses, particularly during the transition from a pluripotent state, to meticulously determine the critical points at which cells shifted to a 'pluripotency low' status. This detailed temporal examination allowed for the classification of cells into either rapid or slow differentiation categories based on their transition timings. For instance, within the 'pluripotency low' cluster, cells crossing the predefined threshold beyond 8 hours were deemed fast differentiating, whereas those crossing after 24 hours were considered slow differentiating. This classification identified a gradient of differentiation speeds within each species, shedding light on the variability of developmental speed.

### 2.2.10 Bioinformatic analysis of single-cell chromatin accessibility data

#### *2.2.10.1 Pre-processing and quality control*

Peaks were called using Macs2, followed by removing peaks located on nonstandard chromosomes and in genomic blocklist regions defined by the ENCODE consortium [208]. To ensure the inclusion of high-quality cells in our dataset, barcodes were removed based on the total distributions of fragments and peaks and visual inspection of each sample. Additionally, barcodes were filtered out with low transcriptional start site (TSS) enrichment scores and a high ratio of mononucleosomal to nucleosome-free fragments. Data normalization was achieved using term frequency-inverse document frequency normalization, implemented through the RunTFIDF function in Signac.

#### *2.2.10.2 Feature selection and visualization in a low-dimensional embedding*

The top 25% variable features were employed for dimension reduction, and singular value decomposition was applied to the TD-IDF normalized matrix. To mitigate the strong correlation between the first LSI component and sequencing depth, this component was excluded before performing UMAP dimension reduction and computing k nearest neighbors. This process was carried out using the RunUMAP and FindNeighbors functions on 30 components.

*2.2.10.3 Peak co-accessibility analysis*

Co-accessibility analysis techniques deduce correlations among accessible genomic regions within single cells, hypothesizing that regions accessible in concurrent cells partake in analogous biological functions and could correlate with the gene expression of proximate genes [209]. This approach, as utilized in ArchR [210], calculates the correlation between the binary accessibility profiles of genomic region pairs, generating a matrix of co-accessibility scores for each peak pair.

# 3 Results

## 3.1 Mammalian PSC cultures were established for subsequent comparative analyses

### 3.1.1 Primed epiblast-like PSCs of diverse mammalian species are adapted to identical conditions

PSCs have emerged as a crucial experimental tool for elucidating species-specific differentiation speeds [20], [21], [83], [148]. Given their capacity to differentiate into any cell type, PSCs, derived either directly from embryos or generated via reprogramming in iPSCs, offer a versatile platform for comparative developmental studies across a broad spectrum of mammalian species [51], [53], [55], [211]. Epiblast-like primed PSCs were chosen as the starting point for comparative analysis due to their availability across different species, including human ESCs, mouse EpiSCs, and iPSCs from non-human primates [64], [82]. This strategic decision guarantees that subsequent analyses are conducted at equivalent developmental stages, allowing for more accurate and meaningful comparisons of differentiation processes across species. This approach addresses inconsistencies in previous studies that used cells maintained under varying conditions. Human ESCs, mouse EpiSCs, cynomolgus iPSCs, and orangutan iPSCs were used for the following harmonization experiments.

The primary goal was to standardize the culture conditions for the various cell lines, establishing a common baseline for comparative analyses. Each cell line was initially obtained with different culturing protocols as specified in **Table 10** and described in detail in the Methods section **2.2.1.1**. Briefly, human ESCs were cultured in feeder-free conditions on Matrigel using StemMACS iPS Brew XF, with routine passaging involving StemMACS Passaging Solution XF. Orangutan and cynomolgus iPSCs were maintained in feeder-free conditions on Geltrex Matrix, utilizing StemFit media. Cells were passaged using 0.5 mM EDTA. Mouse EpiSCs were cultured in EpiSC media, grown in feeder-free conditions on Gelatin with 10% FBS, and passaged using collagenase IV.

The subsequent step involved assessing the efficacy of various media formulations in preserving the pluripotent state across different species. I universally tested media already employed in the different cell lines across all other species. Additionally, I examined the effectiveness of chemically defined medium (CDM) [61] and universal primate pluripotent stem cell (UPPS) medium [198], successfully applied across multiple primed PSC lines and species in previous comparative studies. The exact composition for each medium tested is listed in the Methods section **2.2.1.2** in **Table 11.** The first steps involved the establishment of common coating and passaging procedures to establish consistent culture conditions across all cell lines. Matrigel was adopted as the shared substrate for all cell lines, and the utilization of EDTA for splitting was effective. I evaluated these modifications by assessing regular colony morphology (**Figure 10A**). To ensure a seamless transition to new media, cells were split and gradually adapted over a four-day course, with an incremental increase in the proportion of new media (**Figure 10B**). On the fifth day, cells were passaged again and maintained in the new media for at least three total passages before further evaluation. Initial assessments based on colony morphology indicated positive outcomes for primate cell lines when cross-testing StemFit and iPS Brew medium (**Figure 10C**). However, cultivation in EpiSC media or CDM led to either cell death or differentiation in primate cells. Mouse cells posed more significant challenges, experiencing cell death or differentiation over time in StemFit, iPS Brew, and CDM.

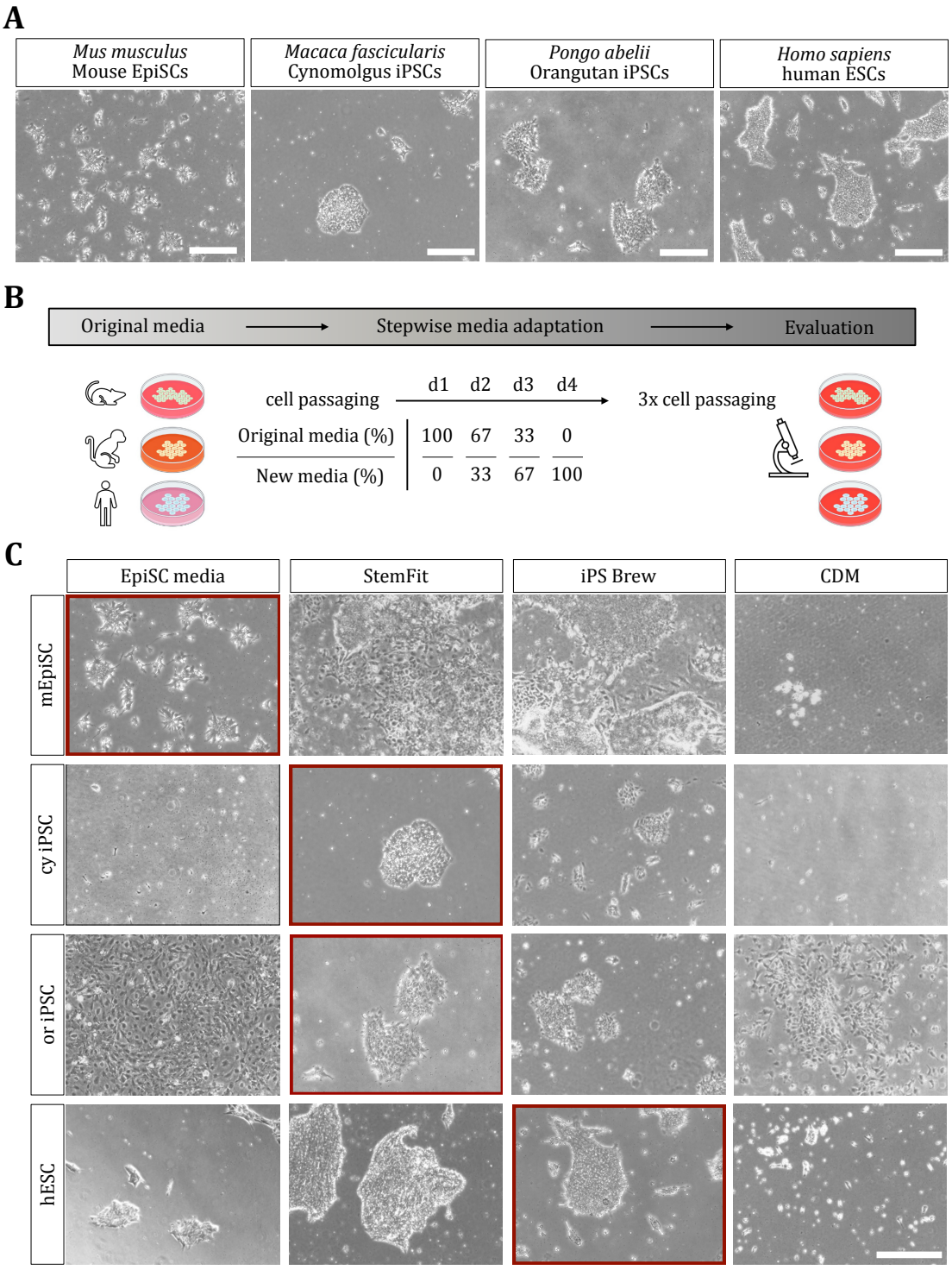


**Figure 10. Harmonization of primed PSCs. (A)** Brightfield images of mouse EpiSC, cynomolgus iPSC, orangutan iPSC, and human ESC (left to right) with adapted coating and passaging but still in the original culture media. Magnification: 5x, scale bar: 500 µm. **(B)** Schematic illustration of the stepwise media adaptation process. **(C)** Brightfield images of mouse EpiSC, cynomolgus (cy) iPSCs, orangutan (or) iPSCs and human ESCs (top to bottom) after three passages in either EpiSC media, StemFit, iPS Brew or CDM (left to right). Red boxes indicate original conditions. Magnification: 5x, scale bar: 500 µm.

Successful maintenance across cell lines was achieved exclusively with UPPS medium. All cell lines exhibit regular colony morphology (**Figure 11A**). Analysis through flow cytometry showed the presence of pluripotency-related transcription factors SOX2, NANOG, and OCT4, along with species-specific stem cell surface markers like TRA-1-60 for primates and SSEA-1 for mice (**Figure 11B**). Immunofluorescence staining further validated the consistent expression of NANOG and SOX2 across the different species (**Figure 11C**).

To summarize, I successfully standardized culture conditions across various species with the harmonization experiments by adapting them to a universally effective medium. This uniformity, confirmed by consistent colony morphology and pluripotency marker expression, facilitates direct comparisons of developmental timelines and sets the stage for further investigations into developmental processes across species.

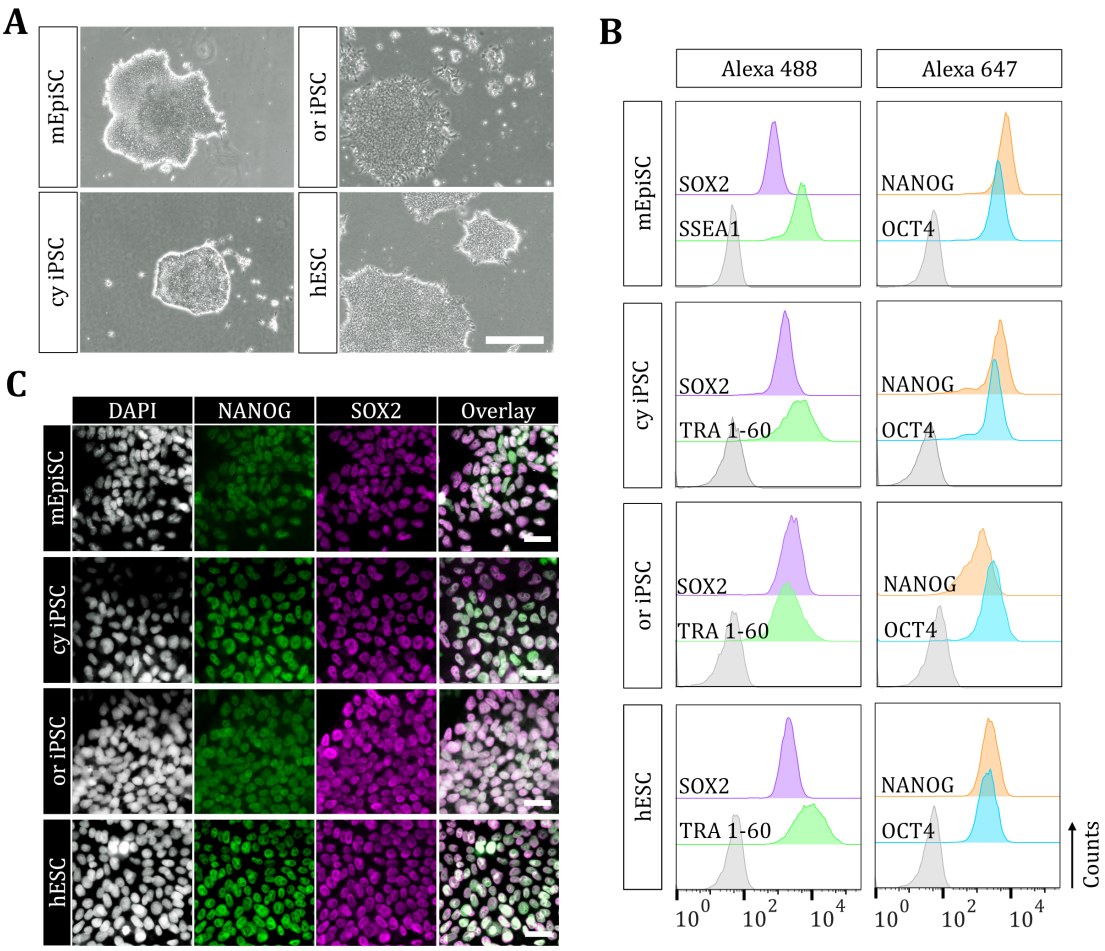


**Figure 11. Successfully adapted cells in UPPS medium.** **(A)** Brightfield images of harmonized mouse EpiSCs (top left), cynomolgus iPSCs (bottom left), orangutan iPSCs (top right), and human ESCs (bottom right) in UPPS medium after three passages. Magnification: 5x, scale bar: 500 µm. **(B)** Histograms of FACS analysis of mouse EpiSCs, cynomolgus iPSCs, orangutan iPSCs and hESC (from top to bottom) for SOX2 and SSEA1 (mouse) or TRA 1-60 (primates) labeled with Alexa-488 (left) and NANOG and OCT4 labeled with Alexa-647 (right). Gray distributions represent unstained control. **(C)** Immunofluorescence imaging of DAPI, NANOG labeled with Alexa-488 and SOX2 labeled with Alexa-647 and the resulting overlay (from left to right) in mouse EpiSCs, cynomolgus iPSCs, orangutan iPSCs and hESC (from top to bottom). Magnification = 40x, scale bar = 25 µm.

### 3.1.2 Generation of elephant shrew iPSCs

Afrotheria, a mammalian superorder originating from Africa, are characterized by their notably slow development relative to other mammals of comparable size [212], [213]. This order provides a unique opportunity to deepen the understanding of developmental biology from tiny golden moles to massive elephants. For this study, a biopsy from a 4.5-year-old male elephant shrew (*Macroscelides proboscideus*), also known as sengi, was procured from the Salzburg Zoo, and provides a valuable resource for generating iPSCs, offering a window into the developmental intricacies of Afrotheria.

The following generation of clonal sengi iPSCs was conducted in the Drukker lab together with Polyxeni Nteli, utilizing a non-integrating, plasmid-based technique [92]. This process involved the use of the 4-in-1 CoMiP vector, incorporating codon-optimized Yamanaka factors and an shRNA targeting p53, in conjunction with the pCXLE-hMLN plasmid, which encodes for human C-MYC, LIN28, and NANOG, thereby assembling a comprehensive genetic toolkit for reprogramming. The strategy employed for generating sengi iPSCs is depicted in **Figure 12A** and described in detail in **2.2.2**. Initially, nucleofection was used to introduce the plasmids into fibroblasts, which were then maintained in fibroblast media for three days, with regular visual monitoring for iPSC growth (**Figure 12B**). On the third day following nucleofection, the medium was replaced with either a LIF-containing naïve medium or an Essential 7 medium for primed conditions. Around day 10, the first iPSC-like colonies emerged, and the switch in medium was prompted to either mTeSR for primed conditions or 2i + LIF for further naïve cultivation. By day 21 post-nucleofection, colonies had predominantly formed under primed conditions, with minimal growth noted under naïve conditions. The culture in mTeSR was then expanded under feeder-free conditions on Matrigel, with individual colonies selected for clonal expansion after 30 days of induction and were eventually transferred to EpiSC media. To verify the successful generation of iPSCs, I stained the cells positively for the crucial pluripotency-related transcription factors OCT4 and SOX2 (**Figure 12C**). Interestingly, sengi iPSCs demonstrated expression of the mouse-specific embryonic surface marker SSEA-1 and the primate-specific TRA-1-60, indicating a complex and unique pluripotency expression pattern (**Figure 12D**).

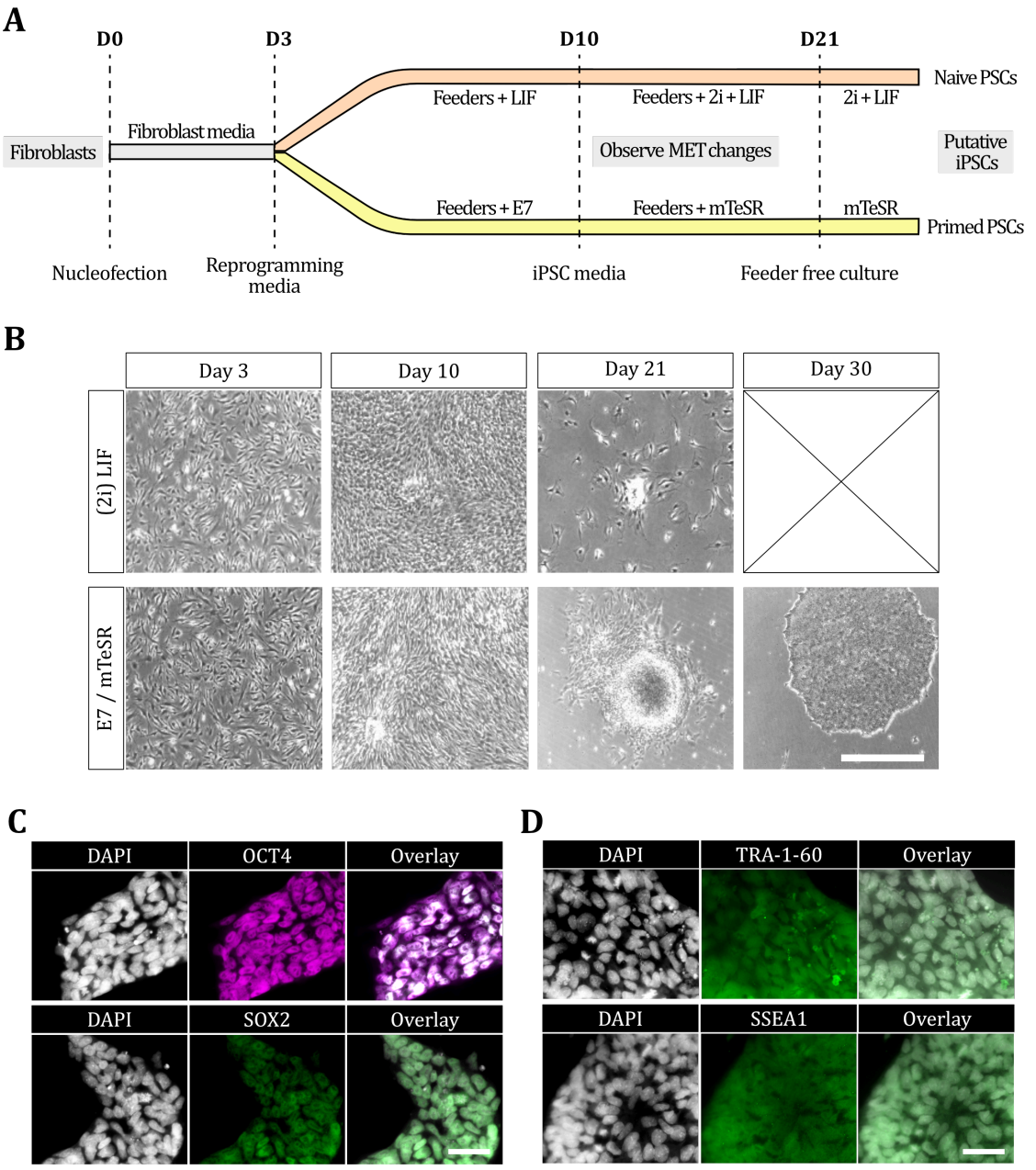


**Figure 12. Generation and evaluation of elephant shrew iPSCs. (A)** Schematic illustration of the strategy used to produce either naïve or primed sengi iPSCs. **(B)** Brightfield images of the induction progression at day 3, day 10, day 21, and day 30 post-nucleofection (left to right) of the sengi fibroblasts in either naïve conditions using LIF until day 10 and 2i + LIF afterward (top) or primed conditions using Essential 7 (E7) until day 10, mTeSR until day 30 and EpiSC medium afterward (bottom). Magnification: 5x, scale bar: 500 µm. **(C-D)** Immunofluorescence imaging of (C) DAPI and OCT4 (top) labeled with Alexa-488 and DAPI and SOX2 (bottom) labeled with Alexa-647 and the resulting overlay (left to right) and of (D) DAPI and TAR-1-60 (top) labeled with Alexa-488 and DAPI and SSEA1 (bottom) labeled with Alexa-488 and the resulting overlay (left to right) in sengi iPSC clone 1. Magnification = 40x, scale bar = 25 µm.

## 3.2 Exploring developmental dynamics via single-cell multiome sequencing in PSCs

With a diverse and harmonized multi-species panel in place, the initial phase involved a pilot study to assess variations in pluripotent states across different species. This step was critical in setting the stage for a broader investigation into the regulatory mechanisms that control developmental timing at both cellular and molecular levels. Utilizing the multiome assay from 10x Genomics, single-cell gene expression and chromatin accessibility data were simultaneously captured, offering insights into molecular differences across species. In the experiment, I pooled PSCs from human, mouse, cynomolgus, and sengi into one sample to employ computational techniques to demultiplex species-specific data afterward. This approach minimized batch effects and optimized the efficiency of sample preparation, paving the way for detailed comparative analyses.

### 3.2.1 Optimization of combined nuclei isolation for minimizing sequencing batch effects

To obtain high-quality sequencing data, the goal was to minimize sequencing batch effects through combined nuclei isolation, with all species mixed at an initial stage for subsequent combined library preparation and computationally demultiplexing the species post-sequencing by aligning them to each species' genome. For PSCs, the original protocol provided by 10x Genomics required optimization. Initially, I assessed the efficiency of nuclei isolation for each species individually, focusing on optimizing lysis time and the detergent amount, as insufficient detergent and lysis time left cells intact while excessive amounts led to nuclear membrane disruption or nuclei clumping.

I established the final protocol with a lysis time of three minutes and a 50% reduction in detergent concentration from the original protocol, illustrated in **Figure 13A**. Verification through Trypan blue staining revealed success for individual species and the combined sample, with bright spots indicating live cells and a blue color marking dead cells in the input sample or isolated nuclei in the processed sample (**Figure 13B**). The isolation quote consistently exceeded 98%, and nuclei remained intact and free from clumping, therefore suited for subsequent single-cell sequencing experiments. While the sequencing was performed on single isolated nuclei, the term ‘single-cell sequencing’ will be employed in the following sections.

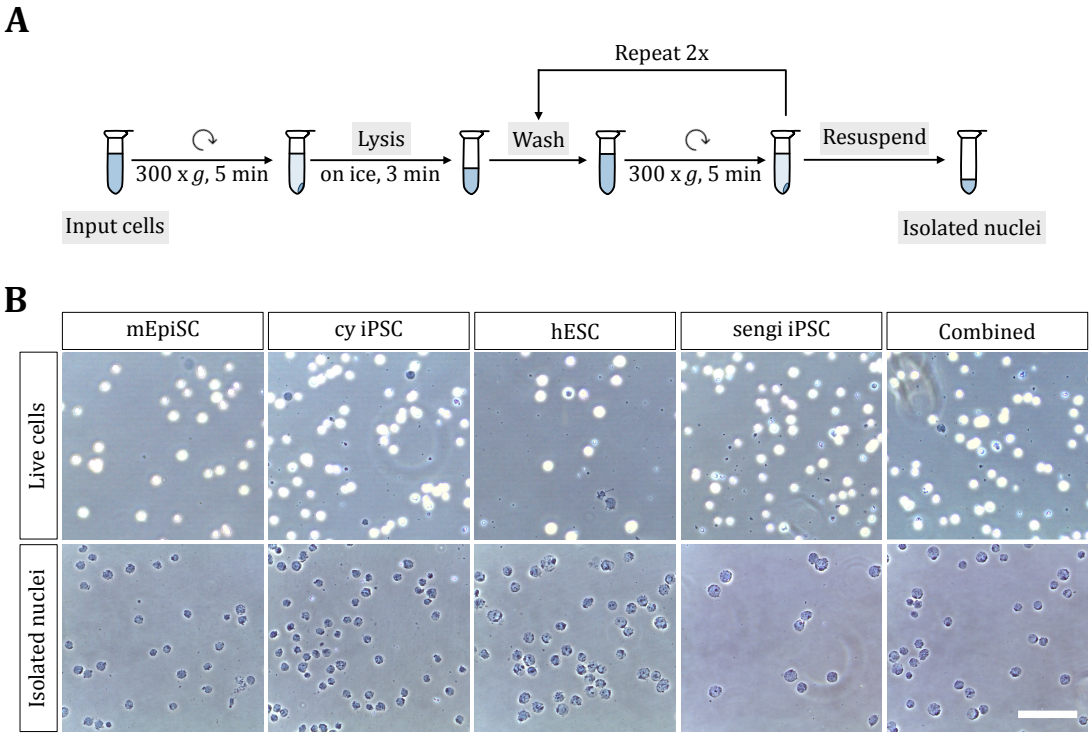


**Figure 13. Optimization of nuclei isolation for single-cell multiome sequencing. (A)** Schematic illustration of the finalized nuclei isolation protocol. **(B)** Brightfield images of mouse EpiSCs, cynomolgus iPSCs, human ESCs, sengi iPSCs, and all species combined (left to right). The top row shows live cells before isolation in Trypan blue, and the bottom row shows isolated nuclei in Trypan blue. Magnification: 20x, scale bar: 100 µm.

### 3.2.2 Correct assignment and high-quality data for well-established model species

All species were mixed pre-nuclei isolation in equal parts to reduce batch effects and treated as one sample for gene expression and ATAC library preparations and subsequent sequencing (**Figure 14A**). This approach required precise alignment of each sequence to reference genomes post-sequencing, which was critical for determining species-specific cellular belonging. I adopted a strategy whereby the alignment efficacy of each cell to its respective reference genome was evaluated based on the prevalence of high genomic counts via maximum count assignment (**Figure 14B**). This measure served as an indicator of each cell's most accurate genomic association. The sole analysis via genome alignment using maximum count assignment revealed a differential alignment success across the species

examined. Specifically, cells from cynomolgus and mouse exhibited expected alignment profiles, indicating a high degree of concordance with their reference genomes, with 2682 cells assigned to the mouse and 3833 cells assigned to cynomolgus (**Table 13**).

In contrast, the sengi presented a considerable challenge, with only 318 cells demonstrating genomic alignment based on counts. Notably, 4604 cells were assigned to the human genome. Further analysis of count distributions highlighted the limitations using the elephant shrew. Unlike mouse and cynomolgus, human samples exhibited many cells with low counts (**Figure 14C**). Subsequently, cells with low total counts were filtered out (**Figure 14D**). The analysis yielded 2477 mouse cells identified in the gene expression dataset and 2175 in the ATAC dataset, with 2148 cells common to both. In the case of cynomolgus, the gene expression data contributed to identifying 3478 cells, while the ATAC data accounted for 3257 cells, and a total of 3083 cells were found in both datasets. For the human samples, 2487 cells were detected in the gene expression dataset, 2318 cells in the ATAC dataset, and 2178 cells were identified in both datasets (**Table 13**). Using the refined threshold, none were confidently assigned to the sengi, so I excluded the sengi from further evaluation.

**Table 13.** Number of cells assigned to each species via maximum count assignment and souporcell genotype assignment.

| | **Mouse** | **Cynomolgus** | **Human** | **Sengi** |
|---|---|---|---|---|
| | **Maximum count assignment** | | | |
| **Unprocessed** | 2682 | 3833 | 4604 | 318 |
| **Combined** | 2148 | 3083 | 2178 | - |
| **GEX** | 2477 | 3478 | 2487 | - |
| **ATAC** | 2175 | 3257 | 2318 | - |
| | **Souporcell genotype assignment** | | | |
| **Combined** | 1977 | 2845 | 1894 | - |
| **GEX** | 2264 | 3214 | 2160 | - |
| **ATAC** | 1993 | 2988 | 1947 | - |

To further refine the assignment of cells to their respective species, the souporcell genotype assignment method was additionally applied to mouse, cynomolgus, and human, following the approach outlined by Heaton et al. [199] This method enabled inferring distinct genotypes from single-cell RNA data without needing a reference genome, allowing for the clustering of cells according to these genotypes. As a result, 2264 cells from the gene expression data were assigned to mouse, with 1993 for ATAC sequencing and 1977 present in both datasets. Gene expression data yielded 3214 cells for the cynomolgus, ATAC sequencing identified 2988 cells, and 2845 cells were found in both datasets. In humans, gene expression data identified 2160 cells, ATAC sequencing found 1947 cells, and 1894 cells were present in both datasets. With this combined approach, leveraging genome alignment via maximum count assignment and genotype-based alignment using souporcell assignment, I confidently demultiplexed data from well-established model species. Demultiplexed datasets then underwent quality control in single-cell data processing. Cells of high quality were selected based on criteria including mitochondrial reads [214], the removal of doublets [200], and the distribution of total UMIs and genes. To adjust for technical variations, the UMI count data underwent normalization [201].

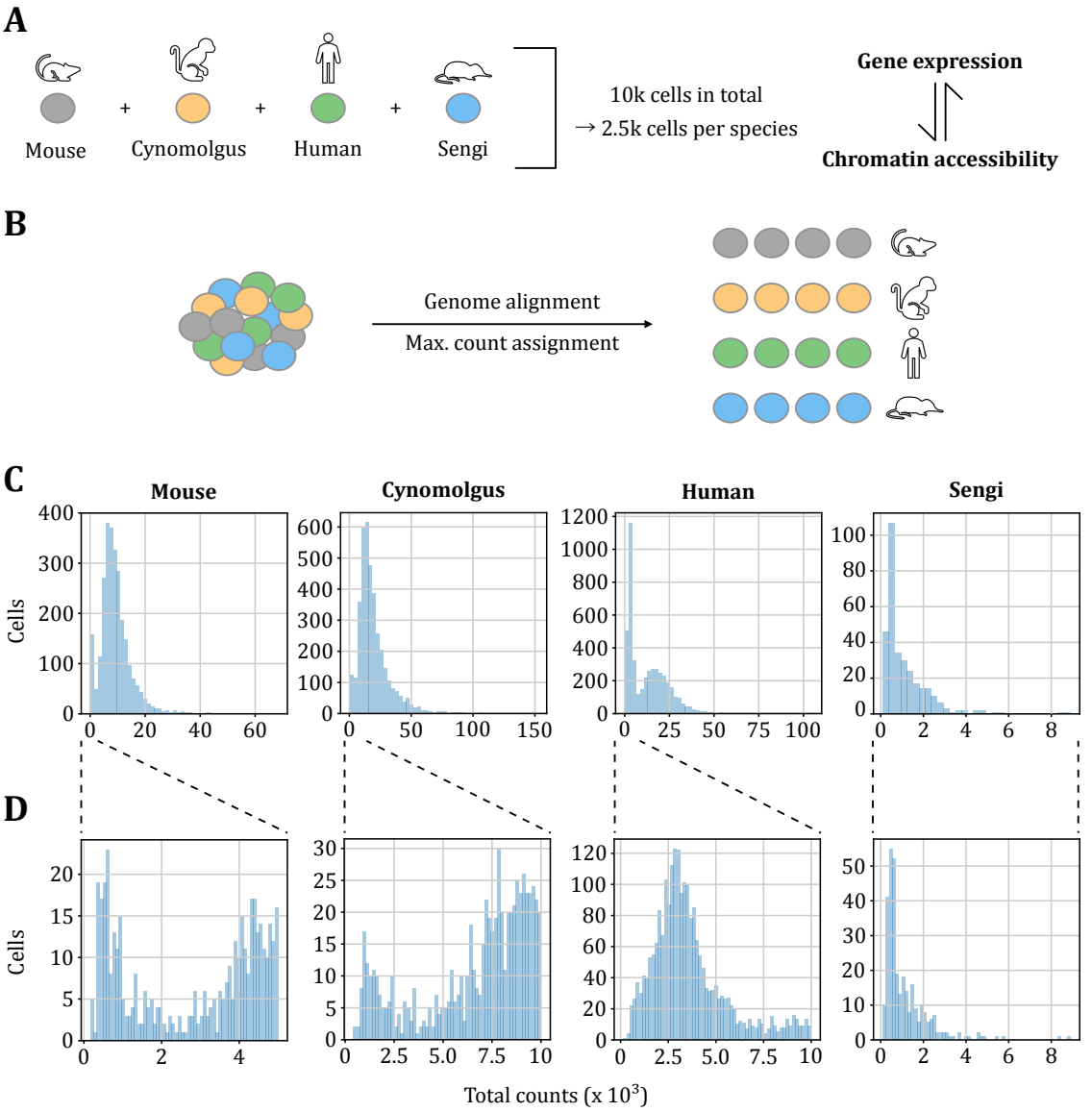


**Figure 14. Pre-processing of single-cell multiome data from multiplexed PSCs. (A)** Schematic illustration of the experimental setup for single-cell multiome sequencing of PSCs. **(B)** Schematic illustration of the bioinformatic demultiplexing approach. **(C)** Histogram showing the total sequencing counts and the number of cells assigned to either mouse, cynomolgus, human, or sengi (left to right). **(D)** Histogram showing cells with low total sequencing counts and the number of cells assigned to either mouse, cynomolgus, human, or sengi (left to right) below the applied thresholds.

### 3.2.3 Highest variance within PSCs of one species is explained by the cell cycle

In the following section, I will focus on the analysis of the scRNA-seq data, as Moritz Thomas exclusively handled the analysis of the pilot scATAC-seq data and is therefore not included in this thesis. Following the pre-processing and quality control, the PSC sequencing data underwent analysis for characteristic gene expression to confirm successful harmonization and establishment of a common baseline for all three species. Utilizing UMAP for visualization [204], pluripotency-related transcription factors OCT4 and SOX2, along with the pluripotency-related RNA-binding protein LIN28a, were found to be highly and uniformly expressed across all three species (**Figure 15A-C**, left column). In contrast, in mouse and human samples, lineage markers such as the mesoderm marker TBXT, the endoderm marker GATA4, and the ectodermal marker PAX6 were absent. However, a small subset of cynomolgus cells showed expression of TBXT, suggesting some degree of differentiation within the culture (**Figure 15A-C**, right column). This analysis highlights the ability of scRNA-seq to capture the transcriptional states across different species and provide a starting point for conducting time-sensitive experiments to explore species-specific developmental speeds.

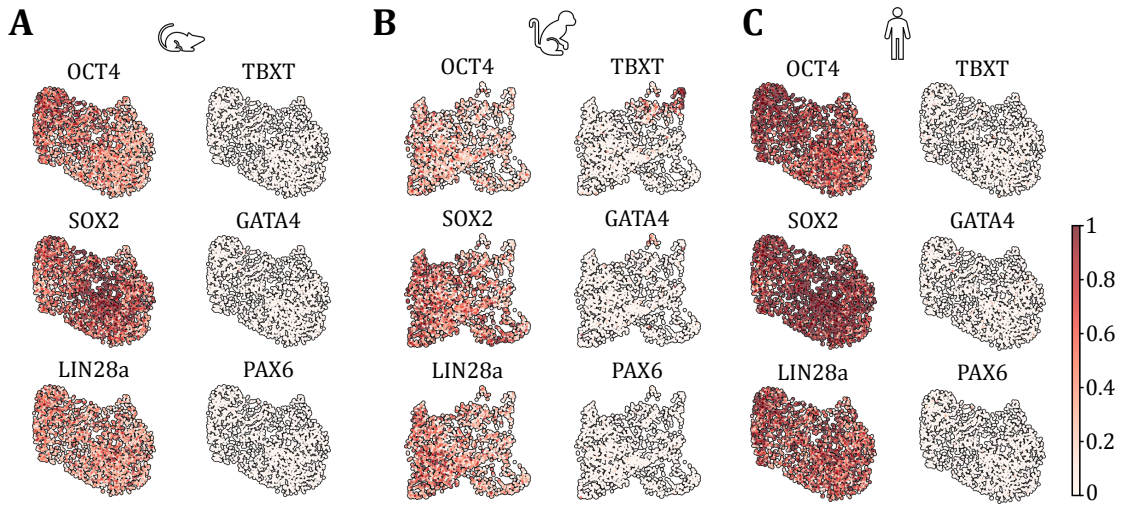


**Figure 15. Expression of pluripotency and lineage markers in scRNA-seq data. (A)** UMAPs showing relative expression of OCT4, TBXT, SOX2, GATA4, LIN28a, and PAX6 (from top left to bottom right) in mouse EpiSCs. **(B)** UMAPs showing relative expression of OCT4, TBXT, SOX2, GATA4, LIN28a, and PAX6 (from top left to bottom right) in cynomolgus iPSCs. **(C)** UMAPs showing relative expression of OCT4, TBXT, SOX2, GATA4, LIN28a, and PAX6 (from top left to bottom right) in human ESCs.

Given the sampling of steady-state pluripotent stem cells, it was anticipated that most underlying dynamics would derive from the cell cycle. The role of the cell cycle was investigated in the scRNA-seq data by compiling cell cycle phase-specific genes from two previously published studies [205], [206]. The average expression of each set of phase-specific genes was calculated for each cell, subtracted by the average expression of a random reference set of genes, leading to the assignment of each cell to either the G1, S, or G2/M phase. The cell cycle explained most of the variation in the data and significantly influenced the 2-dimensional UMAP embedding across all three species (**Figure 16A**). This variation became even more pronounced when PCA was used as the embedding method, with cells clustering according to their cell cycle phase in all three species (**Figure 16B**). An analysis of the relative distribution of the cell cycle phases revealed that all three species exhibited the smallest fraction of cells in G1, with mice at 13.1%, cynomolgus at 13.0%, and humans at 21.5%. Most mouse and cynomolgus cells were in the G2 or M phase, with mice at 49.7% and cynomolgus at 54.1%. For human, 37.7% of cells were in the G2/M phase. Most human cells were in the S-phase at 40.8%, while 37.2% of mouse and 32.9% of cynomolgus cells were in the S-phase (**Figure 16C**). Although very similar overall, slight differences were observed between species.

The scRNA-seq analysis pilot experiment showed consistent high expression of pluripotency markers across species, with only minimal signs of differentiation. I confirmed that transcriptional variability largely stemmed from cell cycle differences between species. Bioinformatics techniques effectively minimized batch effects and accurately assigned species-specific transcriptomic profiles.

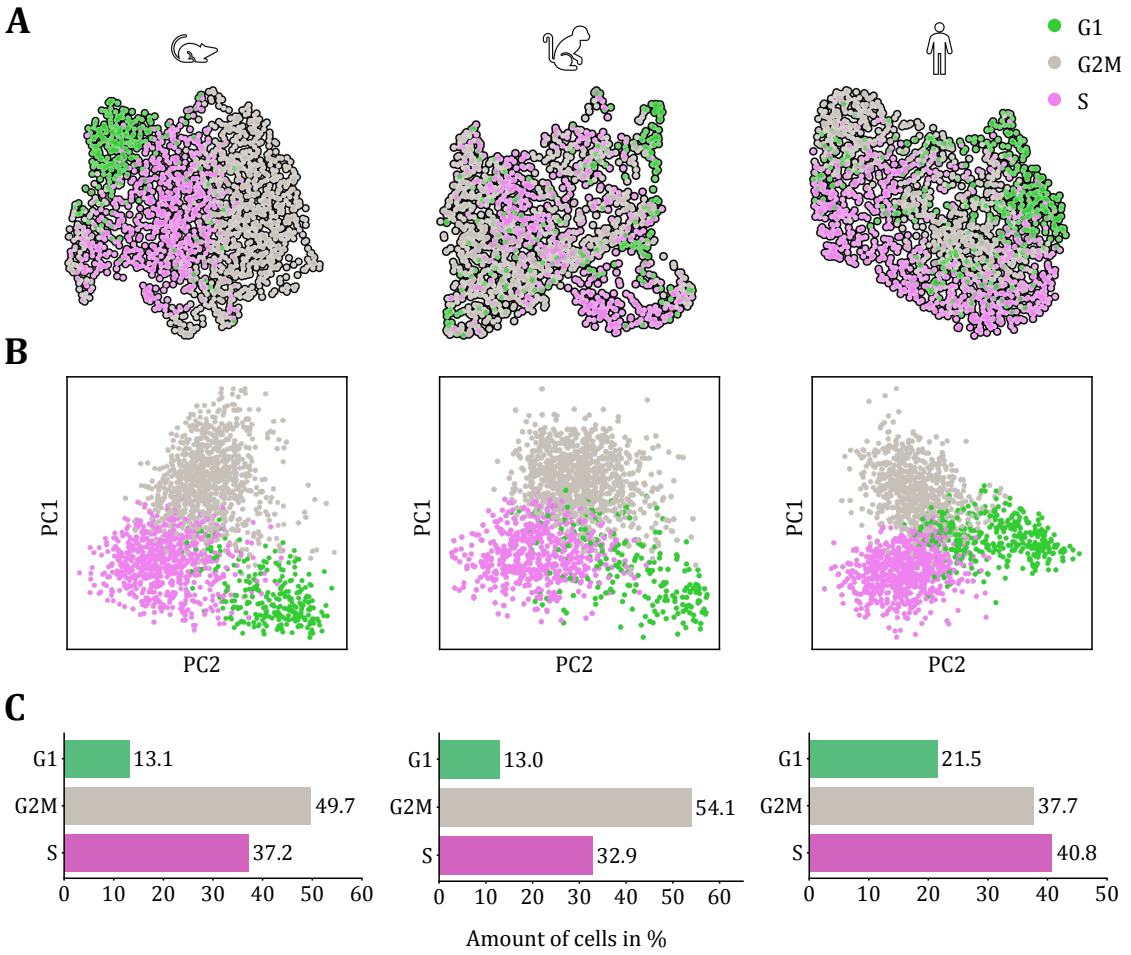


**Figure 16. Cell cycle analysis of single-cell gene expression data in PSCs. (A)** UMAPs showing cell cycle phase distribution of G1, G2/M, and S-phase in mouse EpiSCs, cynomolgus iPSCs, and human ESCs (left to right). **(B)** PCA plots showing cell cycle phase distribution of G1, G2/M, and S-phase in PC1 versus PC2 in mouse EpiSCs, cynomolgus iPSCs, and human ESCs (left to right). **(C)** Bar plots displaying the percental distribution of cell cycle phases in mouse EpiSCs, cynomolgus iPSCs, and human ESCs (left to right).

## 3.3 Directed differentiation of PSCs into NPCs

To explore the developmental speed of various species, I focused on the differentiation of PSCs towards NPCs through the dual inhibition of the SMAD pathway, as described by Chambers et al. [107]. This differentiation progresses through well-defined stages over seven to ten days, varying according to the species. In combination with single-cell sequencing techniques, this approach allows to dissect the underlying regulatory mechanisms that regulate the transition from pluripotency to neural lineage commitment,

highlighting differences in the developmental pace among mouse, cynomolgus, and human cells.

### 3.3.1 Different protocols lead to successful NPC differentiation across species

I evaluated three distinct protocols provided by different groups: the '8GMK' protocol from Prof. Dr. Wolfgang Enard's lab (LMU Munich), the '3N' protocol provided by Prof. Dr. Magdalena Götz's lab (Helmholtz Munich), and the 'NMM' protocol provided by Dr. Christian Schröter's group (MPI of Molecular Physiology). The exact protocols are listed in **Table 12** of the Method section **2.2.5**.

All protocols were tested on mouse EpiSCs, cynomolgus iPSCs, and human ESCs, and I initially assessed the success of neural differentiation via RT-qPCR. By day ten of differentiation, I observed the formation of a neuroepithelial sheet in all species and under all protocols, as evidenced by brightfield microscopy (**Figure 17A**). I particularly noted neuron formation in mouse cells, especially within the context of the 8GMK protocol. Furthermore, the downregulation of pluripotency markers OCT4 and NANOG, alongside the relatively stable levels of SOX2, a marker for pluripotency as well as neural differentiation, were confirmed by RT-qPCR analysis in all three species and all three protocols (**Figure 17B-D**). Additionally, the upregulation of early neural markers SOX1 and PAX6 across all protocols indicated successful differentiation into NPCs.

The establishment of a protocol was met with certain limitations. The decision to employ a consistent protocol for subsequent single-cell multi-omic analysis and time-lapse live imaging performed in collaboration with the Schröter lab led to the exclusive testing of monolayer-based approaches. The '8GMK' protocol resulted in overly dense cell layers. Therefore, for greater precision in seeding density and to ensure the uniform formation of neuroepithelial sheets, the '3N' protocol was selected. This approach, which favored dissociated single cells over cell clumps for seeding, allowed for more manageable control over the initial seeding density, meeting the specific requirements for further analyses conducted.

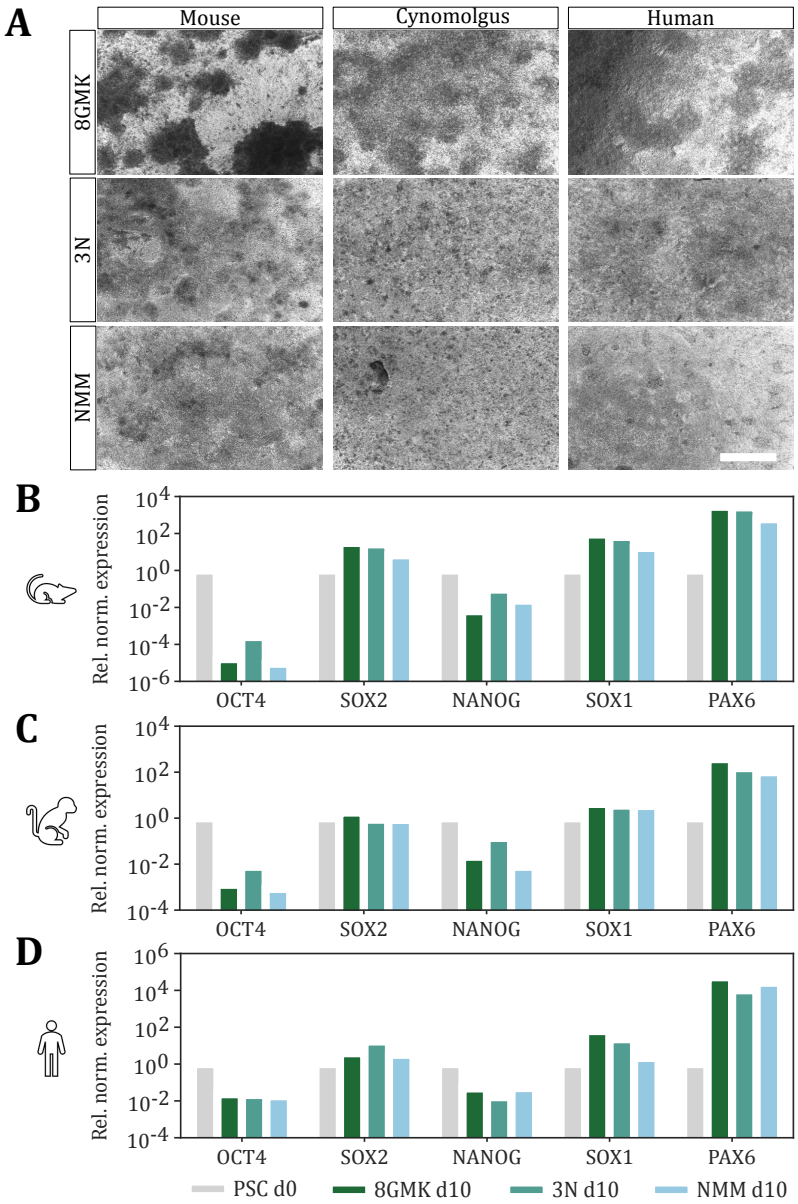


**Figure 17. Successful NPC differentiation is achieved with all three protocols. (A)** Brightfield images of mouse, cynomolgus, and human cell cultures (left to right) show the formation of a neuroepithelial sheet after ten days of differentiation using the '8GMK', '3N', and 'NMM' differentiation protocols (top to bottom). Magnification: 5x, scale bar: 500 µm. **(B-D)** RT-qPCR results for (B) mouse, (C) cynomolgus, and (D) human for NPC differentiation using the '8GMK', '3N', and 'NMM' differentiation protocols. Relative normalized expression was calculated using the $2^{-ddCt}$ method using the respective PSC for normalization. Logarithmic scale.

### 3.3.2 Time-course NPC differentiation for the determination of sampling time points for single-cell multiome sequencing

Daily RT-qPCR samples of neural progenitor differentiation were analyzed over ten days using the '3N' protocol to evaluate the differentiation timelines and critical time points for the three species.

In the initial days, a quick and significant gradual downregulation of pluripotency markers OCT4 and NANOG was observed in all three species, along with a significant gradual upregulation of neural progenitor markers SOX1 and PAX6, indicating a successful linear neural induction (**Figure 18A-C**). Although the general trajectory of differentiation appeared similar, differences in the temporal dynamics were noted early on. While in cynomolgus (**Figure 18B**) and human (**Figure 18C**) SOX1 expression levels gradually increased, in mouse, SOX1 was quickly upregulated upon differentiation induction, peaked around days 2 and 3 and then gradually declined again (**Figure 18A**). Similarly, PAX6 expression steadily increased in cynomolgus and human, but in mouse, the expression peaked at day 6 and then declined.

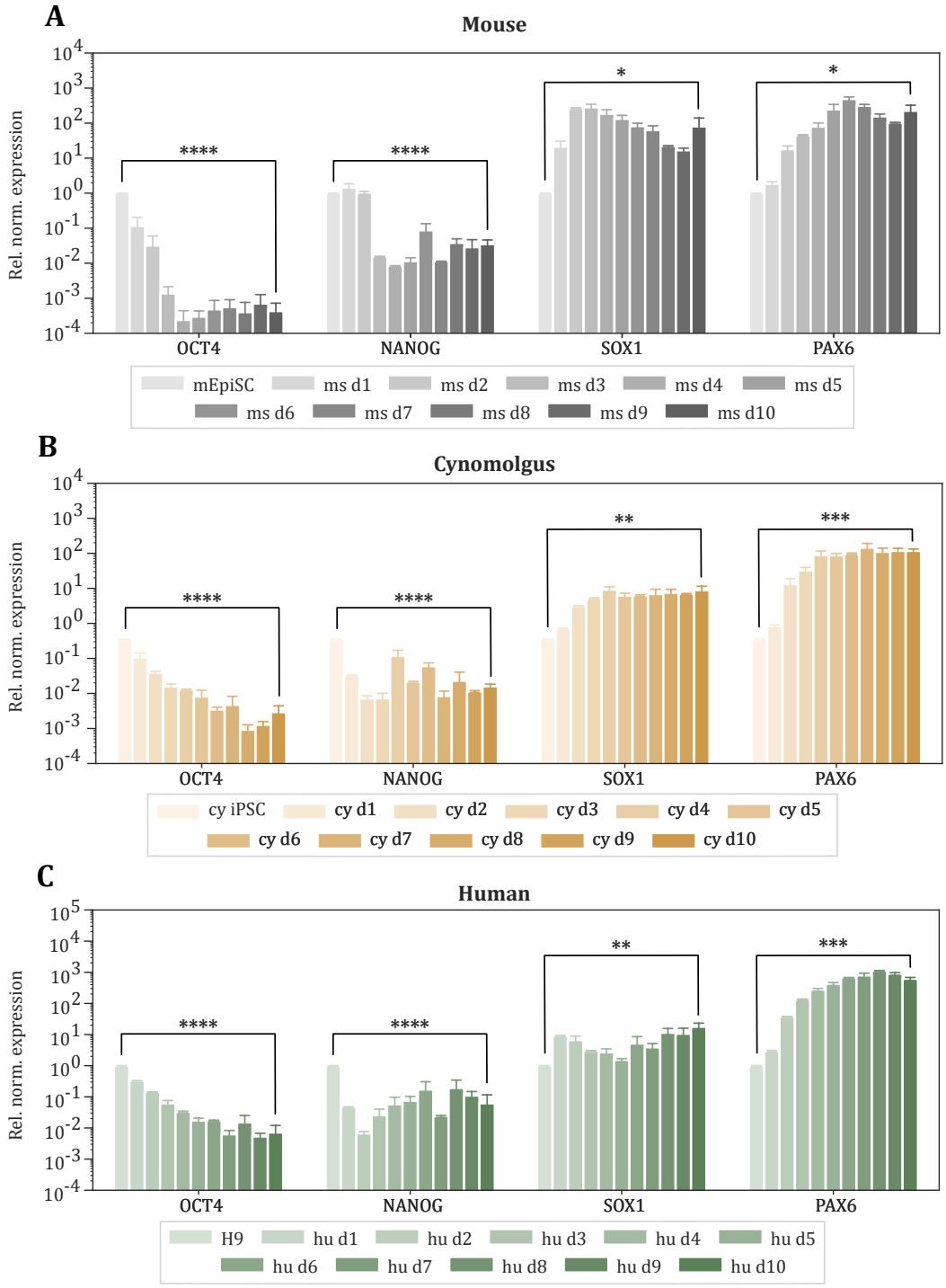


**Figure 18. Time-course RT-qPCR results show gradual neural differentiation. (A)** Mouse, **(B)** Cynomolgus and **(C)** Human RT-qPCR results for time-course NPC differentiation using the '3N' differentiation protocol at daily time points from day 1 to day 10 of differentiation. Relative normalized expression was calculated using the $2^{-ddCt}$ method using the respective PSC for normalization and is shown for OCT4, NANOG, SOX1, and PAX6. Logarithmic scale. Error bars represent standard deviation (n=3), and the p-value of day 0 vs. day 10 was determined using the student's t-test: * $p < 0.05$, ** $p < 0.01$, *** $p < 0.001$, **** $p < 0.0001$.

I further conducted immunofluorescence staining alongside the RT-qPCR analysis to corroborate the successful differentiation at the protein level. Samples were stained for DAPI, OCT4 and SOX1, and PAX6 and SOX2 at various stages of differentiation: day 0, day 2, day 4, and day 6. I observed the disappearance of the pluripotency marker OCT4 after 2 days of induction in mouse cells (**Figure 19A**) and by day 4 of differentiation in cynomolgus (**Figure 19B**) and human cells (**Figure 19C**). Neural progenitor markers SOX1 and PAX6 were detected as early as day 2 in mouse and cynomolgus cells and from day 4 in human cells, already highlighting species-specific variations in the differentiation rate. SOX2 was consistently expressed throughout the differentiation process, aligning with expectations for neural differentiation. To ensure that potential initial changes in RNA levels and chromatin state were thoroughly captured, I planned the sampling to be more frequent during the first days, with designated time points at 0 hours, 8 hours, 1 day, 2 days, 3 days, 4 days, 7 days, and 10 days.

In summary, I tested three NPC differentiation protocols on mouse EpiSCs, cynomolgus iPSCs, and human ESCs, showing successful differentiation into NPCs by day ten. The '3N' protocol demonstrated a consistent transition from pluripotency to neural lineage, as shown by time-course RT-qPCR and immunofluorescence, which recorded the expected changes in key markers. This validated the protocols and provided critical temporal data for future sequencing efforts.

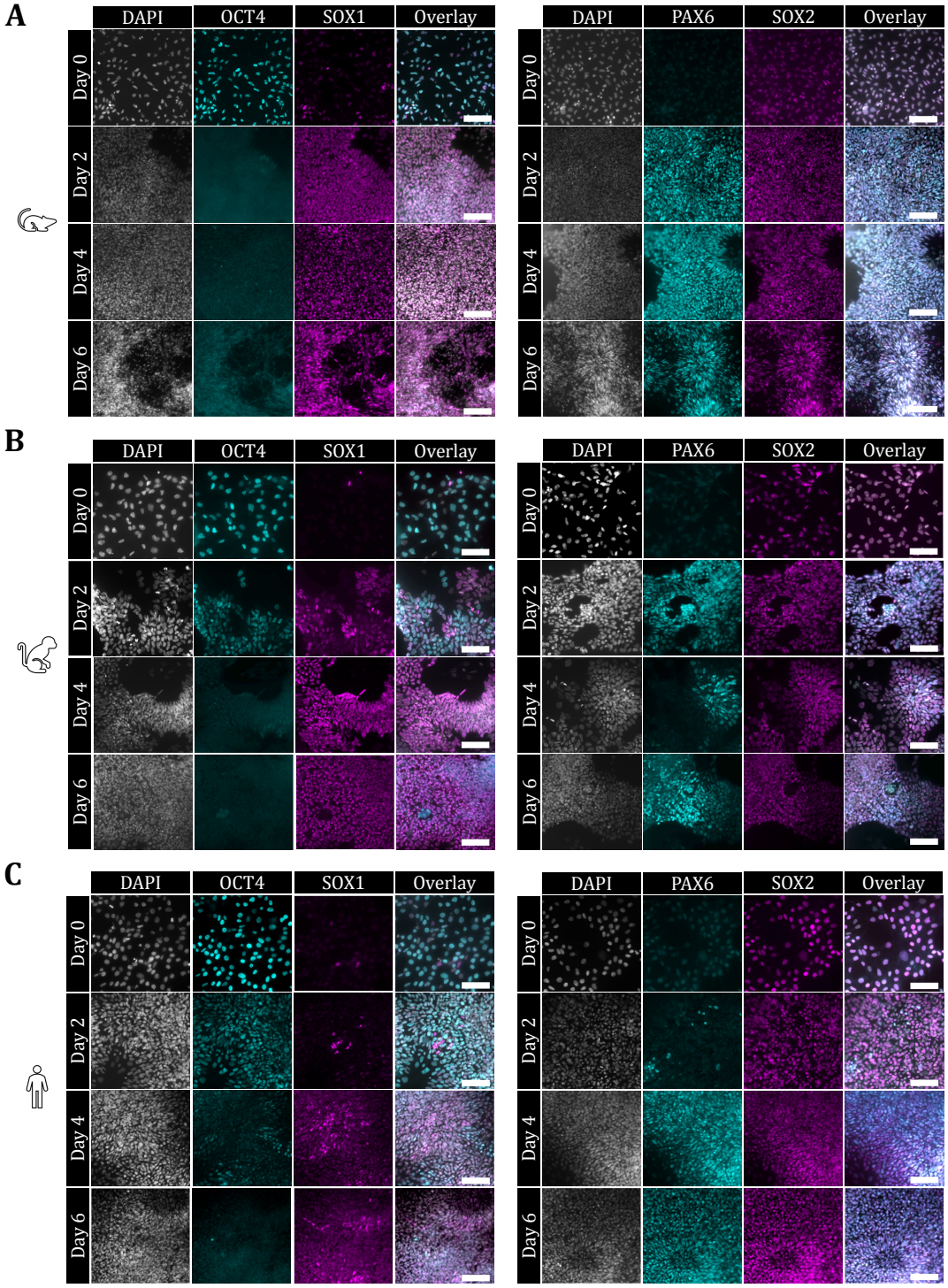


**Figure 19. Immunofluorescence imaging during time course NPC differentiation. (A-C)** Immunofluorescence images of (A) mouse, (B) cynomolgus, and (C) human. The left panel shows DAPI, OCT4 (Alexa-488), SOX1 (Alexa-647) (left to right), and the resulting overlay at day 0, day 2, day 4, and day 6 of NPC differentiation (top to bottom). The right panel shows DAPI, PAX6 (Alexa-488), SOX2 (Alexa-647) (left to right), and the resulting overlay at day 0, day 2, day 4, and day 6 of NPC differentiation (top to bottom). Magnification: 40x, scale bar: 70 µm.

## 3.4 Capturing NPC differentiation through time-course single-cell multiome sequencing

I utilized a combined approach of scRNA and ATAC-seq to investigate the differentiation characteristics unique to each species. Recent advancements in single-cell multi-omic sequencing technologies have improved the exploration of cellular dynamics and diversity [187]. By meticulously capturing the gene expression and chromatin accessibility profiles of individual cells across various developmental stages, this method permits an exhaustive examination of cellular heterogeneity. The preceding pilot experiment confidently identified transcriptional and genomic attributes from multiplexed pluripotent cultures of mouse, cynomolgus, and human. Following this, samples from these species, spanning a ten-day differentiation timeline, were analyzed through single-cell multiome sequencing, aiming to shed light on the temporal dynamics of species-specific developmental speeds.

### 3.4.1 Single-cell multiome sequencing captures neural differentiation trajectory of mouse, cynomolgus, and human

For the experimental setup for single-cell multiome sequencing, I conducted NPC differentiation over ten days for each species, with samples being strategically collected at designated time points (0 hours, 8 hours, 1 day, 2 days, 3 days, 4 days, 7 days, and 10 days) as illustrated in **Figure 20**. To minimize sequencing batch effects and ensure data quality, the cells from a single time point across all three species were pooled to isolate nuclei and prepare the subsequent GEX and ATAC libraries as previously tested in the pilot. An aim was set for 10,000 cells per time point, translating to approximately 3,333 cells for each species, leading to a total of 80,000 cells for the entirety of the experiment. In theory, this amounts to roughly 27,000 cells per species, allowing for optimal data integration and the generation of seamless developmental trajectories. The preparation of libraries from lysed nuclei was carried out immediately, with the libraries being stored for subsequent simultaneous sequencing with all samples to reduce batch effects further.

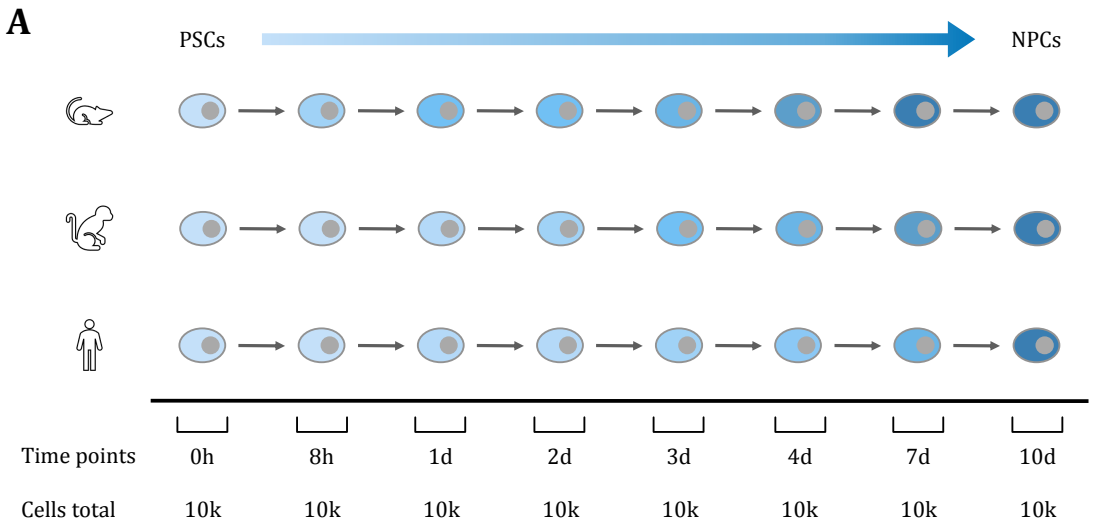


**Figure 20. Experimental setup of time course single-cell multiome sequencing. (A)** Schematic illustration of the experimental single-cell multiome sequencing setup during neural differentiation for mouse, cynomolgus, and human cells.

### *3.4.1.1 Preprocessing of time course single-cell multiome sequencing*

In the preprocessing phase for scRNA-seq data, species-specific demultiplexing was executed, as evaluated in the earlier pilot study. Briefly, sequencing data underwent alignment against each species' reference genome. A preliminary assignment of cells to species was based on the highest sequencing counts per cell per reference genome. This initial step was complemented by the application of souporcell [199] for detecting and eliminating doublet cells and for clustering cells according to genotype and species origin, utilizing single nucleotide polymorphisms. Sample barcodes were filtered only to include cells meeting high-quality criteria, determined by distributions of UMI counts, gene presence, and the proportion of mitochondria-encoded genes. Genes present in fewer than 20 cells were omitted from subsequent analysis. This resulted in 24,157 cells assigned to mouse, 23,914 cells assigned to cynomolgus, and 26,043 cells assigned to human. In total, 74,114 cells passed the preprocessing criteria for the whole time course. The exact distributions for each time point and species are listed in **Table 14**. Preprocessing steps are explained in detail in the Method section **2.2.9**.

**Table 14.** Number of cells assigned to each species and time point for the differentiation time course.

| **Species** | **0h** | **8h** | **1d** | **2d** |
|---|---|---|---|---|
| **Mouse** | 5820 | 5333 | 4041 | 1301 |
| **Cynomolgus** | 4063 | 3017 | 3228 | 1580 |
| **Human** | 2505 | 3405 | 4714 | 1990 |
| **Total** (time point) | **12,388** | **11,755** | **11,983** | **4871** |

| **Species** | **3d** | **4d** | **7d** | **10d** | **Total** (species) |
|---|---|---|---|---|---|
| **Mouse** | 1911 | 2092 | 1770 | 1646 | **24,157** |
| **Cynomolgus** | 3165 | 3559 | 2969 | 4462 | **23,914** |
| **Human** | 3031 | 2206 | 2430 | 3876 | **26,043** |
| **Total** (time point) | **8107** | **7857** | **7169** | **9984** | **74,114** |

*3.4.1.2 Single-cell RNA sequencing captures neural differentiation trajectory*

The UMAP plots derived from the gene expression profiles of cells undergoing differentiation provided a clear visualization of the linear progression of NPC differentiation specific to each species (**Figure 21A**) with cells clustering by sampling time point and aligning from day 0 to day 10. This observation was further corroborated by analyzing the expression of marker genes in a dot plot, where the dynamics aligned with the anticipated differentiation trajectory (**Figure 21B**). During NPC differentiation, I observed a gradual decrease in the expression of the pluripotency marker OCT4, revealing species-specific temporal variations: in the mouse OCT4 signal was absent after just one day, whereas in cynomolgus and humans, OCT4 expression persisted until day 2 (**Figure 21C**). In contrast, the neural marker PAX6 demonstrated a gradual increase in expression, with each species displaying unique expression dynamics as well: emergence was noted in mouse by day 2 and in cynomolgus and humans between days 3 and 4 (**Figure 21D**). SOX2, serving as both a pluripotency and neural differentiation marker, was consistently expressed throughout the differentiation process in varying degrees (**Figure 21E**).

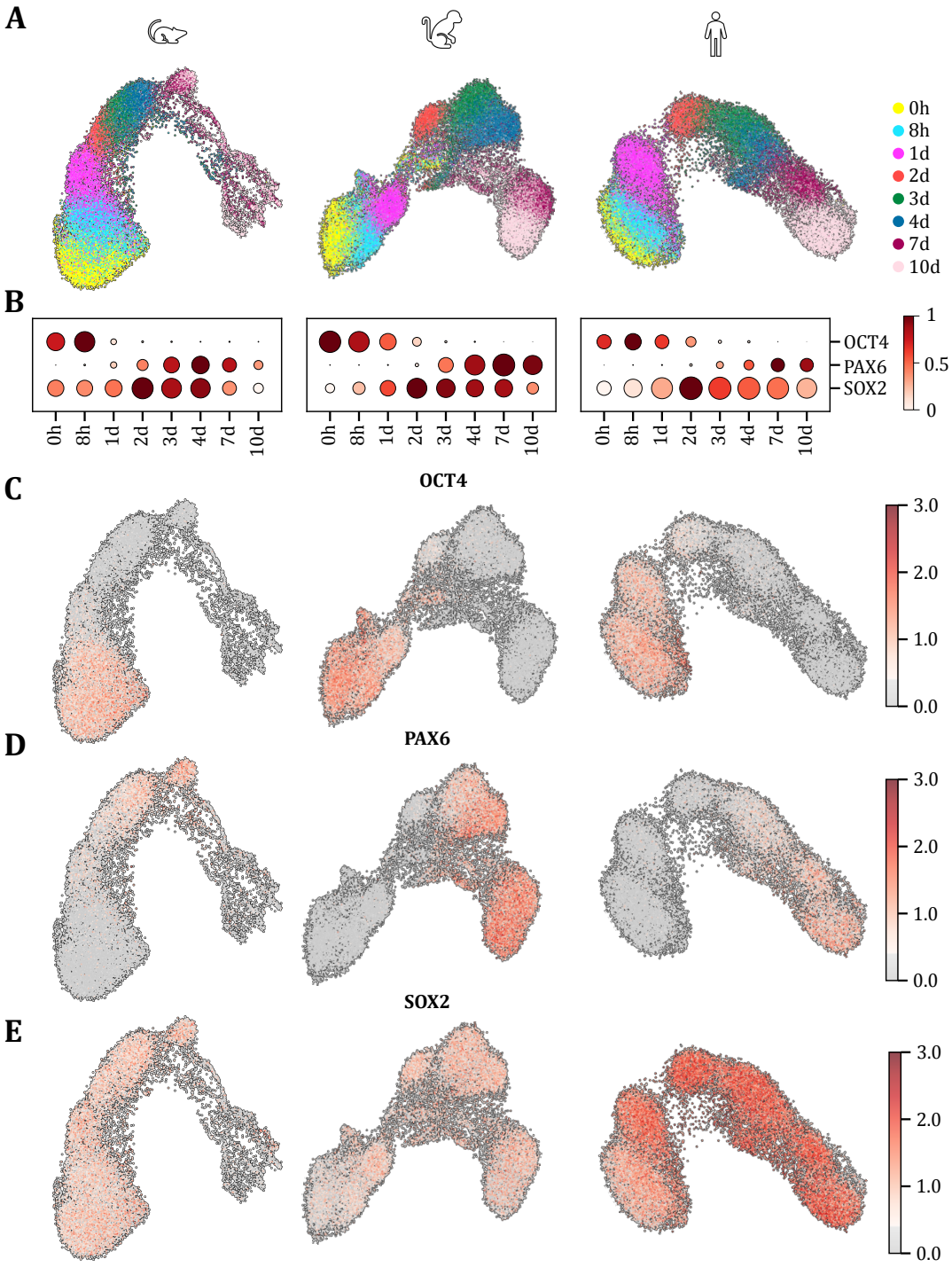


**Figure 21. ScRNA-seq captures neural differentiation trajectory. (A)** Two-dimensional UMAP embedding of mouse, cynomolgus, and human single-cells (left to right) during NPC differentiation at eight distinct time points show a continuous gene expression change. **(B)** Dot plots showing normalized mean expression of OCT4, PAX6, and SOX2 for mouse, cynomolgus, and human cells (left to right). **(C-E)** UMAPs showing OCT4 (C), PAX6 (D), and SOX2 (E) expression for mouse, cynomolgus, and human single-cells (left to right.)

#### *3.4.1.3 Single-cell ATAC sequencing captures neural differentiation trajectory*

Also, the scATAC-seq data supports a linear differentiation process, as evidenced by the gradual reduction in accessible chromatin at the OCT4 gene locus, indicated by the arrows. This correlates with the observed decrease in OCT4 gene expression. I also observed species-specific dynamics within the scATAC-seq data. In mouse cells (**Figure 22A**), accessible chromatin peaks around the OCT4 gene were only detected up to eight hours into NPC differentiation, while in cynomolgus (**Figure 22B**) and human (**Figure 22C**) cells, the chromatin around the OCT4 gene remained accessible up to two days into differentiation. In contrast, chromatin accessibility around the PAX6 gene locus gradually increased following the differentiation pathway, with mouse cells showing accessibility after one day and cynomolgus and human cells showing changes around days 2-3.

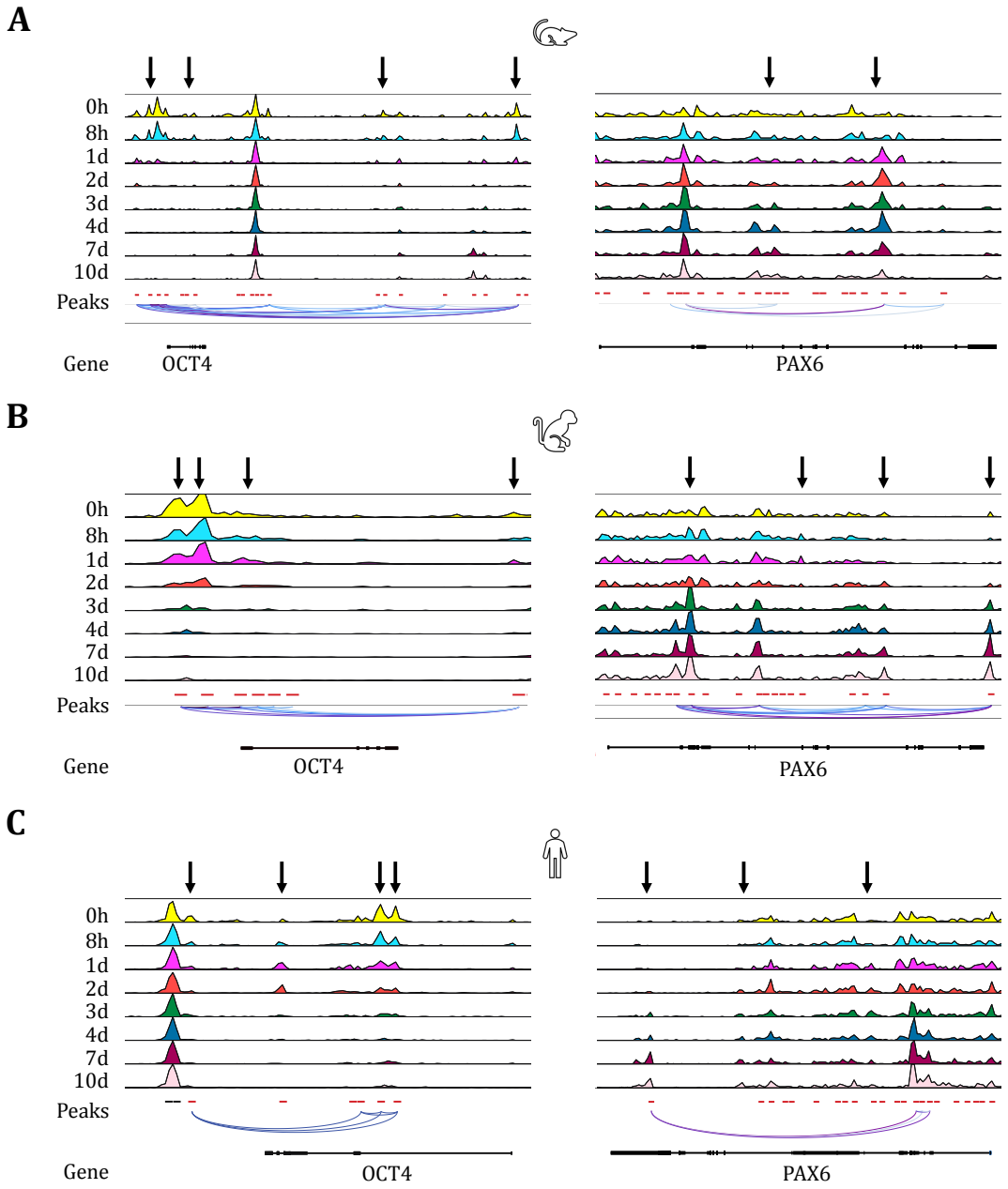


**Figure 22. ScATAC-seq captures neural differentiation trajectory. (A-C)** Local chromatin accessibility of (A) mouse, (B) cynomolgus, and (C) human changes for 10-day neural progenitor differentiation at peaks of interest around the OCT4 (left) and PAX6 (right) locus (indicated by arrows).

### 3.4.2 Correlating biological annotations with the timing of sampling revealed variations in the progression of neural differentiation among species

Cells were grouped using an unsupervised Leiden clustering method to investigate further the biological significance of observed differences in differentiation speed. This approach helped analyze the continuous differentiation trajectory toward a neural fate, a complex task due to the lack of clearly defined cell types. Using the transcriptomic data, I derived lists of marker genes common across all three species from the clusters. These marker genes allowed for the computation of gene scores for each cell, which assisted in categorizing individual cells into specific stages of differentiation (**Figure 23A-C**). The clustering approach is described in detail in the Methods section **2.2.9.5**. This analysis revealed five clusters consistently present across all species during differentiation, defined by their differentiation stage: pluripotency high, pluripotency low, intermediate, neural low, and neural high (**Figure 23D-F**). Mouse cells were distinguished by an additional cluster defined as 'neuronal', suggesting a more extensive differentiation trajectory within the ten days (**Figure 23D**).

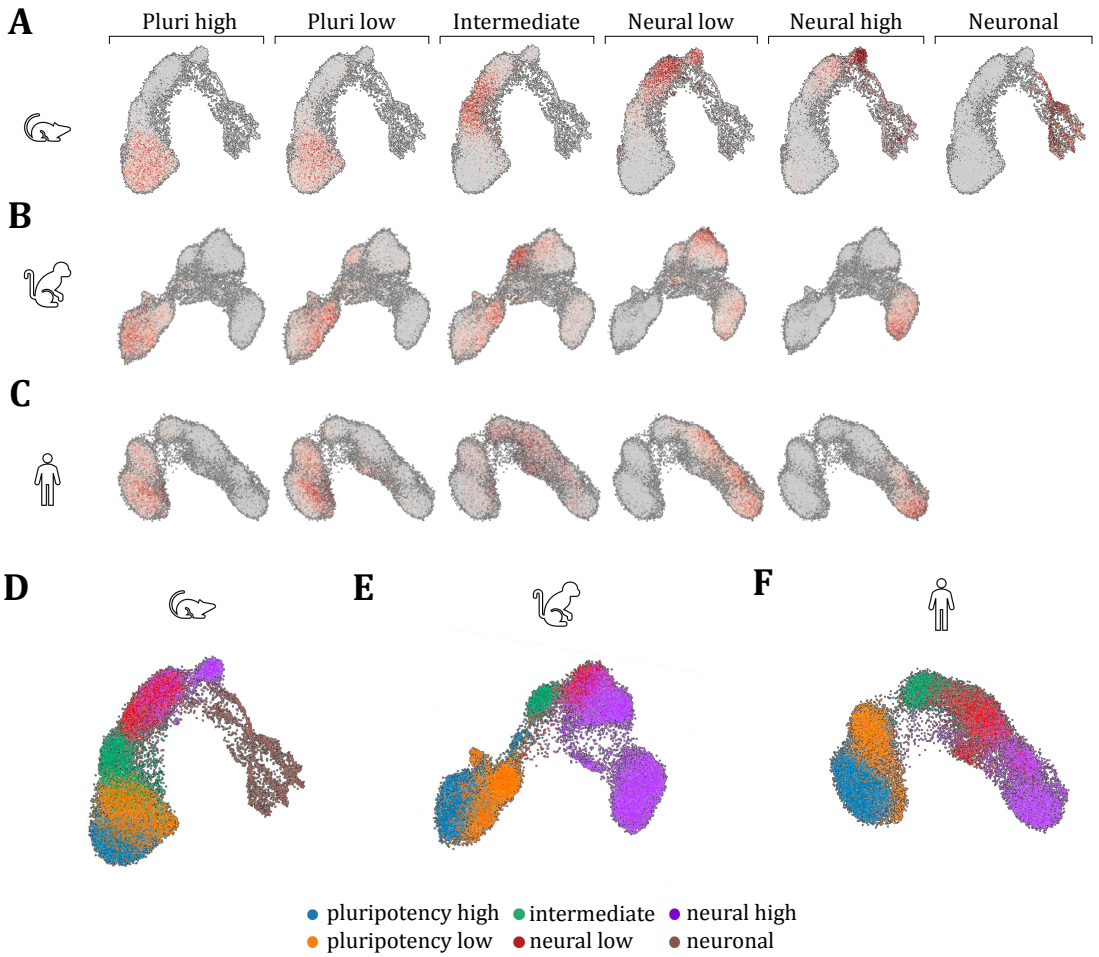


**Figure 23. Gene scores were used to determine clusters in neural progenitor differentiation.** **(A-C)** Gene expression UMAPs showing calculated gene scores for pluripotency high, pluripotency low, intermediate, neural low, neural high and neuronal cluster (left to right) fit with differentiation trajectory for (A) mouse, (B) cynomolgus and (C) human. **(D-F)** Clustering shows mouse cells differentiate further towards neuronal fate. Representation of annotated clusters in UMAP of (D) mouse, (E) cynomolgus, and (F) human during NPC differentiation.

Selected marker genes defining each cluster showed similar temporal dynamics across species, highlighting commonalities in their differentiation processes (**Figure 24A-C**). Then, I correlated biological annotations with actual sampling time points, shedding light on the variations in differentiation progression among species. Mouse cells were noted for their swift progression, reaching the neural stage by day 2 (**Figure 24D**), whereas cynomolgus and human cells took three (**Figure 24E**) and four days (**Figure 24F**), respectively, to arrive at the same stage.

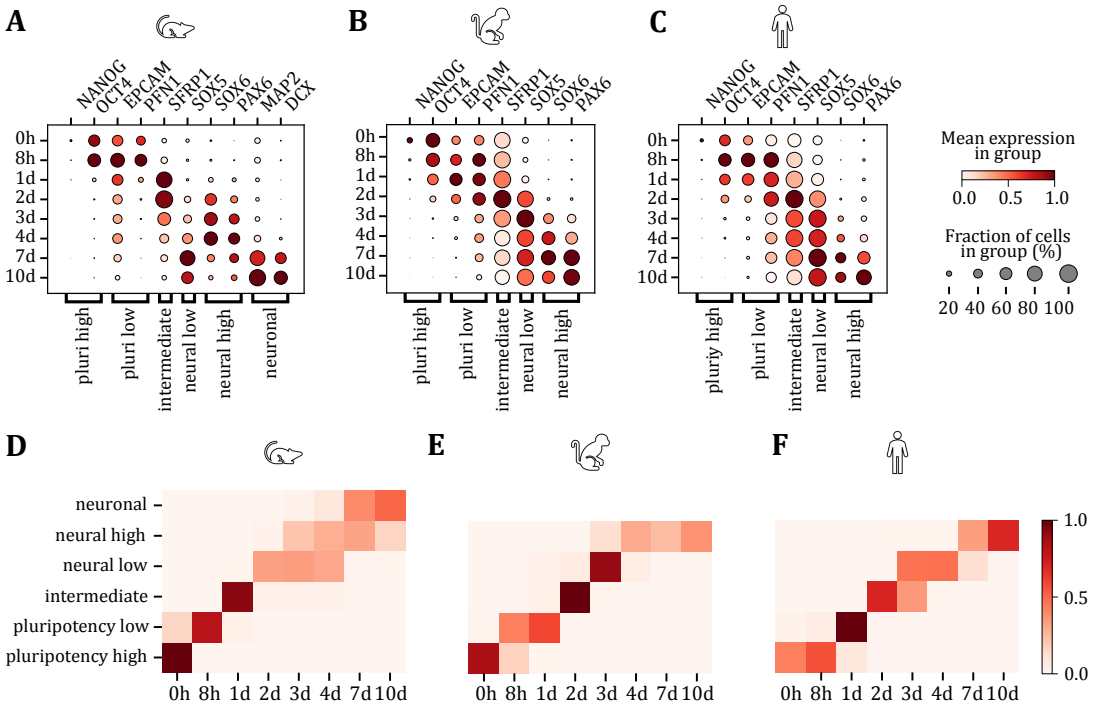


**Figure 24. Stages of neural differentiation correlated with sampling time points. (A-C)** Dot plots showing normalized mean expression of selected marker genes used for biological annotation of (A) mouse, (B) cynomolgus, and (C) human during NPC differentiation. **(D-F)** Matrix plot showing correlation between sampling time and biological annotation for (D) mouse, (E) cynomolgus, and (F) human.

### 3.4.3 Species-specific differentiation rates were determined from multiome data

To explore the differentiation speed across three species, cells were projected onto a joint embedding using the Scanpy 'ingest' tool. This technique involved integrating the embeddings and annotations of cynomolgus and human cells with those of mouse cells, which were chosen as the reference due to their relatively fast pace of differentiation that covered a more comprehensive range of developmental stages. This approach was applied to both gene expression data (**Figure 25A**) and chromatin accessibility data (**Figure 26A**), enabling an examination of how cells from the slower-differentiating species (cynomolgus and human) aligned with the rapidly differentiating mouse reference, thus revealing differences in global differentiation speeds among the species.

#### *3.4.3.1 Calculation of species-specific differentiation rates from scRNA-seq*

For gene expression data, I projected cells from all three species onto a shared embedding (**Figure 25B**). This visualization highlighted that cynomolgus cells were slightly further along in the differentiation trajectory compared to human cells, indicating a marginally faster differentiation pace in cynomolgus cells. The alignment of the sampling times with the mouse reference time was represented in a heatmap, correlating the newly projected time, the so-called 'mouse mapped time', with the actual sampling time for each species. This correlation produced a line of perfect fit for mouse cells, as expected, since their sampling time coincided with the reference time, serving as the benchmark differentiation trajectory (**Figure 25C**). Cynomolgus cells over a 10-day differentiation period only aligned with mouse cells until approximately day 4-7, revealing a noticeable shift between the original and mapped time frames (**Figure 25D**). A more pronounced deviation was seen with human cells, which aligned on day 10 with mouse cells on roughly day 4 (**Figure 25E**). Furthermore, I quantified the differentiation rates relative to mouse cells using a linear regression model to fit through each mapped time point for human ($y = 0.42x$, $R^2 = 0.84$) and cynomolgus ($y = 0.45x$, $R^2 = 0.95$) cells demonstrating that mouse cells differentiated, on average, 2.4 times faster than human cells, and 2.2 times faster compared to cynomolgus cells (**Figure 25F**).

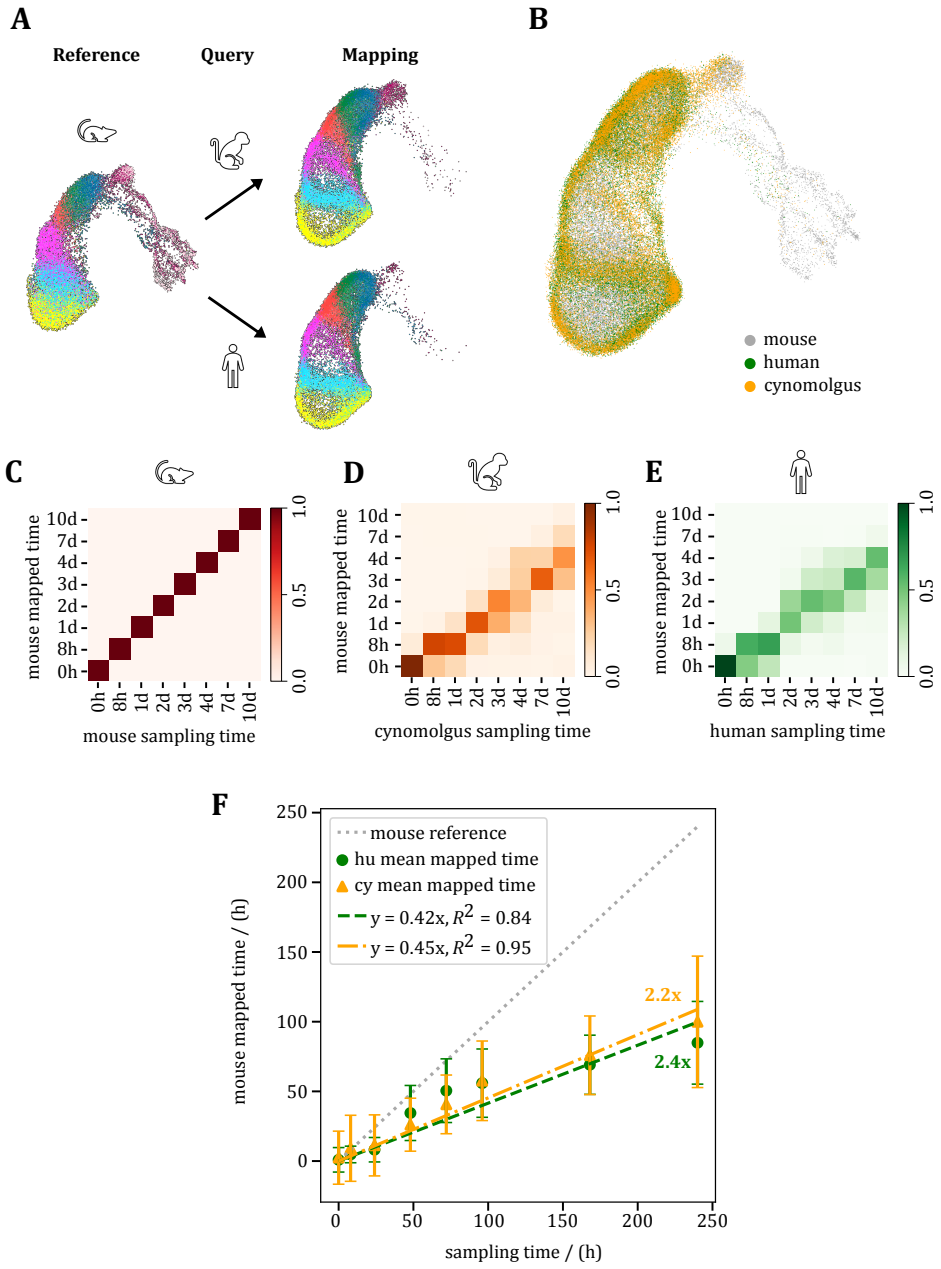


**Figure 25. Ingest mapping for scRNA-seq data. (A)** Ingest mapping for human and cynomolgus transcriptomic data using mouse UMAP as reference. **(B)** Overlay of UMAPs resulting from ingest mapping. **(C)** Heatmap of correlation between original sampling time and novel mouse mapped time annotation for mouse used as reference to calculate differences in neural differentiation speed. **(D)** Heatmap of correlation between original sampling time and novel mouse mapped time annotation for cynomolgus. **(E)** Correlation between original sampling time and novel mouse mapped time annotation for human. **(F)** Linear regression model of ingest mapping for single-cell RNA sequencing data. Mouse differentiation is 2.2 and 2.4 times faster than cynomolgus and human, respectively. Mean mapped time of human (circle) and cynomolgus (triangle) development. Error bars represent standard deviation. Mouse (dotted line) as reference.

#### *3.4.3.2 Calculation of species-specific differentiation rates from scATAC-seq*

The same analytical approach applied to RNA data was extended to ATAC data, incorporating simulated gene expression to facilitate the visualization and interpretation of scATAC Seq data. By leveraging chromatin accessibility patterns, gene expression profiles for cell state-specific marker genes were estimated. This involved calculating gene scores based on the local accessibility of gene regions, including promoters and gene bodies, across all cells while adjusting for gene distances and variations in gene size using ArchR [210].

Although the results mirrored the trends observed in the scRNA-seq data, the ATAC data presented more noise, highlighting the inherent challenges and the fact that many analytical tools are primarily designed for scRNA-seq data. Despite these challenges, the same analysis steps were applied: cells from human and cynomolgus were mapped onto the mouse reference using the simulated gene expression derived from the ATAC data (**Figure 26A**). The UMAP embedding did not reveal a clear linear trajectory, making it difficult to discern differences in differentiation speed (**Figure 26B**). However, progression was visualized using a heatmap, once again with the mouse correlation as the benchmark for the differentiation trajectory, represented by a perfect fit line (**Figure 26C**). In this context, cynomolgus cells aligned with the 0-hour mouse PSC reference until day 2, with day 10 cells approximately mapping to mouse day 7 (**Figure 26D**).

Similarly, human cells mostly mapped to mouse cells at 0 or 8 hours until day 2 and then progressed to approximately mouse day 4 (**Figure 26E**). As for the gene expression data, I quantified differentiation rates relative to mouse cells using a linear regression model to fit through each mapped time point for human ($y = 0.53x$, $R^2 = 0.89$) and cynomolgus ($y = 0.59x$, $R^2 = 0.95$) cells, revealing that, based on the ATAC simulated gene expression, mouse cells differentiated 1.9 times faster than human cells and 1.7 times faster than cynomolgus cells (**Figure 26F**). Although there was a slight variance compared to the gene expression data, the overall trend remained consistent.

The comparative analysis of cross-species gene expression and chromatin accessibility provided crucial insights into the variations in differentiation speeds among species. It highlighted distinct progression patterns and how cells from cynomolgus and human species align with those from the mouse, which differentiates at a quicker pace. This analysis highlighted that among the species studied, the mouse exhibited the fastest differentiation speed, followed by cynomolgus in the intermediate position, and human cells showed the slowest differentiation rate. The next step was identifying the mechanisms that determine these species-specific differentiation speeds.

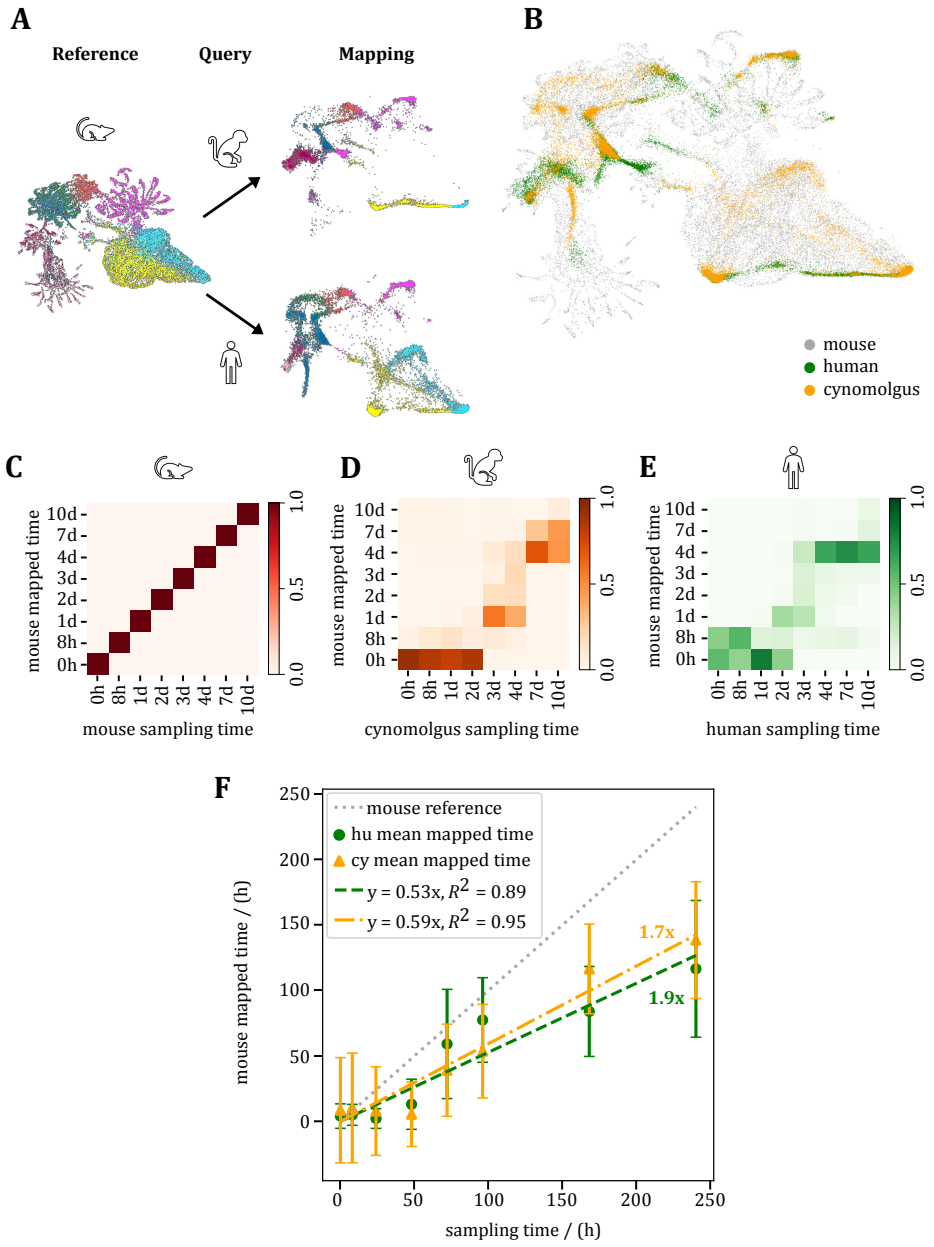


**Figure 26. Ingest mapping for simulated gene expression of scATAC-seq data. (A)** Ingest mapping for human and cynomolgus transcriptomic data using mouse UMAP as reference. **(B)** Overlay of UMAPs resulting from ingest mapping. **(C)** Heatmap of correlation between original sampling time and novel mouse mapped time annotation for mouse used as reference to calculate differences in neural differentiation speed. **(D)** Heatmap of correlation between original sampling time and novel mouse mapped time annotation for cynomolgus. **(E)** Correlation between original sampling time and novel mouse mapped time annotation for human. **(F)** Linear regression model of ingest mapping for simulated gene expression of single-cell ATAC sequencing data. Mouse differentiation is 1.7 and 1.9 times faster than cynomolgus and human, respectively. Mean mapped time of human (circle) and cynomolgus (triangle) development. Error bars represent standard deviation. Mouse (dotted line) as reference.

### 3.4.4 Dissecting the relationship between cell cycle and differentiation speed

Previous studies have suggested a correlation between the duration of the species-specific cell cycle and the pace of differentiation at the population level [20], [148]. Leveraging single-cell technologies, this relationship was investigated at the individual cell level to determine whether the cell cycle has a causal effect on the differentiation rate.

A comprehensive examination of the cell cycle phase compositions across three species was facilitated by assigning individual cells to specific cell cycle phases based on gene scores derived from phase-associated marker genes [205], [206]. UMAP visualizations revealed that mouse cells transitioned towards later time points into a post-mitotic state, exhibiting G1 arrest (**Figure 27A**). In contrast, cells from cynomolgus (**Figure 27B**) and human (**Figure 27C**) demonstrated an even distribution of cell cycle phases throughout the differentiation process. A more detailed analysis of the distribution of cell cycle phases at each time point highlighted that mouse cells progressively became post-mitotic during NPC differentiation. Initially, a small fraction of cells was in the G1 phase, with most cells in the S-phase. However, the fraction of cells in G1 increased over time, reaching approximately 73% by day 7 and 88% by day 10 (**Figure 27D**). Meanwhile, even upon closer inspection, human (**Figure 27E**) and cynomolgus (**Figure 27F**) cells showed a consistent distribution across all three cell cycle phases, with minor variations between different days, indicating distinct cell cycle dynamics across species.

Cell culture experiments investigating species-specific cell cycle differences and their effect on differentiation speed were exclusively conducted by my collaborators Dr. Christian Schröter from the Max-Planck-Institute of Molecular Physiology in Dortmund and his Ph.D. student Julia Schröder as part of her thesis. Consequently, the results are not included in this thesis but will contribute to the discussion.

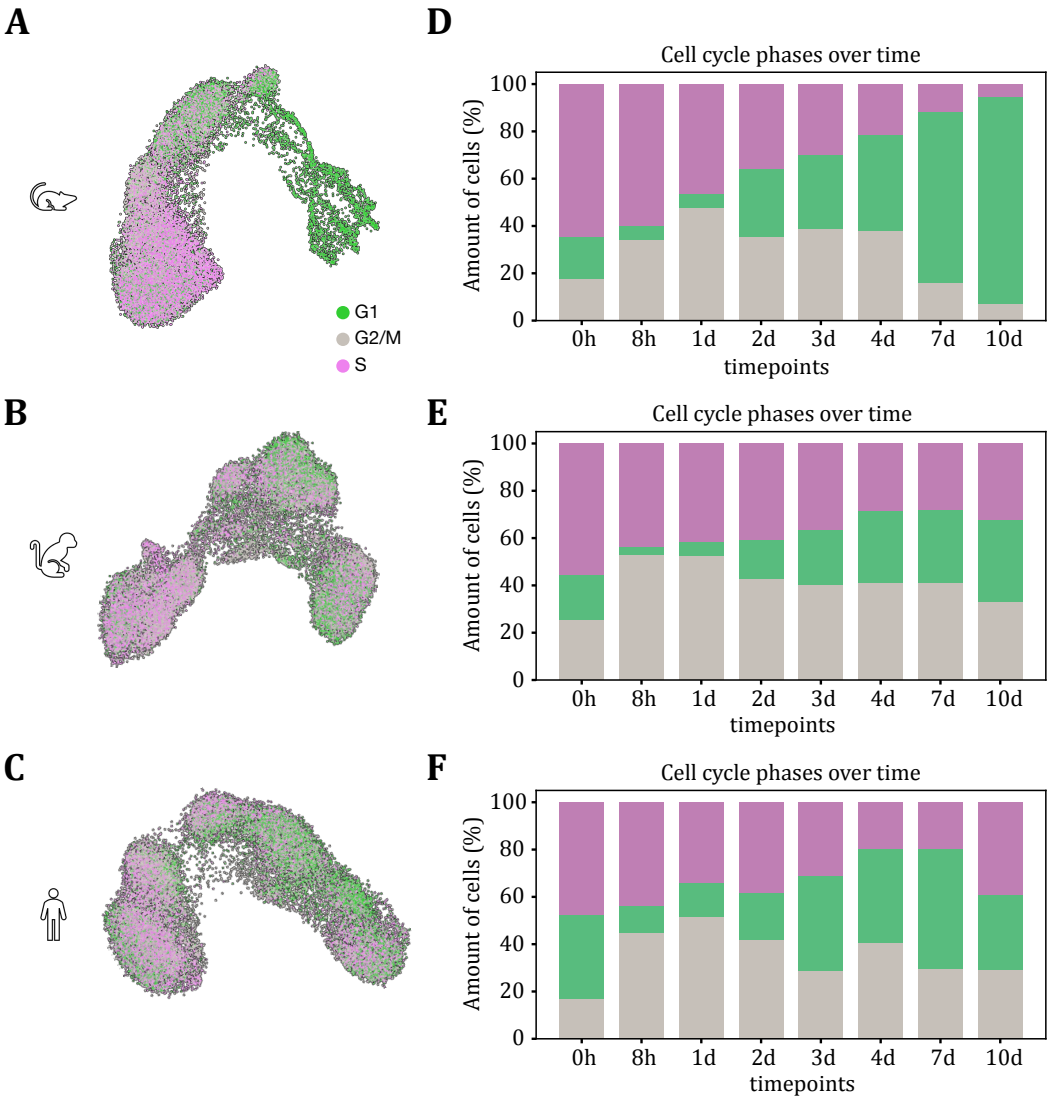


**Figure 27. Cell cycle phase distribution during neural progenitor differentiation. (A-C)** UMAPs showing cell cycle phase distribution inferred from gene expression data for (A) mouse, (B) cynomolgus, and (C) human. **(D-F)** Percental distribution of cell cycle phases for each time point of the 10-day NPC differentiation course inferred from gene expression data for (D) mouse, (E) cynomolgus, and (F) human.

### 3.4.5 Identification of candidates regulating neural differentiation speed

Within the time course transcriptomic data, I noted that differentiation speeds, while generally following a similar trend, displayed some heterogeneity among cells within the same species (**Figure 24D-F**). Therefore, besides comparing the different species to each other, I broadened the exploration to consider whether mechanisms responsible for differences in developmental speed between different species could also underlie the differences observed within a species. This hypothesis proposes that the determinants of developmental pace, genetic, epigenetic, metabolic, or related to cell signaling pathways, might account for inter-species variation and play a pivotal role in explaining the intra-species disparities. The analytical framework encompassed three steps: initially, a comparative analysis of biological processes across species was conducted to identify universal developmental differences. This was succeeded by a targeted examination of genes within these processes, focusing on those demonstrating species-specific expression dynamics, aiming to identify pivotal genes responsible for differential developmental tempos. Subsequently, in the last phase, the analysis focused on examining individual cell trajectories to elucidate differences in differentiation speed within one species (**Figure 28A**).

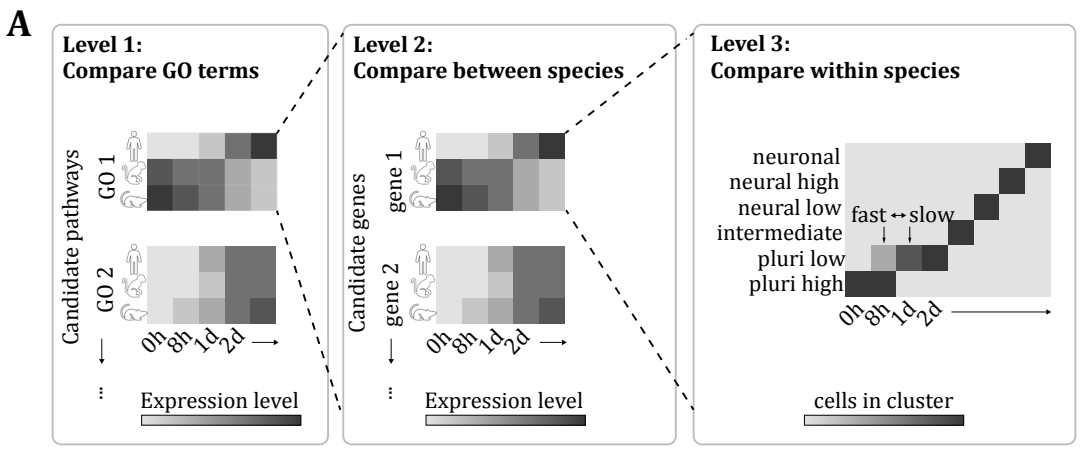


**Figure 28. Identification of genes of interest for the regulation of developmental speed. (A)** Schematic illustration of the methodology behind identifying genes of interest for regulating inter and intra-species development speed.

#### *3.4.5.1 Cross-species comparison for the identification of candidate mechanisms*

I explored biological mechanisms beyond the cell cycle that may account for species-specific differences in differentiation speeds, which led to a focused investigation of metabolic and epigenetic factors. Building upon literature that underscored the significant roles of these factors in developmental pacing [20], [21], [148], I embarked on a comprehensive examination of shared genes across mouse, cynomolgus, and human species.

Initial analyses, including GO analysis of differentially expressed genes comparing the different species with each other, yielded broad outcomes pointing to general metabolic and cellular processes (**Figure 29A-C**). Seeking a more detailed understanding, I curated distinct gene lists from GO categories such as energy metabolism, protein biosynthesis, and epigenetic regulation and modification (**Figure 29D**), revealing unique expression profiles for each species at various time points. The data was normalized for each biological pathway and scaled from -2 to 2. This normalization helped to highlight differences between species that were otherwise quite homogeneous. Notably, human cells showed a higher expression of epigenetic regulators and DNA modifiers, whereas cynomolgus cells displayed an increased expression of genes associated with glycogenolysis and biological oxidations. Mouse cells had the most significant upregulation in glucose-related metabolic processes, setting them apart from humans and cynomolgus. Interestingly, the TCA cycle and NADH metabolism exhibited similar patterns across all species, hinting at cross-species conserved metabolic pathways.

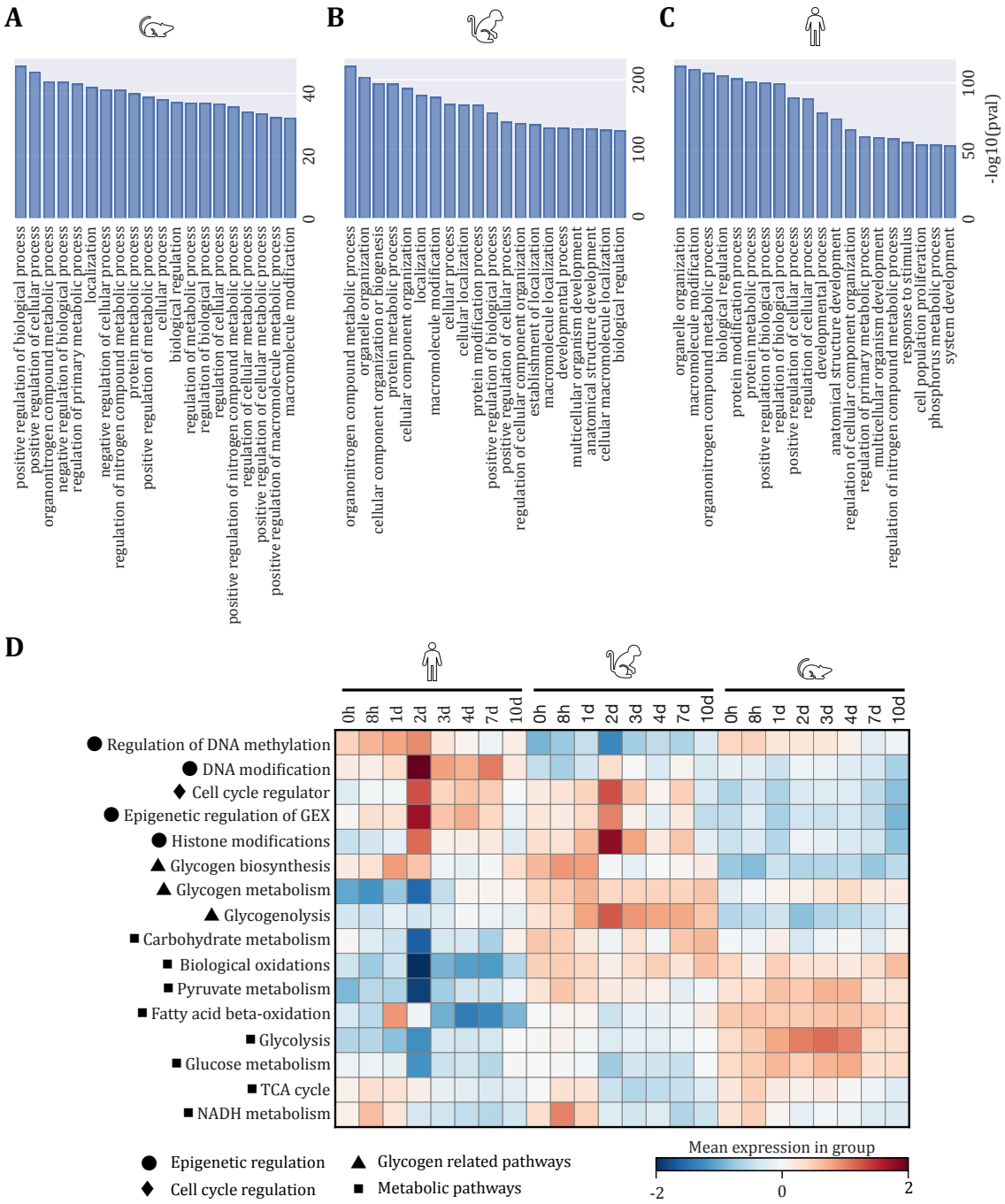


**Figure 29. Genes in defined biological pathways are differentially expressed across species.** **(A-C)** GO analysis for differentially expressed genes in (A) mouse, (B) cynomolgus, and (C) human shows similar and imprecise results for enriched biological processes. **(D)** Expression analysis of selected biological pathways in shared dataset. Matrix plot showing normalized mean expression of genes in selected biological pathways for human, cynomolgus and mouse from a comprehensive shared dataset for each timepoint of the NPC differentiation course.

Progressing, selected biological processes and gene lists were scrutinized to isolate based on their distinctive expression profiles across species. With this analysis, I narrowed the list of potential candidate genes. One such candidate was, for example, the phosphoglycerate kinase PGK1, an enzyme crucial for the dephosphorylation of 1,3-Bisphosphoglycerate to 3-Phosphoglyceric acid during glycolysis. It was initially observed to have higher expression in differentiating mouse cells (**Figure 30A**). However, upon further examination through a normalized dot plot, the disparity in expression appeared less pronounced, with high levels also observed in human and cynomolgus cells during differentiation (**Figure 30C**). Another gene of interest, UGP2, which functions as a UDP-glucose pyrophosphorylase critical for glycogen synthesis (**Figure 30B**), was found to have notably higher expression in the slower-differentiating species, human and cynomolgus, particularly at the start of neural differentiation, contrasting significantly with the faster-differentiating mouse (**Figure 30D**). Through UMAP visualizations examining UGP2 expression across the differentiation timeline, I noted consistently low levels of UGP2 in mouse cells (**Figure 30E**). At the same time, I observed elevated expression at the onset of differentiation in both cynomolgus (**Figure 30F**) and human cells (**Figure 30G**), indicating the varied influence of UGP2 on the differentiation processes among the species.

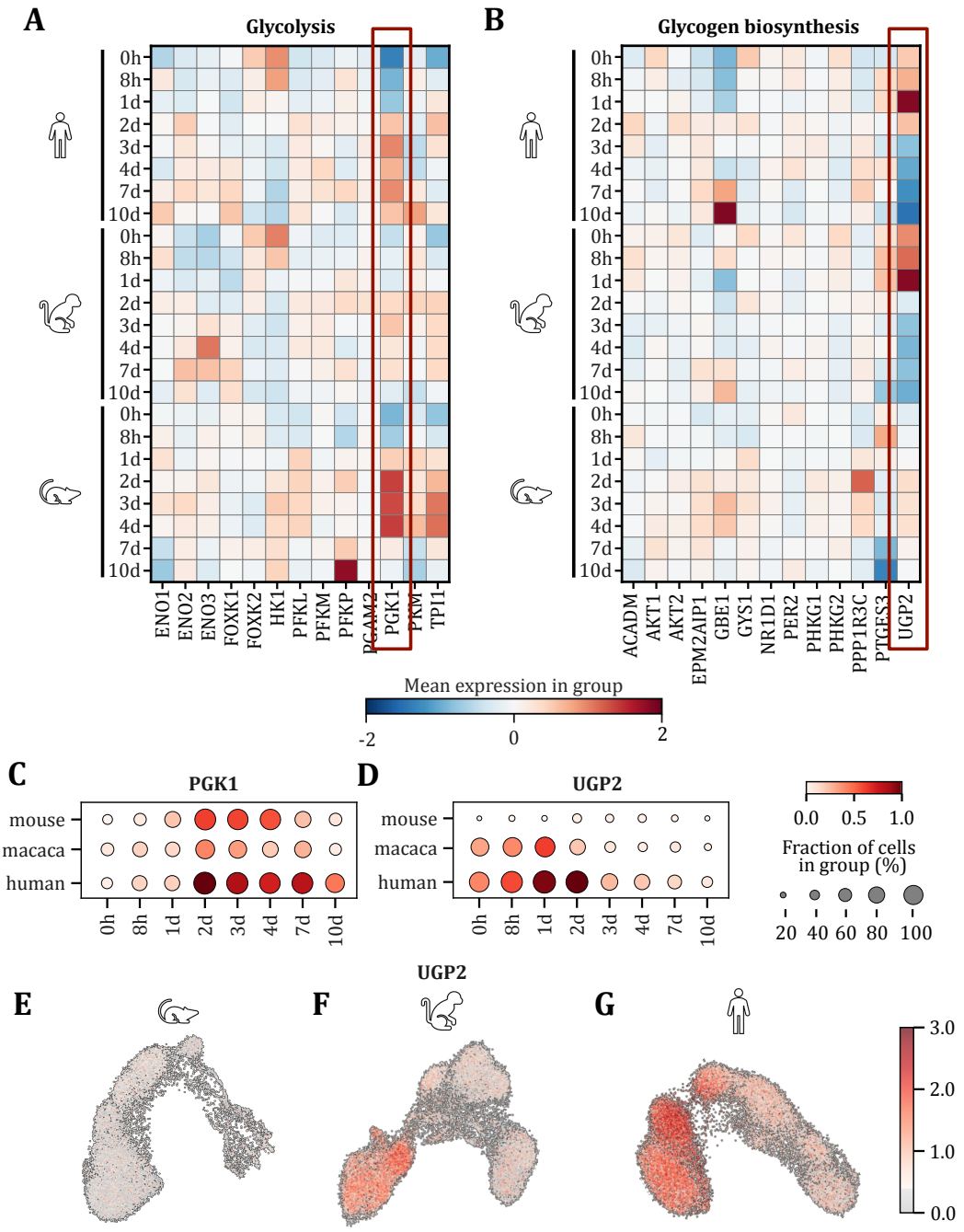


**Figure 30. Glycogen biosynthesis-related UGP2 is upregulated in slower species. (A-B)** Matrix plot showing mean expression of genes relevant for (A) glycolysis and (B) glycogen biosynthesis in human, cynomolgus, and mouse for each timepoint of the NPC differentiation. **(C-D)** Dot plot showing the mean expression of (C) PGK1 and (D) UGP2 in mouse, cynomolgus, and human for each timepoint of the NPC differentiation course. **(E-G)** Gene expression UMAPs for UGP2 show differences in expression in (E) mouse, (F) cynomolgus, and (G) human and over the differentiation time course.

### 3.4.6 UGP2 is upregulated in slower differentiating cells within a species

Cells with nearly identical gene expression profiles were closely examined, as determined through the biological annotation of data at distinct developmental time points, revealing cells that displayed rapid differentiation and those that progressed at a slower pace within each species. At the exit of pluripotency, a detailed temporal analysis was conducted to ascertain the exact junctures at which cells transitioned into a 'pluripotency low' classification, surpassing a set threshold based on gene scores. This defined cells as rapidly or slowly differentiating based on their transition timing. In the case of the pluripotency low cluster, cells surpassing the set gene scoring threshold after 8 hours were classified as fast-differentiating cells. At the same time, those exceeding the threshold after one day of differentiation were classified as slowly differentiating (**Figure 31A**). A direct comparison between fast and slow-differentiating cells highlighted only UGP2 as a gene of significant interest from the previously narrowed candidates in the inter-species comparison. Although less pronounced in mouse cells, UGP2 exhibited higher expression in slower-differentiating cells than their faster counterparts across all three species (**Figure 31B**).

In summary, initial explorations through GO analysis prompted a detailed investigation into distinct gene lists across various biological pathways. Further analysis within species unveils that mechanisms affecting inter-species developmental speed variations may similarly influence intra-species differentiation rates. Heightened expression of UGP2 in slower-differentiating species and cells was observed, potentially linking glycogen biosynthesis and metabolic processes with developmental timing.

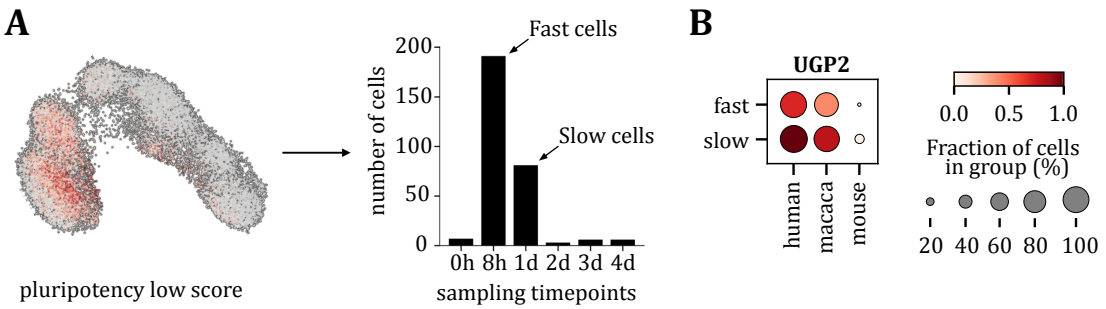


**Figure 31. Glycogen biosynthesis-related UGP2 is upregulated in slower differentiating cells.** **(A)** Visualization of the method for identification of fast and slow differentiating cells (here fast or slow exit from pluripotency) from gene expression data. **(B)** Dot plot showing the mean expression of UGP2 in mouse, cynomolgus, and human cells identified as fast or slowly differentiating.

## 3.5 UGP2 KO in human and cynomolgus leads to accelerated neural differentiation

UGP2 plays a pivotal role in glycogen biosynthesis and influences cellular metabolism and energy balance. Given its critical function in synthesizing UDP-glucose, an essential precursor for glycogen, glycoproteins, and glycolipids synthesis, UGP2 impacts the cellular capacity for glucose storage and energy regulation [215], [216]. This regulatory potential prompted the hypothesis that the deletion of UGP2 might significantly alter neural differentiation dynamics, particularly in species exhibiting slower differentiation speeds. Given the integral function of UGP2 in producing UDP-glucose for glycogen biosynthesis, its absence could severely affect cellular metabolism, impacting the energy storage capability of cells and potentially altering the pathways and efficiency of neural differentiation and development [217].

### 3.5.1 Generation of UGP2 KO for functional studies

The compelling observations from the single-cell gene expression data concerning UGP2 prompted the hypothesis that this gene could significantly influence the regulation of neural differentiation. A comprehensive series of targeted experiments was initiated to pursue this hypothesis. I kindly obtained a human ESC UGP2 KO line from Dr. Stefan Barakat's lab (Erasmus MC). In addition, I generated a UGP2 KO model in cynomolgus iPSCs to determine

the effects of these genetic deletions on the pace of neural differentiation in the slower species. By employing these genetic modifications, the aim was to ascertain whether the absence of UGP2 would manifest in alterations in differentiation dynamics, thereby substantiating the role of glycogen metabolism in the neural development process.

I employed a methodology similar to that described in Perenthaler et al., 2020 [217] to create a cynomolgus UGP2 KO line, taking advantage of the highly conserved nature of the UGP2 gene, which is characterized by ten exons in both human (**Figure 32A**) and cynomolgus (**Figure 32B**), with only the first and tenth exon differing in length aside from a 98% sequence similarity. I applied CRISPR editing to cynomolgus iPSCs, targeting exon 2 for deletion, which is explained in detail in the Method section **2.2.7**. This process involved testing two distinct guide RNA combinations (**Figure 32C**), from which single clones were selected for further examination. I extracted genomic DNA from these clones for PCR analysis. The wild type resulted in a PCR product with a length of 297bp, while successful deletions were expected to produce PCR products of 177bp and 168bp for the sgRNA 2+9 and 3+9 combinations, respectively. Based on PCR and gel electrophoresis results, six clones were chosen for additional verification through Sanger sequencing (**Figure 32D**). Only the cynomolgus iPSCs UGP2 KO sgRNA 2+9 clone 6 (29cl6) exhibited a successful homozygous deletion, as confirmed by Sanger sequencing.

The absence of UGP2 protein in both human and cynomolgus KO lines was verified via Western Blot analysis, contrasting with its pronounced presence in the wild types. UGP2 protein was also absent in the mouse EpiSC wildtype (**Figure 32E**). Both human and cynomolgus KO cell lines maintained typical cell culture morphology (**Figure 32F**), providing a solid foundation for subsequent functional experiments to explore the impact of UGP2 KO on the pace of neural differentiation.

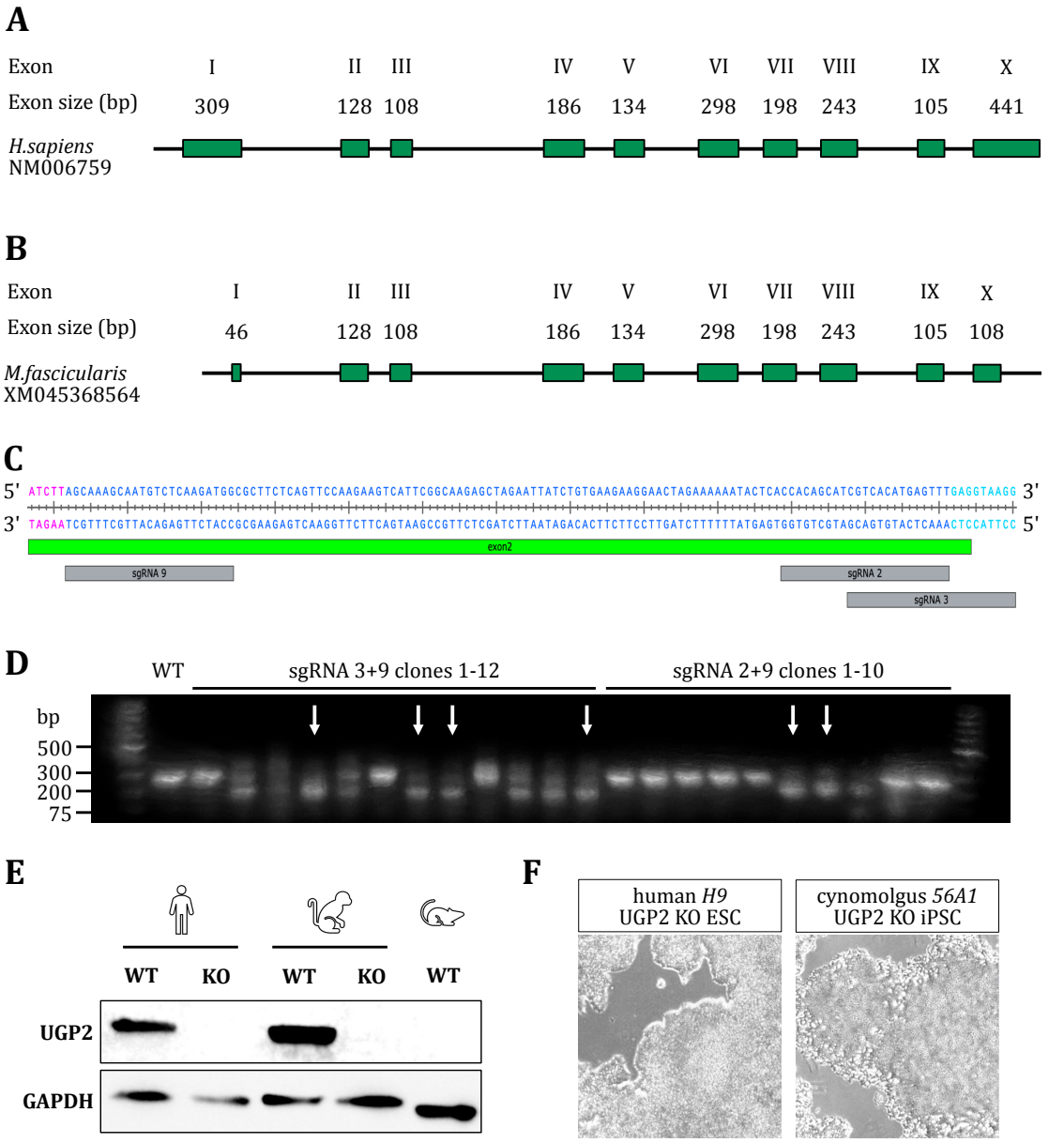


**Figure 32. Generation of UGP2 KO for functional studies. (A-B)** Illustrative representation of the (A) human and (B) cynomolgus UGP2 gene locus. Exons are depicted as boxes, with the coding regions highlighted in green. **(C)** Strategy for CRISPR-cas9 editing of the cynomolgus UGP2 gene. The Coding region of exon 2 is highlighted in blue, indicating the binding sites of sgRNAs. **(D)** Gel electrophoresis analysis of PCR products of single clones. Arrows indicate clones selected for Sanger sequencing. **(E)** Western blot quantification of UGP2 protein in human ESC, cynomolgus iPSC and mouse EpiSC wildtype (WT) and human and cynomolgus KO lines (KO). GAPDH is used as housekeeping control. **(F)** Brightfield images of human ESC H9 3-35 (left) and cynomolgus iPSC 29cl6 (right) UGP2 KO lines. Magnification = 5x.

### 3.5.2 Neural markers are significantly upregulated in UGP2 KO lines

With the generation of UGP2 knockouts in human and cynomolgus PSCs, I repeated neural differentiation experiments with these lines to assess the impact of UGP2 depletion on the speed of neural differentiation. RT-qPCR was employed to analyze the outcomes.

In human cells, a gradual downregulation of the pluripotency marker OCT4 (**Figure 33A**) was observed, occurring to a slightly greater extent in the KO cells compared to the wild type. Additionally, the early neural markers SOX1 (**Figure 33B**) and PAX6 (**Figure 33C**) were significantly more expressed in the KO starting from day 4. Most notably, the later-stage neural marker FOXG1, while barely expressed in the wild type, showed significant upregulation from day 6 of NPC differentiation onwards in the KO cells (**Figure 33D**). In cynomolgus cells, the UGP2 KO effects were not as pronounced as in human cells. OCT4 was gradually downregulated upon differentiation (**Figure 33A**). The early neural progenitor marker SOX1 did not significantly differ between wildtype and KO except for a notable upregulation at day 6 in the KO versus the wildtype (**Figure 33B**). However, the later-stage neural marker FOXG1 was significantly upregulated in the KO as early as day 4 of NPC differentiation but was not expressed in the wild type throughout the differentiation process.

Notably, NPC differentiation with the cynomolgus UGP2 KO could only proceed until day 8. After prolonged differentiation, cells aggregated similarly to mouse wild-type cells and detached, preventing further maintenance and analysis.

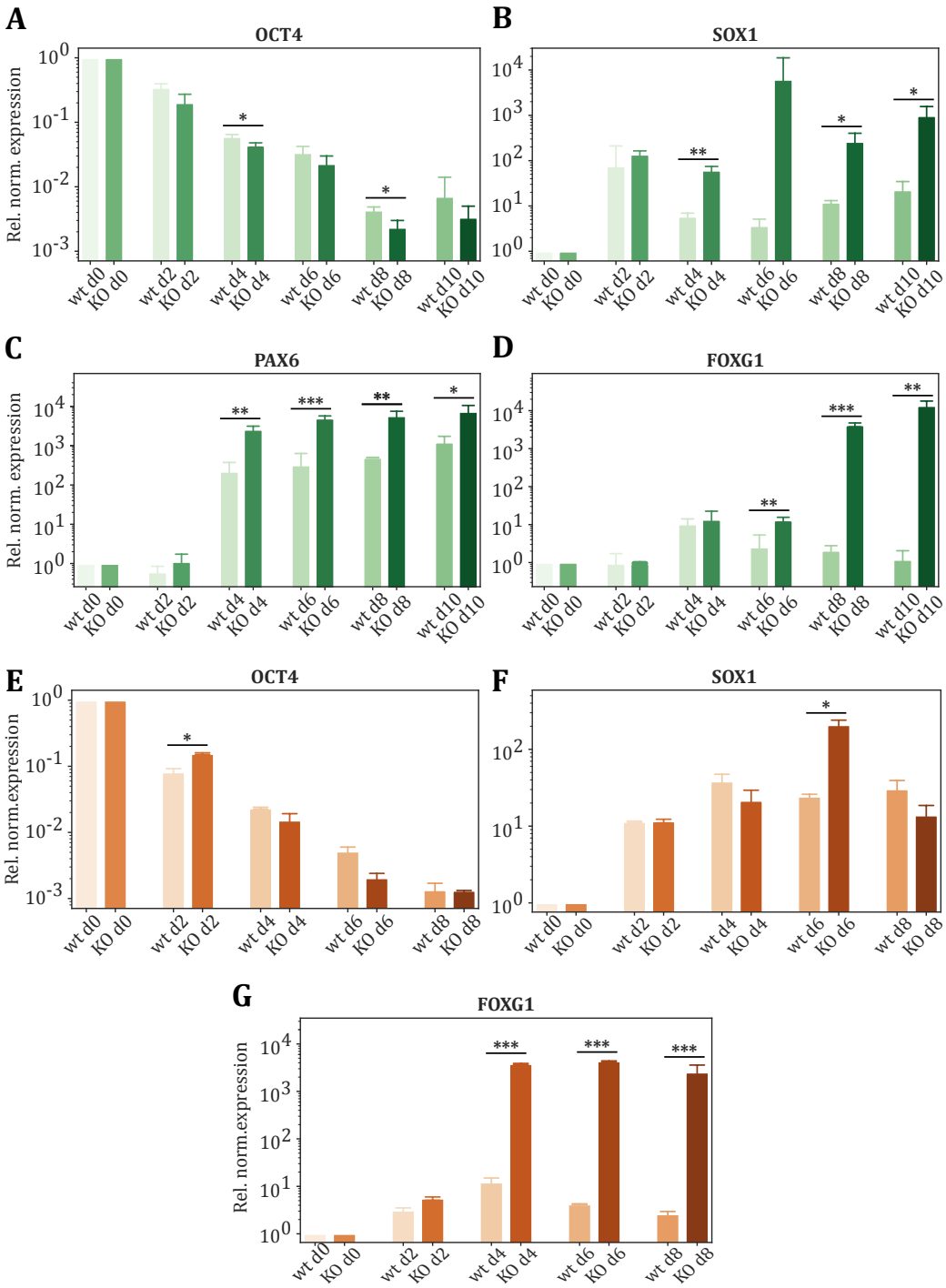


**Figure 33. RT-qPCR analysis of human and cynomolgus UGP2 KO during neural differentiation.** **(A)** OCT4, **(B)** SOX1, **(C)** PAX6, and **(D)** FOXG1 RT-qPCR results for time-course NPC differentiation in human wildtype versus UGP2 KO. **(E)** OCT4, **(F)** SOX1, and **(G)** FOXG1 RT-qPCR results for time-course NPC differentiation in cynomolgus wildtype versus UGP2 KO. Relative normalized expression was calculated using the $2^{-ddCt}$ method using the respective PSC for normalization. Logarithmic scale. Error bars represent standard deviation (n=3), p-value was determined using the student's t-test: * $p < 0.05$, ** $p < 0.01$, *** $p < 0.001$, **** $p < 0.0001$.

# 4 Discussion

## 4.1 The regulation of developmental timing is a multifaceted process

The regulation of developmental timing in mammals is a pivotal process, directing the intricate transition from a zygote to a complex, multicellular organism through a sophisticated network of genetic, epigenetic, and extracellular interactions [20], [21], [83], [148], [168], [218]. In my thesis, I aimed to uncover the molecular mechanisms that govern this crucial aspect of developmental biology, particularly emphasizing how intrinsic cellular processes dictate the developmental timeline across mammalian species.

My investigation led to discoveries that enrich our understanding of developmental and stem cell biology. By leveraging *in vitro* models and innovative single-cell sequencing techniques, I identified a complex relationship between the transcriptional properties of PSCs and their developmental speed, revealing how metabolic regulation influences differentiation potentials. I highlighted intrinsic species differences and similarities through comparative analyses across mammals, uncovering both conserved and divergent biological pathways. Moreover, utilizing CRISPR/Cas9 gene editing, I dissected the functional roles of UGP2 in influencing differentiation speed, offering new perspectives on the metabolic and genetic regulation of developmental processes.

### 4.1.1 Standardization of PSC culture conditions reveals conserved cross-species pluripotency and differentiation mechanisms

#### *4.1.1.1 PSCs of various species are maintained in harmonized culture conditions*

The intrinsic regulation of a cell, and therefore likely the developmental pace, depends on extrinsic influences and signals [165], [219]. For this thesis, the culturing conditions for PSCs were harmonized across multiple mammalian species, thereby creating a common ground for comparative analyses and enabling the examination of intrinsic pluripotency and differentiation mechanisms without disturbance of extrinsic factors.

Culturing human ESCs, mouse EpiSCs, and iPSCs from cynomolgus and orangutans under harmonized conditions has led to the observation that primed mammalian PSCs can grow under identical culture conditions (**Figure 11**). This confirms the presence of a robust, universal system regulating the delicate equilibrium between self-renewal and differentiation within the mammalian lineage [220]. After a variety of cell culture media were tested, UPPS media was initially chosen as the most promising candidate based on the morphology of the colonies (**Figure 11A**) [198]. The composition of UPPS uniquely modifies the Wnt signaling pathway and allows for the self-renewal of epiblast-like cells. It incorporates CHIR, a GSK3 inhibitor and, therefore, a Wnt signaling activator, and IWR-1, an Axin, part of the β-catenin destruction complex, activator and, therefore, a Wnt signaling inhibitor [221]. In combination, this leads to the cytoplasmatic accumulation of β-catenin. This ultimately leads to the binding of β-catenin to TAZ, a transcription factor within the Hippo pathway. The Hippo signaling pathway is critical in limiting cell proliferation and promoting apoptosis [222], [223]. Consequently, neither can be translocated to the nucleus, inhibiting the activation of differentiation signals. Zhou et al. demonstrated the significance of this interaction for the self-renewal of primed PSCs [224].

Establishing harmonized conditions significantly facilitated a fruitful collaboration with Prof. Dr. Heinrich Leonhardt and Dr. Enes Ugur from LMU Munich. My expertise in mammalian PSC culture played a crucial role in this partnership, leading to my co-authorship on the publication "Comprehensive chromatin proteomics resolves functional phases of pluripotency and identifies changes in regulatory components," featured in Nucleic Acids Research [225]. I utilized harmonized primed conditions for human ESCs and mouse EpiSCs and transformed ground mouse ESCs in 2i+LIF into formative mouse EpiLCs using UPPS for comparative studies. This allowed us to analyze the proteome and chromatome—the proteome associated with the chromatin—of different pluripotency states in mice and compare it with human ESCs. Dr. Enes Ugur made significant contributions by developing a robust protocol to confidently analyze the chromatome via mass spectrometry. The study provides a detailed analysis of chromatin proteome dynamics across different states of pluripotency in both human and mouse cells, identifying three main phases: ground, formative, and primed. Each phase is characterized by distinct chromatin configurations and transcriptional activities, integral to the developmental potential and cellular identity. In the ground state, mouse ESCs exhibit a transcriptionally permissive chromatin environment with low levels of repressive epigenetic marks, which allows for high cellular plasticity. As cells transition to the formative phase, they gain additional epigenetic modifications, such as H3K27me3, preparing them for subsequent

differentiation pathways. The primed state is marked by a more restricted chromatin structure that supports specific differentiation paths, indicating a progression toward lineage commitment. The study highlights notable species-specific differences in the chromatin landscapes between human and mouse PSCs. Human cells maintained under UPPS culture conditions, which reflect a primed state, show similarities to mouse primed EpiSCs and exhibit unique chromatin features distinct from those observed in mouse cells. Furthermore, essential proteins such as OCT4, SOX2, and NANOG are found to interact differently with chromatin across these states. This dynamic interaction influences the cells' developmental capacities and underscores the complexity of pluripotency regulation. It highlights the critical role of chromatin modifications in governing cell fate decisions across different species, offering a comprehensive view of the molecular dynamics at play during cellular differentiation and identity formation.

#### *4.1.1.2 Exploring pluripotency in PSCs through single-cell sequencing*

The pilot experiment utilizing single-cell sequencing to explore the PSC populations across mouse, cynomolgus, and human has shed light on the foundational aspects of pluripotency at a molecular level (**Figure 14**). ScRNA-seq data analysis provided a detailed map of the transcriptional states of PSCs, unveiling the shared gene expression profiles that highlight pluripotency across species (**Figure 15**). This accomplishment aligns with prior research showing the conservation of core pluripotency factors, such as OCT4, SOX2, and NANOG, in epiblast-like primed PSCs across various mammalian species [40], [64]. Furthermore, studies highlighting the preservation of the LIF/STAT3 signaling pathway in maintaining pluripotency across mouse and human stem cells, as well as research showing that the Activin/Nodal signaling pathway sustains pluripotency and is conserved among mammals, emphasize the evolutionary conservation of pluripotency regulatory mechanisms [226], [227]. Combined with the observations from the harmonization experiments, it is suggested that fundamental regulatory mechanisms, which control the pluripotent state, are conserved across different mammals, regardless of evolutionary differences. Nonetheless, fully harmonized conditions for comparative studies haven’t been realized before. The ability to standardize culturing conditions across species marks a significant breakthrough, significantly improving the ability to conduct precise experiments sensitive to both time and developmental stages.

#### *4.1.1.3 PSCs of various species are differentiated into NPCs using a standardized protocol*

Besides harmonizing PSC maintenance conditions, a uniform protocol was employed to differentiate PSCs from various mammalian species into NPCs, highlighting the conserved mechanisms underlying neural differentiation across mammals. The literature suggests that specific differentiation protocols can direct PSCs of different species toward neural lineages [61], [228], [229], [230]. I employed a dual SMAD inhibition protocol for anterior neural cell differentiation in mouse, cynomolgus, and human cells. However, multiple studies have demonstrated that a range of protocols and 2D and 3D culture systems similarly influence the timing of neural marker expression [107], [149], [231], [232], [233], [234], [235]. This strategy was confirmed to be highly efficient in neural conversion and the rapid generation of neural progenitors, demonstrated by the accelerated differentiation of PAX6 and SOX1 positive neural progenitors [236]. Three distinct differentiation protocols utilizing dual SMAD inhibition allowed for a comprehensive assessment of neural differentiation efficacy across species (**Table 12**). The observation of neuroepithelial sheet formation across all species and protocols by day ten, as evidenced by brightfield microscopy (**Figure 17A**) and subsequently confirmed by RT-qPCR (**Figure 17B-D**), highlights the robustness of the differentiation process.

The directed differentiation of PSCs into NPCs has illuminated the nuanced differences in developmental speed among the mouse, cynomolgus, and human species. RT-qPCR analysis of daily time points until day ten of differentiation confirmed the anticipated downregulation of pluripotency markers alongside the upregulation of neural markers, indicating successful NPC differentiation under the well-established '3N' protocol in all three species (**Figure 18**). The temporal analysis further refined the understanding of differentiation dynamics, revealing species-specific variations in the differentiation rate, already visible at the bulk level. Immunofluorescence staining provided additional layers of confirmation, visually demonstrating the progressive disappearance of pluripotency markers and the emergence of neural progenitor markers, further validating the RT-qPCR findings and highlighting species-specific differences during NPC differentiation (**Figure 19**). Such differences indicate that the general mechanisms behind differentiation may be conserved, but variability exists in the timing of these processes across species. Additionally, the time course RT-qPCR data revealed a remarkably rapid downregulation of pluripotent markers, emphasizing the importance of determining sampling time points for capturing the initial changes in RNA levels and chromatin states, which were analyzed in subsequent time course single-cell multiome sequencing studies (**Figure 20**). Therefore, I included a sample as early as 8 hours into the differentiation.

Numerous studies suggest that developmental timing can be modestly accelerated through various means [237], [238], [239], [240], [241], [242]. For example, modifying culture conditions has reduced the time needed to derive different types of neural cells from the human ESCs [241], [243], [244]. However, due to limited access to embryonic material, it is not entirely clear whether these methods genuinely change developmental timing or optimize conditions to more closely reflect natural *in vivo* rates [143], [245], [246]. By standardizing protocols, I addressed the issue of varying external factors affecting differentiation. Harmonizing culture conditions provides crucial insights into the mechanisms regulating development by removing external variables. The development of such standardized protocols represents a significant step forward in research on developmental timing, offering a robust framework for exploring developmental speeds across different PSCs, given their highly conserved nature of pluripotency and differentiation regulation.

### 4.1.2 Unraveling species-specific developmental timescales of mouse, cynomolgus, and human through single-cell multiome sequencing

#### *4.1.2.1 Single-cell sequencing reveals species-specific patterns of neural differentiation*

Through the application of time-course single-cell multiome sequencing, I provided an in-depth view of the transcriptional and chromatin changes during the neural differentiation of mouse, cynomolgus, and human PSCs. This method produced a detailed temporal map of gene expression (**Figure 21**) and chromatin accessibility dynamics (**Figure 22**), offering profound insights into the developmental mechanisms across these species.

Single-cell sequencing technologies, especially single-cell transcriptomics, have significantly advanced comparative analyses in developmental biology, offering detailed insights into early differentiation dynamics across various species, including mice, humans, monkeys, pigs, and rabbits [247], [248], [249], [250], [251], [252], [253]. These analyses have been supported by recent single-cell atlases of gastrulation-stage embryos, which enable quantitative comparisons of transcriptional landscapes to identify both conserved and divergent aspects of developmental control. Combined with functional studies, such atlases are crucial for investigating the molecular bases of developmental processes and associated disorders and align with the objectives of examining species-specific developmental timing. However, challenges such as small sample sizes in human datasets sometimes limit the scope of definitive conclusions in these studies. To address this, I implemented single-cell

multiome sequencing with a sampling of 10,000 cells at each time point, equating to approximately 3,333 cells per species. In the experiment, this approach accumulated a total of 74,000 cells, roughly 25,000 per species (**Table 14**), thereby enabling optimal data integration and the creation of the first comparative and comprehensive single-cell multiome sequencing data set for *in vitro* neural trajectories for each species, uncovering both shared features, such as the general linear neural differentiation trajectory across all species, and distinct features, such as species-specific dynamics of specific marker genes like SOX1 during the differentiation of PSCs. This robust experimental design involved directing the differentiation of NPCs over ten days for each species, with strategic sample collection at specific intervals aimed at minimizing sequencing batch effects and ensuring the production of high-quality data.

ScRNA-seq data revealed a continuous change in gene expression, effectively mapping the linear progression of NPC differentiation for each species (**Figure 21**). This analysis was further supported by scATAC-seq insights, which provided a view into the evolving landscape of chromatin accessibility that corresponded with the observed gene expression patterns, highlighting species-specific variations in the timing of these changes (**Figure 22**). For instance, all three species demonstrated decreased transcription and accessible chromatin at pluripotency markers such as OCT4 and NANOG, alongside increased PAX6 and SOX1 during NPC differentiation. These findings affirm the expected linear trajectory of neural progenitor differentiation and highlight the utility of single-cell multiome sequencing as an effective tool for capturing differentiation dynamics at a cellular level across species. Unlike bulk data, single-cell techniques enable detailed examination of individual cells and allow for analysis that yields more refined insights (**Figure 23**). Significant differences included mouse-specific expression of late-stage neuronal genes, indicating a more advanced differentiation stage within the ten days, especially highlighted by the ingest mapping analysis (**Figure 25**). Mouse cells advanced further along the differentiation trajectory and progressed rapidly, reaching the neural stage by day 2 (**Figure 24D**).

In contrast, cynomolgus and human cells took three (**Figure 24E**) and four days (**Figure 24F**) to reach the same stage. Further scRNA-seq analysis identified distinct signaling pathways active within human, cynomolgus, and mouse PSCs during neural differentiation (**Figure 29D**). Notably, cynomolgus cells exhibited higher expression levels of genes associated with glycogen metabolism compared to other species, underscoring how even closely related species like humans and macaques can display differences in their transcriptional programs.

#### *4.1.2.2 Quantification of species-specific differentiation rates from single-cell sequencing*

Furthermore, by applying linear regression models, I calculated the species-specific differentiation rates in both the transcriptomic and chromatin accessibility data between human and mouse, and for the first time between cynomolgus and mouse. The results indicated that mouse cells differentiate approximately 2.4 times faster than human cells and 2.2 times faster than cynomolgus cells based on gene expression data (**Figure 25F**). Despite the scATAC-seq data containing more noise, it demonstrated similar trends, with mouse cells differentiating 1.9 times faster than human cells and 1.7 times faster than cynomolgus cells (**Figure 26F**). This comprehensive analysis underscores how cells from different species align and differ in their differentiation trajectories. It shows that mouse cells exhibit the fastest differentiation speeds, followed by cynomolgus, with human cells progressing slowest. These findings confirmed that cells maintained species-specific differentiation rates *in vitro* and resemble others previously reported in comparative developmental speed research comparing human and mouse development in different contexts. Rayon et al. reported a scaling factor of 2.5x between human and mouse during motor neuron differentiation from bulk scRNA-seq data [148]. In pulse-chase experiments, human neural proteins were twice as stable as those in mice. EdU labeling of mouse and human NPCs also demonstrated that the cell cycle in mouse cells is approximately 2.5 times faster than in human cells. Matsuda et al. reported that the oscillation periods of HES7 in mouse PSM cells are 2 to 3 times faster than those in human cells, corresponding with the differences in protein half-lives observed between the two species [20]. Furthermore, Diaz-Cuadros et al. linked the HES7 oscillation periods to the mass-specific oxygen consumption rates and glycolytic rates, which were approximately two times higher in mouse PSM cells compared to human cells [21].

Furthermore, I observed genes with species-specific temporal expression differences, mostly related to neural differentiation (**Figure 21B**), reinforcing bulk RNA sequencing experiments conducted by Barry et al. [83]. Their study observed that despite varied experimental conditions, the intrinsic species-specific differentiation rates were consistently maintained *in vitro*. Their findings further reveal that when differentiated in teratomas within a mouse host, human ESCs retain their species-specific developmental timing rather than adopting the host's, suggesting an intrinsic mechanism governing developmental timing. Despite the longer duration generally required for differentiation procedures in human PSCs compared to mouse PSCs, the results underscore a remarkable degree of cell autonomy in maintaining species-specific developmental timing *ex utero*. Thus, by creating a consistent environment for differentiation for time course single-cell

multiome experiments, the results highlighted the intrinsic nature of species-specific developmental timing, mirroring principles observed in classical transplantation experiments across various biological systems. Species-specific autonomy in developmental timing and size regulation is a well-documented phenomenon that spans cellular to tissue levels. Historical amphibian transplantation experiments have shown that the properties of the transplant, are predominantly determined by the species of origin rather than the host, demonstrating significant species-specific autonomy [140], [141]. More recent studies, such as chick limb transplants between chicks at different developmental stages, have similarly observed the retention of donor stage-specific intrinsic timing [142]. Furthermore, autonomy in the timing of neural and glial precursor differentiation, fate choices, and apoptosis has been well-established in mouse and rat studies, as well as in transplants and *ex vivo* cultures [144], [145], [146], [147], [254]. These patterns highlight the robustness of species-specific developmental mechanisms, which operate independently of the surrounding environment. In contrast, when rat PSCs were injected into pancreatogenesis-disabled mouse blastocysts, the resulting chimeras developed into fully functional organisms with properties of the host and species-specific organogenesis. This suggests that environmental control over development is still possible and requires further investigation [179].

#### *4.1.2.3 Using single-cell data to identify variances in differentiation speed within a species*

Investigation was conducted to identify processes that might influence developmental timing. Initially, I performed GO analysis on differentially expressed genes across species, but the results only vaguely described general biological processes (**Figure 29A-C**). After a literature review, I corroborated lists of biological processes known to impact developmental speed [20], [21], [83], [148], [152], [158], [160], [165], [166], [167], [168], [255]. Comparative models of differentiation in PSM cells and motor neurons in mice and humans provided insights into the mechanisms affecting developmental speed [20]. It was suggested that inter-species period differences depend on transcription and translation kinetics. The significance of protein turnover was underscored by treatments with translation inhibitors in human PSM cells, further slowing down HES7 oscillations. However, previous studies have not identified specific genes that govern these species-specific differences. Additionally, my analysis of the transcriptomic data did not reveal any species-specific expression patterns that might suggest variations in protein turnover on a transcriptomic level (**Figure 29D**).

However, through single-cell transcriptomic analysis, I identified UGP2 as a candidate gene upregulated in slower-differentiating species, particularly at the exit of pluripotency (**Figure 30D**). In addition, the possibility that mechanisms responsible for variations in developmental speed within a species might also contribute to differences between species was investigated. By comparing individual cells with nearly identical gene expression profiles from separate time points, cells that rapidly differentiate and those that differentiate at a slower pace within each species were identified (**Figure 28**). A comparison between fast-differentiating cells and their slower counterparts allowed for determining a set of candidate genes. Notably, UGP2 emerged as a gene of significant interest during these comparisons. I observed that UGP2 exhibited higher expression in slower-differentiating cells compared to their faster counterparts across all three species, although this was less pronounced in mouse cells (**Figure 31**). This detailed analysis was made possible through the resolution provided by single-cell sequencing.

The analysis of gene expression and chromatin accessibility profiles from single-cells across mouse, cynomolgus, and human species has illuminated the distinct dynamics of NPC differentiation, highlighting marked differences in developmental timelines. Single-cell multiome sequencing data has offered profound temporal insights into differentiation, revealing that each species strictly adheres to its intrinsic developmental timeline despite employing a uniform differentiation protocol. This finding emphasizes a significant degree of cellular autonomy in developmental pacing [83]. Integrating previously observed findings in the literature with time course single-cell sequencing data from this thesis highlights a complex landscape in developmental biology, demonstrating that species-specific differentiation rates are maintained through a remarkable degree of cell autonomy.

### 4.1.3 The computational study of non-model organisms in developmental biology

Since Yamanaka's groundbreaking generation of the first iPSCs, researchers have established iPSC lines from diverse species, but with varying degrees of success [82], [256], [257], [258], [259]. These efforts have significant implications, broadening our understanding of developmental biology across different species and offering a potential tool for conservation efforts to save animals from extinction, such as the northern white rhino [260]. Furthermore, iPSCs have opened new avenues to study the embryonic development of species where obtaining embryonic material is challenging, highlighting the impact of this technology on the study of developmental biology and timing.

Studying less commonly researched non-model organisms holds significant potential for advancing developmental studies. The study by Lázaro et al. [160] explores how various mammalian species, including marmosets, rabbits, cattle, southern white rhinos, mice, and humans, regulate the pace of cellular development through a diverse array of stem cell models referred to as a 'stem cell zoo.' By differentiating PSCs into PSM-like cells, the research team can replicate the segmentation clock *in vitro*, offering a controlled environment to dissect the cellular mechanisms behind developmental timing. By employing live-cell imaging with a HES7 reporter and fluorescent markers, they can monitor cell behavior and protein dynamics in real-time, enabling them to study developmental timing effectively. Although single-cell sequencing data provides a deeper insight into the molecular mechanisms that govern developmental speed, it has certain limitations when working with non-model organisms. There are challenges with unavailable or poorly annotated reference genomes. For instance, in this thesis, genome alignment using maximum count assignment indicated variable success across different species (**Figure 14C-D**). Cells from cynomolgus and mouse aligned well with their reference genomes, showcasing a high concordance. However, the sengi presented significant difficulties, with only 318 cells aligning correctly, while 4604 cells were assigned to the human genome (**Table 13**). This misalignment was likely not due to the genetic similarity of the sengi to the human but rather the superior quality of the human genome reference.

Further examination of count distributions highlighted the challenges faced by the sengi cells. Unlike in samples from mouse and cynomolgus, the human samples displayed a substantial number of cells with low counts, possibly stemming from erroneously annotated sengi cells (**Figure 14C**). Consequently, the sengi cells were excluded from further analyses due to the recurrent inaccuracies in cell mapping and the limitations of the current genomic tools. The strategic exclusion of sengi cells from the time course experiments highlights the broader challenges faced in the field, where the reliability of data from well-characterized species far exceeds that from less studied ones, directing the focus towards organisms with better-established genomes. In addition, even when cell assignment was successful, analyzing the cynomolgus dataset proved challenging due to its non-standard model status. This issue was particularly pronounced during ATAC sequencing, which required significant adaptations since many of the available analysis tools were primarily optimized for human or mouse datasets, further complicating the analysis of cynomolgus data [210].

However, there is still much to be gained by including these non-model species. I added one more species to the comparison panel by incorporating the cynomolgus. This allowed me to examine an organism whose physiology is intermediate between humans and mice,

providing a more comprehensive analysis beyond the previous studies that only compared humans and mice at a functional level [20], [21], [83], [148].
In summary, using iPSCs and a 'stem cell zoo' enables detailed developmental biology studies across various species, employing advanced techniques like live-cell imaging and single-cell sequencing. Challenges such as inadequate reference genomes for non-model organisms complicate data analysis, highlighting the need for improved genomic tools.

### 4.1.4 Dissecting the relationship between the cell cycle and differentiation speed

#### *4.1.4.1 Species-specific differences are reflected in the cell cycle*

Previous research has indicated a correlation between species-specific cell cycle duration and the rate of differentiation at the population level [20], [21], [148]. Additionally, during *in vitro* neural differentiation, it was observed that both human and non-human primate pluripotent cells regulate their cell cycle and post-mitotic states of maturation in ways that reflect their species of origin [150], [152], [156]. This consistency suggests that the cell cycle may play a significant role in regulating developmental speed, providing a compelling perspective for investigation into how cell cycle dynamics influence developmental processes. To investigate the role of the cell cycle in NPC differentiation, single-cell technologies such as single-cell sequencing, and live-cell imaging were utilized. This approach was employed to test whether the relationship between cell cycle duration and differentiation speed persists at the individual cell level and to determine if the cell cycle causally influences differentiation speed.
Using transcriptomic data, individual cells were assigned to specific cell cycle phases based on gene scores calculated from marker genes associated with each phase [205], [206]. This method facilitated a detailed examination of cell cycle phase compositions across mouse, cynomolgus, and human PSCs and NPCs. I observed that the fewest cells were in the G1 phase, supporting literature suggesting that PSCs typically have a shortened G1 phase, and consequently, fewer cells are captured in this phase (**Figure 16**) [111], [261], [262], [263]. Generally, mouse ESCs are characterized by a highly abbreviated G1 phase, which facilitates rapid cycling between cell division during M-phase and DNA synthesis during S-phase, allowing these cells to progress quickly through the cell cycle [109], [264], [265]. Across species, ESCs, particularly mouse ESC, have notably short G1 phases, approximately 1 hour, compared to 2–3 hours in human [111]. This difference reflects the more naïve/ground pluripotent state of mouse ESCs in contrast to the primed pluripotent state of primate ESCs.

Therefore, mouse EpiSCs, which more closely resemble human ESCs, exhibit slightly longer cell cycles than mouse ESCs [62]. The analysis of cell cycle phase distributions during NPC differentiation revealed species-specific patterns of cellular dynamics (**Figure 27**). UMAP visualizations and detailed phase distributions indicated that mouse cells transition uniquely towards a post-mitotic state, contrasting with the more evenly distributed cell cycle phases observed in cynomolgus and human cells throughout the differentiation process. These observations coincide with detecting a more mature neuronal state in mouse EpiSCs, indicating that mouse cells surpass the progenitor state and differentiate into neurons over the ten days [83]. This comprehensive exploration into the cell cycle and differentiation dynamics offers valuable insights into the complex interplay between these two fundamental aspects of developmental biology.

#### *4.1.4.2 Exploring the impact of cell cycle manipulation on neural differentiation speed*

Furthermore, my collaborators explored how manipulating the cell cycle affects the differentiation speed, explicitly investigating whether cells with extended or reduced cell cycle durations could still differentiate into neural progenitors and how these alterations might influence differentiation speed. As previously mentioned, the research conducted by Dr. Christian Schröter and his Ph.D. student Julia Schröder is pivotal to the context of my thesis. It will be part of a jointly drafted manuscript with shared authorship (unpublished data). Given the significance, I will discuss their unpublished findings to provide a comprehensive understanding of the investigations into the role of the cell cycle.

PSC lines from all species were generated to examine cell cycle duration differences between species, expressing the PIP-FUCCI sensor [266], [267]. This sensor allowed for precise tracking of cell cycle phases by expressing two fluorescent reporter proteins, facilitating live-cell imaging of these lines. During the pluripotent stage, this imaging confirmed that all cells maintained a typical pluripotency-associated cell cycle structure characterized by an elongated S-phase and a very short G1-phase. Significant differences were observed in the total cell cycle durations across species. It was noted that mouse cells exhibited the shortest cell cycle, averaging 10.1 hours, while human cells had the longest average duration of 14.8 hours, corresponding to 1.47 times the duration of the mouse cell cycle. Cynomolgus cells displayed an intermediate duration, averaging 14.3 hours, which is 1.42 times the duration of the mouse cell cycle, aligning closely with human cells and consistent with established literature [111], [261], [263]. This variation in cell cycle rates correlated with differences in cell differentiation rates among the species (**Figure 25F, Figure 26F**). Additionally, when the durations of individual cell cycle phases were

normalized to the total cell cycle length, the cell cycle structure appeared very similar across species, indicating that the shortening or lengthening of specific cell cycle phases did not influence species-specific differentiation speeds.

Investigations were conducted to explore further the relationship between cell cycle duration and differentiation speed to determine whether cells with altered cell cycle lengths could still effectively differentiate into neural progenitors. The focus was on how metabolic pathways, particularly the mTOR pathway, influence differentiation speed. Various techniques were employed to manipulate the cell cycle, explicitly targeting the mTOR pathway using the small molecule inhibitor INK128 [161]. This intervention significantly extended the cell cycle duration, which was meticulously monitored using time-lapse imaging of PIP-FUCCI reporter lines. Despite the prolongation induced by mTOR inhibition, the proportions of the cell cycle phases relative to the overall duration were maintained consistently. However, this extensive alteration in cell cycle duration didn't strongly influence the timing of neural marker expression, evidenced by specifically PAX6 and SOX1 stainings. Similarly, Okamoto et al. [268] demonstrated that during cerebral development, the differentiation of apical progenitors into mature neurons is unaffected by an induced cell cycle arrest, suggesting that this phenomenon might be a unique aspect of neural development. ScRNA-seq was conducted on both cells treated with the mTOR pathway inhibitor INK128 and untreated cells to verify this unexpected result further. The findings reinforce the earlier notion that the cell cycle does not causally influence the differentiation speed.

While a similar trend between cell cycle duration and differentiation speed is evident across species, the cell cycle itself may not directly cause species-specific differences in differentiation speed. Although these two factors follow the same pattern within inter-species comparisons, the impact of the cell cycle on the timing of differentiation appears to be more subtle, highlighting the complexity of the mechanisms governing developmental speed.

### 4.1.5 The role of UGP2 in metabolic regulation of developmental timing

#### *4.1.5.1 The impact of metabolic regulation on developmental timing*

Single-cell transcriptomic analysis revealed that UGP2 is a candidate gene upregulated in species and cells that differentiate more slowly, especially at the transition from pluripotency (**Figure 30**). The findings suggest that glycogen metabolism may play a

significant role in regulating developmental speed. UGP2, or UDP-glucose pyrophosphorylase 2, is crucial in mammalian carbohydrate metabolism. It functions as an enzyme to form UDP-glucose, which is ultimately stored as glycogen molecules. This enzyme activity is essential for glucose conversion, supporting various cellular metabolic pathways [215].

Recent research has focused on how metabolism influences developmental timing. Mouse PSM cells exhibited higher metabolic rates and faster HES7 oscillations than humans [21]. Pharmacological inhibition of the electron transport chain in human PSM cells slows the HES7 period, while overexpression of NADH oxidase speeds up the segmentation clock by increasing translation rates. From the cross-species transcriptome comparison, I couldn't link transcriptional differences in the electron transport chain or NADH metabolism to these observations as other post-transcriptional mechanisms might be at play here (**Figure 29D**). Similar behavior was noted during the *in vitro* differentiation of mouse and human ESCs into motor neurons, where human cells exhibited slower progression linked to greater protein stability [148]. Further studies have shown that larger animals have more stable proteomes and slower protein turnover, which correlates with lower ATP production rates [158]. These findings suggest that differences in metabolic rates might regulate varying developmental timelines, linking developmental timing with cellular and metabolic states and implying that environmental and metabolic conditions significantly impact developmental programs.

UGP2 may serve as a crucial regulator of metabolic rates by limiting glucose availability within cells, thereby restricting downstream metabolic processes. The hypothesis suggests that glucose is stored as glycogen in primate cells where UGP2 is active, limiting the cell's energy supply and influencing the differentiation speed. Conversely, in mice, where UGP2 is not expressed in the pluripotent state, glucose is more readily available, ultimately leading to faster differentiation. This hypothesis was tested through functional experiments by deleting UGP2 in slower-differentiating primate species to accelerate their differentiation processes.

#### *4.1.5.2 KO of UGP2 in slow-differentiating species manipulates developmental speed*

The application of CRISPR/Cas9 technology for editing the UGP2 gene in human and cynomolgus PSCs has enhanced our understanding of its role in developmental timing (**Figure 32**). NPC differentiation was performed for UGP2 KO cell lines, compared to wildtype differentiation, and analyzed via RT-qPCR. An upregulation of neural markers SOX1 and PAX6 and earlier onset of late-stage neural marker FOXG1 in human (**Figure 33A-D**), as

well as early onset of FOXG1 expression in cynomolgus (**Figure 33E-G**), was observed in UGP2 KO, indicating accelerated neural differentiation. Furthermore, immunostainings performed by my collaborator, Julia Schröder, at the Max Planck Institute of Molecular Physiology, demonstrated that during neural differentiation of UGP2 KO lines, the expression of later-stage neural marker FOXG1 was significantly accelerated in cells lacking functional UGP2 (unpublished data). Additionally, it was observed that UGP2 KO cells had substantially lower glycogen storage than their wild-type counterparts.

Interestingly, the wild-type mouse cells exhibited very low glycogen storage, similar to primate KO cells. This substantial reduction in glycogen granules further emphasizes the crucial function of UGP2 in glycogen metabolism and storage, affirming its importance in maintaining cellular energy homeostasis and overseeing critical metabolic activities. These findings highlight the vital influence of UGP2 in developmental biology, aligning with Perenthaler et al.'s research that associates UGP2 loss with a severe developmental neurological disorder [217]. Developmental and/or epileptic encephalopathies are severe genetic conditions characterized by early-onset seizures resistant to treatment, developmental delays, progressive microcephaly, visual impairments, and subtle facial dysmorphisms. In their study, they examined 22 individuals from 15 families with a severe type of treatment-resistant epilepsy. A consistent homozygous mutation was discovered in the UGP2 gene, leading to decreased levels of this critical enzyme in neural stem cells. Consequently, this impacts glycogen metabolism and causes premature neuronal differentiation in *in vitro* models.

In both human and mouse models, ESCs shift from a high rate of glycolysis to greater reliance on oxidative phosphorylation, thus increasing their mitochondrial respiratory capacity as they differentiate, and their rate of cell division slows. Notably, variations in UGP2 expression between and within species are most marked during the pluripotent state and at the exit of pluripotency (**Figure 30D**). Glycolysis plays a crucial role in the rapid expansion of PSCs, providing quick energy despite its lower ATP efficiency compared to oxidative phosphorylation, which is essential for the growth and proliferation of these cells [269]. The KO of the UGP2 gene in stem cells significantly impacts glycogen storage capacity, potentially increasing glucose availability from the culture media for glycolysis. Research shows that rapidly proliferating mouse ESCs heavily utilize aerobic glycolysis [269], as evidenced by the upregulation of glycolytic pathways in mouse samples in scRNA-seq data (**Figure 29D**). This dependency on glycolysis indicates the importance of accessible glucose for rapid energy production in faster-dividing mouse and UGP2 KO primate cells with accelerated neural differentiation.

In conclusion, using CRISPR/Cas9 technology to delete UGP2 in human and cynomolgus PSCs has revealed its significant role in impacting glycogen metabolism and, therefore, regulating the pace of neural differentiation. These findings offer evidence supporting the hypothesis that UGP2 functions as a crucial regulator of metabolic rates by controlling glucose availability, thereby influencing downstream metabolic processes and the speed of cellular differentiation. Furthermore, this indicates that in wild-type primate PSCs where UGP2 is present, glucose is stored as glycogen, limiting the immediate energy supply and potentially slowing the differentiation process (**Figure 34**). Conversely, in mouse cells where UGP2 expression is absent in the pluripotent state and throughout neural differentiation, glucose remains more readily available, ultimately leading to faster differentiation rates. This dynamic suggests that UGP2 may serve as a metabolic gatekeeper, dictating the availability of glucose for energy production and, thus, the pace of stem cell differentiation across different species. The link between UGP2 deficiency and severe developmental disorders such as developmental and/or epileptic encephalopathies, characterized by treatment-resistant seizures and developmental delays, underlines the fundamental role of UGP2 in neural development and metabolic regulation [217]. This investigation enhances our understanding of cellular metabolism by correlating these findings with the hypothesis that UGP2 regulates glucose availability, thereby influencing species-specific differentiation speeds and lays the groundwork for future studies into species-specific developmental timing mechanisms.

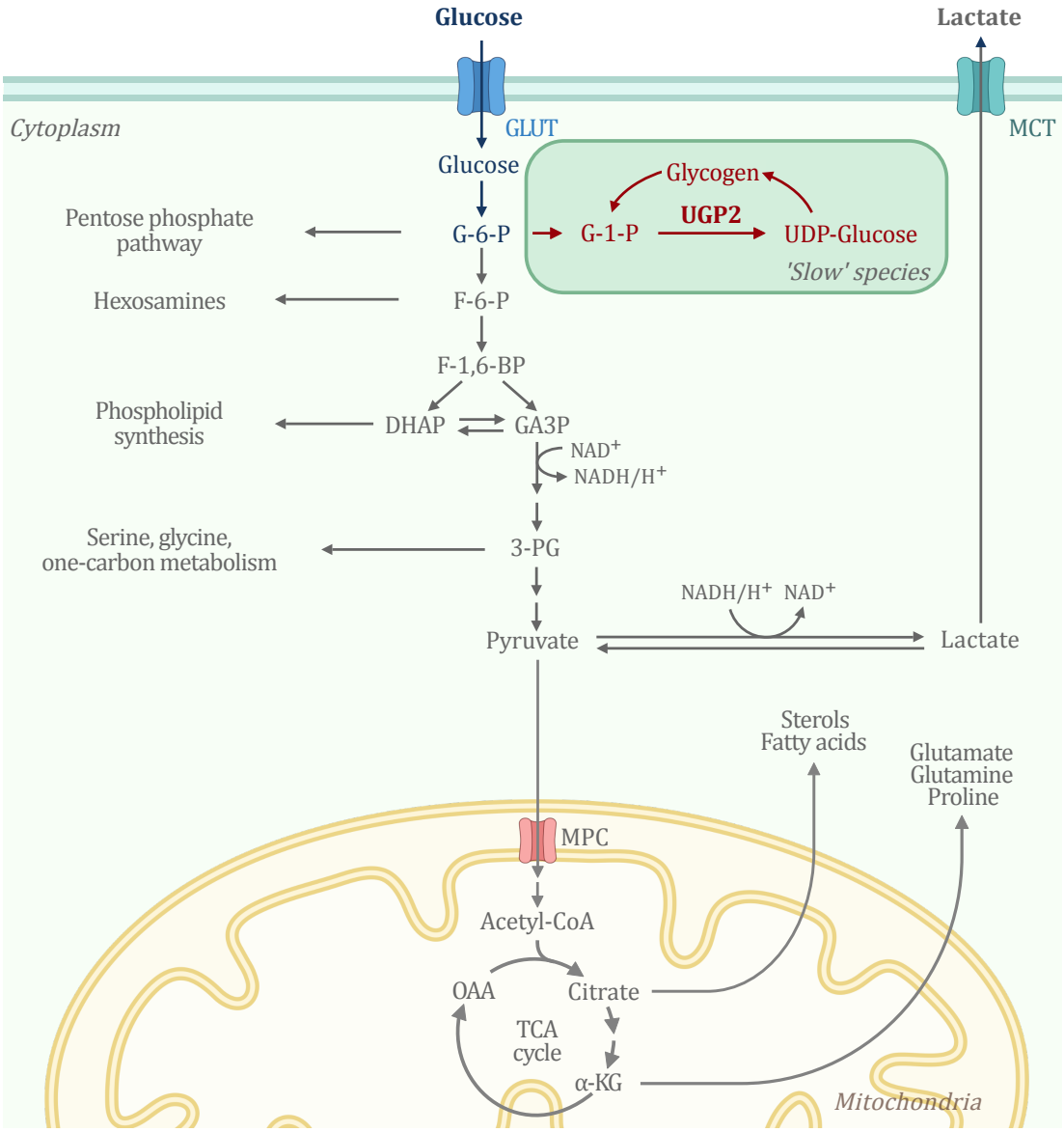


**Figure 34. Function of UGP2 in glucose metabolism of PSCs.** Schematic illustration of the function of UGP2. Active UGP2 leads to the conversion of G-1-P to UDP-Glucose and subsequent glycogen synthesis. GLUT = Glucosetransporter, MCT = Monocarboxylate transporter, G-6-P = Glucose 6-phosphate, G-1-P = Glucose 1-phosphate, UDP = Uridine diphosphate, UGP2 = UDP-glucose pyrophosphorylase 2, F-6-P = Fructose 6-phosphate, F-1,6-BP = Fructose 1,6-Bisphosphate, DHAP = Dihydroxyacetone phosphate, GA3P = Glyceraldehyde 3-phosphate, 3-PG = 3-Phosphoglycerate, TCA = Tricarboxylic acid, MPC = Mitochondrial pyruvate carrier, α-KG = α-Ketoglutarate, OAA = Oxaloacetic acid. Created with BioRender.com.

## 4.2 Conclusion and outlook

In this thesis, I investigated the regulation of developmental timing across mammals, revealing a complex and multifaceted nature. It emphasizes the intricate interplay among genetic, epigenetic, and extracellular factors that guide the transition from a fertilized oocyte to a mature organism. Notably, single-cell sequencing to identify UGP2 as a gene of interest and the functional analysis of UGP2 through CRISPR/Cas9 gene editing has enhanced our understanding of the molecular mechanisms that govern developmental speed across species. Developing refined and universally applicable *in vitro* models, demonstrated by the successful harmonization of PSC culture conditions, also marks a promising direction for future research. These models enable more standardized and replicable studies, thereby improving the reliability and broader applicability of developmental biology research.

Looking forward, the research initiated by Yamanaka and continued through diverse efforts like those by Lázaro et al. show where iPSCs can serve as pivotal tools for comparative developmental biology. The ability to generate iPSC lines from under-studied species opens promising avenues for investigating the unique developmental processes of non-model organisms. Despite the challenges associated with genome sequencing inaccuracies and the limitations of analytical tools primarily designed for model species, single-cell sequencing techniques are still beneficial for future advancements. Emerging technologies and improved computational methods are expected to enhance genome annotation and alignment processes, increasing the accuracy of developmental studies involving less common species [270], [271]. Nanopore sequencing of the sengi genome has recently been performed and is currently being assembled. This pivotal advancement provides a foundational basis that, it is hoped, will eventually facilitate detailed studies into sengi developmental speed regulation and significantly enrich our understanding of mammalian development by shedding light on the complex biology of the Afrotheria. This evolution in tools and techniques will likely expand the accessibility of the 'stem cell zoo' concept in bioinformatic studies to include an even broader array of species, offering more refined insights into the molecular mechanisms of development across mammals. Future research should aim to extend the scope of current studies to a broader array of species and developmental stages, particularly by leveraging advances in genome quality and availability for 'exotic' species. This expansion is crucial for enhancing our understanding of how developmental timing is conserved or varies across the mammalian clade, offering more profound insights into evolutionary biology and species adaptation.

Furthermore, an essential tool in this endeavor could be MultiVelo [272]. This computational tool enhances the analysis of multi-omic single-cell datasets by integrating both epigenomic and transcriptomic data. MultiVelo builds on the RNA velocity concept to include epigenomic information, significantly improving the accuracy of cell fate predictions beyond traditional RNA-only methods. Utilizing MultiVelo in future analysis could prove exceptionally beneficial for dissecting the complex temporal dynamics between the epigenome and transcriptome during development across different species. This approach could facilitate a more profound understanding of species-specific regulatory mechanisms that influence developmental timing and may uncover evolutionary variations in gene regulation and cell state transitions, potentially elucidating regulatory differences in developmental speeds.

Recent research has shed light on the role of epigenetic factors in regulating developmental timing, especially in the context of neuronal development. Studies have shown that specific epigenetic barriers set up during the progenitor stage can delay the maturation of human cortical neurons, with key enzymes such as EZH2, EHMT1/2, or DOT1L playing vital roles in maintaining these barriers [168]. Additionally, the translational regulation of histone modification enzymes, mainly through the rRNA methyltransferase FBL, has been shown to impact the timing of neural stem cell development by modifying H3K27 trimethylation [167]. Moreover, research has revealed that PCR2 is crucial for temporal patterning during mouse corticogenesis, as it establishes 'temporal molecular birthmarks' in progenitors that significantly affect adult neuronal diversity [166]. These discoveries underscore the potential of targeting epigenetic factors to manipulate developmental speeds, offering promising new directions for understanding evolutionary variances in development across species. Such insights pave the way for epigenetic modulation techniques to either accelerate or delay cellular differentiation, providing essential tools for studying and potentially controlling developmental timing.

The role of UGP2 in metabolic regulation and its implications for developmental timing merits further investigation. Observations that UGP2 KO accelerates neural differentiation in specific mammalian models suggest potential strategies for modulating this pathway to manipulate cell maturation. To better understand how UGP2 influences developmental pacing, scRNA-seq of wildtype versus KO models will provide detailed insights into the developmental differences and impacts of UGP2 KO during cell differentiation. Another interesting angle would include overexpressing UGP2 in mouse EpiSCs to determine if this can slow down differentiation speeds, providing further insights into its regulatory mechanisms.

Additionally, investigating the metabolism of PSCs from different species during differentiation and how UGP2 KO affects glycolytic metabolic pathways will be crucial. This approach will help to understand the broader metabolic impacts of UGP2 and its potential as a target for controlling developmental processes across species. Mammalian development is intricately regulated, involving critical developmental decisions influenced by interactions among various tissues. Although this study highlights cell autonomous, species-specific developmental timings, it also acknowledges that they are not immune to external influences. While developmental timing was consistent during anterior neural differentiation, this consistency may not extend to the differentiation processes of other organ systems. Future research should involve differentiating wildtype and KO cells into other germ layers to further explore whether the regulation of differentiation speed is specific to neuro-ectodermal tissues or represents a broader mechanism. This approach will enable functional studies that provide deeper insights into the specificities and generalities of developmental speed regulation across different cell types.

Furthermore, the regulation of cell cycle speed is closely linked to metabolism, which can significantly influence cell proliferation. Research indicates that metabolic pathways are responsive to changes in proliferation and can also regulate it [273]. In mammalian cells, where nutrients are typically plentiful, decisions about cell division are primarily driven by signaling pathways. However, under certain conditions, nutrient availability can become a pivotal factor. For example, ATP/AMP ratios have been shown to play a critical role in deciding whether cells commit to proliferation or enter quiescence [274]. Specifically, in glucose and energy scarcity conditions, cells may lack sufficient energy to complete a cell cycle [273]. Conversely, in pancreatic beta-cells, glucose uptake has been observed to promote cell proliferation by activating the PI3K and AKT pathways, activating forkhead box O transcription factors [273], [275]. These transcription factors then downregulate the cyclin D2 repressor BCL-6, leading to increased transcription of cyclin D2 and promoting beta-cell division [275]. This mechanism illustrates how glucose availability can drive the proliferation of insulin-secreting cells within the pancreas. Exploring whether UGP2 might also regulate cell cycle speed could provide deeper insights into the global machinery behind species-specific developmental speed differences.

The findings from this research pave the way for multiple new paths of investigation. A deeper understanding of the factors that regulate the pace of cell differentiation could enhance methods used in tissue engineering and stem cell therapy, where precise timing and synchronization of cell maturation are essential for the successful integration and functionality of tissues.

In conclusion, the insights garnered from this thesis not only deepen our fundamental comprehension of developmental biology and species-specific developmental timing but also lay the groundwork for forthcoming advancements. The future direction will involve further merging these discoveries with the latest technologies in genomics and bioinformatics to elucidate the complex mechanisms of developmental timing and regulation.

# Bibliography

[1] A. E. Rougvie, “Control of developmental timing in animals,” *Nat. Rev. Genet.*, vol. 2, no. 9, pp. 690–701, Sep. 2001, doi: 10.1038/35088566.

[2] A. E. Rougvie, “Intrinsic and extrinsic regulators of developmental timing: from miRNAs to nutritional cues,” *Development*, vol. 132, no. 17, pp. 3787–3798, Sep. 2005, doi: 10.1242/dev.01972.

[3] M. Kohwi and C. Q. Doe, “Temporal fate specification and neural progenitor competence during development,” *Nat. Rev. Neurosci.*, vol. 14, no. 12, pp. 823–838, Dec. 2013, doi: 10.1038/nrn3618.

[4] G. N. Wilson, J. M. Optiz, and J. F. Reynolds, “Heterochrony and human malformation,” *Am. J. Med. Genet.*, vol. 29, no. 2, pp. 311–321, 1988, doi: 10.1002/ajmg.1320290210.

[5] D. Duboule, “Temporal colinearity and the phylotypic progression: a basis for the stability of a vertebrate Bauplan and the evolution of morphologies through heterochrony,” *Dev. Camb. Engl. Suppl.*, pp. 135–142, 1994.

[6] A. S. Mao and D. J. Mooney, “Regenerative medicine: Current therapies and future directions,” *Proc. Natl. Acad. Sci.*, vol. 112, no. 47, pp. 14452–14459, Nov. 2015, doi: 10.1073/pnas.1508520112.

[7] S. Y. Sokol, “Spatial and temporal aspects of Wnt signaling and planar cell polarity during vertebrate embryonic development,” *Semin. Cell Dev. Biol.*, vol. 42, pp. 78–85, Jun. 2015, doi: 10.1016/j.semcdb.2015.05.002.

[8] S. B. Carroll, “Evo-Devo and an Expanding Evolutionary Synthesis: A Genetic Theory of Morphological Evolution,” *Cell*, vol. 134, no. 1, pp. 25–36, Jul. 2008, doi: 10.1016/j.cell.2008.06.030.

[9] B. K. Hall, “Evo-Devo: evolutionary developmental mechanisms,” 2003.

[10] M. H. Johnson and M. L. Day, “Egg timers: how is developmental time measured in the early vertebrate embryo?,” *BioEssays*, vol. 22, no. 1, pp. 57–63, 2000, doi: 10.1002/(SICI)1521-1878(200001)22:1<57::AID-BIES10>3.0.CO;2-L.

[11] R. C. Beattie, R. Tyler-.Tones, and M. J. Baxter, “The effects of pH, aluminium concentration and temperature on the embryonic development of the European common frog, Rana temporaria,” *J. Zool.*, vol. 228, no. 4, pp. 557–570, 1992, doi: 10.1111/j.1469-7998.1992.tb04455.x.

[12] S. Yahav and J. Brake, “Chick embryogenesis: a unique platform to study the effects of environmental factors on embryo development,” *J. Stem Cells*, vol. 9, no. 1, pp. 17–37, 2014.

[13] M. Seron-Ferre, G. J. Valenzuela, and C. Torres-Farfan, “Circadian clocks during embryonic and fetal development,” *Birth Defects Res. Part C Embryo Today Rev.*, vol. 81, no. 3, pp. 204–214, 2007, doi: 10.1002/bdrc.20101.

[14] D. Vallone, K. Lahiri, T. Dickmeis, and N. S. Foulkes, “Start the clock! Circadian rhythms and development,” *Dev. Dyn.*, vol. 236, no. 1, pp. 142–155, 2007, doi: 10.1002/dvdy.20998.

[15] T. Rayon, “Cell time: How cells control developmental timetables,” *Sci. Adv.*, vol. 9, no. 10, p. eadh1849, Mar. 2023, doi: 10.1126/sciadv.adh1849.

[16] R. Aires, A. D. Jurberg, F. Leal, A. Nóvoa, M. J. Cohn, and M. Mallo, “Oct4 Is a Key Regulator of Vertebrate Trunk Length Diversity,” *Dev. Cell*, vol. 38, no. 3, pp. 262–274, Aug. 2016, doi: 10.1016/j.devcel.2016.06.021.

[17] I. T. Fiddes *et al.*, “Human-Specific NOTCH2NL Genes Affect Notch Signaling and Cortical Neurogenesis,” *Cell*, vol. 173, no. 6, pp. 1356-1369.e22, May 2018, doi: 10.1016/j.cell.2018.03.051.

[18] R. Mallarino, P. R. Grant, B. R. Grant, A. Herrel, W. P. Kuo, and A. Abzhanov, “Two developmental modules establish 3D beak-shape variation in Darwin’s finches,” *Proc. Natl. Acad. Sci. U. S. A.*, vol. 108, no. 10, pp. 4057–4062, Mar. 2011, doi: 10.1073/pnas.1011480108.

[19] N. L. Badlangana, J. W. Adams, and P. R. Manger, “The giraffe (Giraffa camelopardalis) cervical vertebral column: a heuristic example in understanding evolutionary processes?,” *Zool. J. Linn. Soc.*, vol. 155, no. 3, pp. 736–757, 2009, doi: 10.1111/j.1096-3642.2008.00458.x.

[20] M. Matsuda *et al.*, “Species-specific segmentation clock periods are due to differential biochemical reaction speeds,” *Science*, vol. 369, no. 6510, pp. 1450–1455, Sep. 2020, doi: 10.1126/science.aba7668.

[21] M. Diaz-Cuadros *et al.*, “Metabolic regulation of species-specific developmental rates,” *Nature*, vol. 613, no. 7944, Art. no. 7944, Jan. 2023, doi: 10.1038/s41586-022-05574-4.

[22] S. Ladstätter and K. Tachibana, “Genomic insights into chromatin reprogramming to totipotency in embryos,” *J. Cell Biol.*, vol. 218, no. 1, pp. 70–82, Jan. 2019, doi: 10.1083/jcb.201807044.

[23] M. A. Eckersley-Maslin, C. Alda-Catalinas, and W. Reik, “Dynamics of the epigenetic landscape during the maternal-to-zygotic transition,” *Nat. Rev. Mol. Cell Biol.*, vol. 19, no. 7, pp. 436–450, Jul. 2018, doi: 10.1038/s41580-018-0008-z.

[24] D. Jukam, S. A. M. Shariati, and J. M. Skotheim, “Zygotic Genome Activation in Vertebrates,” *Dev. Cell*, vol. 42, no. 4, pp. 316–332, Aug. 2017, doi: 10.1016/j.devcel.2017.07.026.

[25] C. Zhang, M. Wang, Y. Li, and Y. Zhang, “Profiling and functional characterization of maternal mRNA translation during mouse maternal-to-zygotic transition,” *Sci. Adv.*, vol. 8, no. 5, p. eabj3967, Feb. 2022, doi: 10.1126/sciadv.abj3967.

[26] H. P. Pratt, C. A. Ziomek, W. J. Reeve, and M. H. Johnson, "Compaction of the mouse embryo: an analysis of its components," *J. Embryol. Exp. Morphol.*, vol. 70, pp. 113–132, Aug. 1982.

[27] G. Nikas, A. Ao, R. M. L. Winston, and A. H. Handyside, "Compaction and Surface Polarity in the Human Embryo in Vitro," *Biol. Reprod.*, vol. 55, no. 1, pp. 32–37, Jul. 1996, doi: 10.1095/biolreprod55.1.32.

[28] T. P. Fleming, Q. Javed, J. Collins, and M. Hay, "Biogenesis of structural intercellular junctions during cleavage in the mouse embryo," *J. Cell Sci. Suppl.*, vol. 17, pp. 119–125, 1993, doi: 10.1242/jcs.1993.supplement_17.17.

[29] H. Koyama, H. Suzuki, X. Yang, S. Jiang, and R. H. Foote, "Analysis of Polarity of Bovine and Rabbit Embryos by Scanning Electron Microscopy1," *Biol. Reprod.*, vol. 50, no. 1, pp. 163–170, Jan. 1994, doi: 10.1095/biolreprod50.1.163.

[30] J. Fiorentino, M.-E. Torres-Padilla, and A. Scialdone, "Measuring and Modeling Single-Cell Heterogeneity and Fate Decision in Mouse Embryos," *Annu. Rev. Genet.*, vol. 54, no. Volume 54, 2020, pp. 167–187, Nov. 2020, doi: 10.1146/annurev-genet-021920-110200.

[31] Y. Marikawa and V. B. Alarcón, "Establishment of trophectoderm and inner cell mass lineages in the mouse embryo," *Mol. Reprod. Dev.*, vol. 76, no. 11, pp. 1019–1032, 2009, doi: 10.1002/mrd.21057.

[32] A. Suwińska, R. Czołowska, W. Ożdżeński, and A. K. Tarkowski, "Blastomeres of the mouse embryo lose totipotency after the fifth cleavage division: Expression of *Cdx2* and *Oct4* and developmental potential of inner and outer blastomeres of 16- and 32-cell embryos," *Dev. Biol.*, vol. 322, no. 1, pp. 133–144, Oct. 2008, doi: 10.1016/j.ydbio.2008.07.019.

[33] R. Suzuki and S. Niimura, "Hatching and Distribution of Actin Filaments in Mouse Blastocysts Whose Activities of Protein Kinase A were Suppressed by H-89," *J. Reprod. Dev.*, vol. 56, no. 1, pp. 103–109, 2010, doi: 10.1262/jrd.09-144M.

[34] P. P. L. Tam and D. A. F. Loebel, "Gene function in mouse embryogenesis: get set for gastrulation," *Nat. Rev. Genet.*, vol. 8, no. 5, pp. 368–381, May 2007, doi: 10.1038/nrg2084.

[35] K. Elliott and M. O'Connor, *Embryogenesis in Mammals*. John Wiley & Sons, 2009.

[36] J.-F. Colas and G. C. Schoenwolf, "Towards a cellular and molecular understanding of neurulation," *Dev. Dyn.*, vol. 221, no. 2, pp. 117–145, 2001, doi: 10.1002/dvdy.1144.

[37] G. Cossu and U. Borello, "Wnt signaling and the activation of myogenesis in mammals," *EMBO J.*, vol. 18, no. 24, pp. 6867–6872, Dec. 1999, doi: 10.1093/emboj/18.24.6867.

[38] R. S. P. Beddington and E. J. Robertson, "Axis Development and Early Asymmetry in Mammals," *Cell*, vol. 96, no. 2, pp. 195–209, Jan. 1999, doi: 10.1016/S0092-8674(00)80560-7.

[39] J. H. Hanna, K. Saha, and R. Jaenisch, "Pluripotency and Cellular Reprogramming: Facts, Hypotheses, Unresolved Issues," *Cell*, vol. 143, no. 4, pp. 508–525, Nov. 2010, doi: 10.1016/j.cell.2010.10.008.

[40] J. Nichols and A. Smith, "Pluripotency in the Embryo and in Culture," *Cold Spring Harb. Perspect. Biol.*, vol. 4, no. 8, p. a008128, Aug. 2012, doi: 10.1101/cshperspect.a008128.

[41] J. A. Hackett and M. A. Surani, "Regulatory Principles of Pluripotency: From the Ground State Up," *Cell Stem Cell*, vol. 15, no. 4, pp. 416–430, Oct. 2014, doi: 10.1016/j.stem.2014.09.015.

[42] Y. S. Manor, R. Massarwa, and J. H. Hanna, "Establishing the human naïve pluripotent state," *Curr. Opin. Genet. Dev.*, vol. 34, pp. 35–45, Oct. 2015, doi: 10.1016/j.gde.2015.07.005.

[43] H. Inoue, N. Nagata, H. Kurokawa, and S. Yamanaka, "iPS cells: a game changer for future medicine," *EMBO J.*, vol. 33, no. 5, pp. 409–417, Mar. 2014, doi: 10.1002/embj.201387098.

[44] I. Chambers and S. R. Tomlinson, "The transcriptional foundation of pluripotency," *Dev. Camb. Engl.*, vol. 136, no. 14, pp. 2311–2322, Jul. 2009, doi: 10.1242/dev.024398.

[45] J.-L. Chew *et al.*, "Reciprocal Transcriptional Regulation of Pou5f1 and Sox2 via the Oct4/Sox2 Complex in Embryonic Stem Cells," *Mol. Cell. Biol.*, vol. 25, no. 14, pp. 6031–6046, Jul. 2005, doi: 10.1128/MCB.25.14.6031-6046.2005.

[46] H. Niwa *et al.*, "Interaction between Oct3/4 and Cdx2 Determines Trophectoderm Differentiation," *Cell*, vol. 123, no. 5, pp. 917–929, Dec. 2005, doi: 10.1016/j.cell.2005.08.040.

[47] N. Festuccia *et al.*, "Esrrb Is a Direct Nanog Target Gene that Can Substitute for Nanog Function in Pluripotent Cells," *Cell Stem Cell*, vol. 11, no. 4, pp. 477–490, Oct. 2012, doi: 10.1016/j.stem.2012.08.002.

[48] A. A. Sharov *et al.*, "Identification of Pou5f1, Sox2, and Nanog downstream target genes with statistical confidence by applying a novel algorithm to time course microarray and genome-wide chromatin immunoprecipitation data," *BMC Genomics*, vol. 9, p. 269, Jun. 2008, doi: 10.1186/1471-2164-9-269.

[49] J. Zhang *et al.*, "Sall4 modulates embryonic stem cell pluripotency and early embryonic development by the transcriptional regulation of Pou5f1," *Nat. Cell Biol.*, vol. 8, no. 10, pp. 1114–1123, Oct. 2006, doi: 10.1038/ncb1481.

[50] X. Chen *et al.*, "Integration of External Signaling Pathways with the Core Transcriptional Network in Embryonic Stem Cells," *Cell*, vol. 133, no. 6, pp. 1106–1117, Jun. 2008, doi: 10.1016/j.cell.2008.04.043.

[51] K. Takahashi and S. Yamanaka, "Induction of Pluripotent Stem Cells from Mouse Embryonic and Adult Fibroblast Cultures by Defined Factors," *Cell*, vol. 126, no. 4, pp. 663–676, Aug. 2006, doi: 10.1016/j.cell.2006.07.024.

[52] M. J. Evans and M. H. Kaufman, "Establishment in culture of pluripotential cells from mouse embryos," *Nature*, vol. 292, no. 5819, pp. 154–156, Jul. 1981, doi: 10.1038/292154a0.

[53] G. R. Martin, "Isolation of a pluripotent cell line from early mouse embryos cultured in medium conditioned by teratocarcinoma stem cells.," *Proc. Natl. Acad. Sci.*, vol. 78, no. 12, pp. 7634–7638, Dec. 1981, doi: 10.1073/pnas.78.12.7634.

[54] J. A. Thomson *et al.*, "Isolation of a primate embryonic stem cell line," *Proc. Natl. Acad. Sci. U. S. A.*, vol. 92, no. 17, pp. 7844–7848, Aug. 1995, doi: 10.1073/pnas.92.17.7844.

[55] J. A. Thomson *et al.*, "Embryonic Stem Cell Lines Derived from Human Blastocysts," *Science*, vol. 282, no. 5391, pp. 1145–1147, Nov. 1998, doi: 10.1126/science.282.5391.1145.

[56] B. E. Reubinoff, M. F. Pera, C.-Y. Fong, A. Trounson, and A. Bongso, "Embryonic stem cell lines from human blastocysts: somatic differentiation in vitro," *Nat. Biotechnol.*, vol. 18, no. 4, pp. 399–404, Apr. 2000, doi: 10.1038/74447.

[57] C. S. Navara *et al.*, "Derivation and Characterization of Nonhuman Primate Embryonic Stem Cells," *Curr. Protoc. Stem Cell Biol.*, vol. 1, no. 1, p. 1A.1.1-1A.1.21, 2007, doi: 10.1002/9780470151808.sc01a01s1.

[58] M. Buehr *et al.*, "Capture of Authentic Embryonic Stem Cells from Rat Blastocysts," *Cell*, vol. 135, no. 7, pp. 1287–1298, Dec. 2008, doi: 10.1016/j.cell.2008.12.007.

[59] M. Dattena *et al.*, "Isolation, culture, and characterization of embryonic cell lines from vitrified sheep blastocysts," *Mol. Reprod. Dev.*, vol. 73, no. 1, pp. 31–39, 2006, doi: 10.1002/mrd.20378.

[60] K.-H. Choi *et al.*, "Pluripotent pig embryonic stem cell lines originating from *in vitro*-fertilized and parthenogenetic embryos," *Stem Cell Res.*, vol. 49, p. 102093, Dec. 2020, doi: 10.1016/j.scr.2020.102093.

[61] I. G. M. Brons *et al.*, "Derivation of pluripotent epiblast stem cells from mammalian embryos," *Nature*, vol. 448, no. 7150, pp. 191–195, Jul. 2007, doi: 10.1038/nature05950.

[62] P. J. Tesar *et al.*, "New cell lines from mouse epiblast share defining features with human embryonic stem cells," *Nature*, vol. 448, no. 7150, pp. 196–199, Jul. 2007, doi: 10.1038/nature05972.

[63] J. Nichols and A. Smith, "Naive and Primed Pluripotent States," *Cell Stem Cell*, vol. 4, no. 6, pp. 487–492, Jun. 2009, doi: 10.1016/j.stem.2009.05.015.

[64] L. Weinberger, M. Ayyash, N. Novershtern, and J. H. Hanna, "Dynamic stem cell states: naive to primed pluripotency in rodents and humans," *Nat. Rev. Mol. Cell Biol.*, vol. 17, no. 3, pp. 155–169, Mar. 2016, doi: 10.1038/nrm.2015.28.

[65] S. Chandrasekaran *et al.*, "Comprehensive Mapping of Pluripotent Stem Cell Metabolism Using Dynamic Genome-Scale Network Modeling," *Cell Rep.*, vol. 21, no. 10, pp. 2965–2977, Dec. 2017, doi: 10.1016/j.celrep.2017.07.048.

[66] K.-J. Choi *et al.*, "NANOG prion-like assembly mediates DNA bridging to facilitate chromatin reorganization and activation of pluripotency," *Nat. Cell Biol.*, vol. 24, no. 5, pp. 737–747, May 2022, doi: 10.1038/s41556-022-00896-x.

[67] A. G. Smith *et al.*, "Inhibition of pluripotential embryonic stem cell differentiation by purified polypeptides," *Nature*, vol. 336, no. 6200, pp. 688–690, Dec. 1988, doi: 10.1038/336688a0.

[68] C. A. C. Williams, R. Fernandez-Alonso, J. Wang, R. Toth, N. S. Gray, and G. M. Findlay, "Erk5 Is a Key Regulator of Naive-Primed Transition and Embryonic Stem Cell Identity," *Cell Rep.*, vol. 16, no. 7, pp. 1820–1828, Aug. 2016, doi: 10.1016/j.celrep.2016.07.033.

[69] H. Marks *et al.*, "The Transcriptional and Epigenomic Foundations of Ground State Pluripotency," *Cell*, vol. 149, no. 3, pp. 590–604, Apr. 2012, doi: 10.1016/j.cell.2012.03.026.

[70] J. Silva, O. Barrandon, J. Nichols, J. Kawaguchi, T. W. Theunissen, and A. Smith, "Promotion of Reprogramming to Ground State Pluripotency by Signal Inhibition," *PLOS Biol.*, vol. 6, no. 10, p. e253, Oct. 2008, doi: 10.1371/journal.pbio.0060253.

[71] Q.-L. Ying and A. Smith, "The Art of Capturing Pluripotency: Creating the Right Culture," *Stem Cell Rep.*, vol. 8, no. 6, pp. 1457–1464, Jun. 2017, doi: 10.1016/j.stemcr.2017.05.020.

[72] D. Cornacchia *et al.*, "Lipid Deprivation Induces a Stable, Naive-to-Primed Intermediate State of Pluripotency in Human PSCs," *Cell Stem Cell*, vol. 25, no. 1, pp. 120-136.e10, Jul. 2019, doi: 10.1016/j.stem.2019.05.001.

[73] L. E. Bates and J. C. Silva, "Reprogramming human cells to naïve pluripotency: how close are we?," *Curr. Opin. Genet. Dev.*, vol. 46, pp. 58–65, Oct. 2017, doi: 10.1016/j.gde.2017.06.009.

[74] C. B. Ware, "Concise Review: Lessons from Naïve Human Pluripotent Cells," *Stem Cells*, vol. 35, no. 1, pp. 35–41, Jan. 2017, doi: 10.1002/stem.2507.

[75] S.-M. Kim *et al.*, "Dichotomous role of Shp2 for naïve and primed pluripotency maintenance in embryonic stem cells," *Stem Cell Res. Ther.*, vol. 13, no. 1, p. 329, Jul. 2022, doi: 10.1186/s13287-022-02976-z.

[76] M. Boiani and H. R. Schöler, "Regulatory networks in embryo-derived pluripotent stem cells," *Nat. Rev. Mol. Cell Biol.*, vol. 6, no. 11, pp. 872–881, Nov. 2005, doi: 10.1038/nrm1744.

[77] T. Boroviak *et al.*, "Lineage-Specific Profiling Delineates the Emergence and Progression of Naive Pluripotency in Mammalian Embryogenesis," *Dev. Cell*, vol. 35, no. 3, pp. 366–382, Nov. 2015, doi: 10.1016/j.devcel.2015.10.011.

[78] M. Kinoshita *et al.*, "Capture of Mouse and Human Stem Cells with Features of Formative Pluripotency," *Cell Stem Cell*, vol. 28, no. 3, pp. 453-471.e8, Mar. 2021, doi: 10.1016/j.stem.2020.11.005.

[79] S. Geula *et al.*, "m6A mRNA methylation facilitates resolution of naïve pluripotency toward differentiation," *Science*, vol. 347, no. 6225, pp. 1002–1006, Feb. 2015, doi: 10.1126/science.1261417.

[80] K. Van Bortle and V. G. Corces, "Lost in Transition: Dynamic Enhancer Organization across Naive and Primed Stem Cell States," *Cell Stem Cell*, vol. 14, no. 6, pp. 693–694, Jun. 2014, doi: 10.1016/j.stem.2014.05.004.

[81] H. Hirai, M. Firpo, and N. Kikyo, "Establishment of leukemia inhibitory factor (LIF)-independent iPS cells with potentiated Oct4," *Stem Cell Res.*, vol. 15, no. 3, pp. 469–480, Nov. 2015, doi: 10.1016/j.scr.2015.09.002.

[82] J. Geuder *et al.*, "A non-invasive method to generate induced pluripotent stem cells from primate urine," *Sci. Rep.*, vol. 11, no. 1, Art. no. 1, Feb. 2021, doi: 10.1038/s41598-021-82883-0.

[83] C. Barry *et al.*, "Species-specific developmental timing is maintained by pluripotent stem cells ex utero," *Dev. Biol.*, vol. 423, no. 2, pp. 101–110, Mar. 2017, doi: 10.1016/j.ydbio.2017.02.002.

[84] J. B. Gurdon, "The developmental capacity of nuclei taken from intestinal epithelium cells of feeding tadpoles," *J. Embryol. Exp. Morphol.*, vol. 10, pp. 622–640, Dec. 1962.

[85] I. Wilmut, A. E. Schnieke, J. McWhir, A. J. Kind, and K. H. S. Campbell, "Viable offspring derived from fetal and adult mammalian cells," *Nature*, vol. 385, no. 6619, pp. 810–813, Feb. 1997, doi: 10.1038/385810a0.

[86] R. P. Lanza, J. B. Cibelli, and M. D. West, "Human therapeutic cloning," *Nat. Med.*, vol. 5, no. 9, pp. 975–977, Sep. 1999, doi: 10.1038/12404.

[87] C. A. Cowan, J. Atienza, D. A. Melton, and K. Eggan, "Nuclear reprogramming of somatic cells after fusion with human embryonic stem cells," *Science*, vol. 309, no. 5739, pp. 1369–1373, Aug. 2005, doi: 10.1126/science.1116447.

[88] N. Nagata and S. Yamanaka, "Perspectives for Induced Pluripotent Stem Cell Technology," *Circ. Res.*, vol. 114, no. 3, pp. 505–510, Jan. 2014, doi: 10.1161/CIRCRESAHA.114.303043.

[89] K. Kim *et al.*, "Epigenetic memory in induced pluripotent stem cells," *Nature*, vol. 467, no. 7313, pp. 285–290, Sep. 2010, doi: 10.1038/nature09342.

[90] I.-H. Park *et al.*, "Disease-Specific Induced Pluripotent Stem Cells," *Cell*, vol. 134, no. 5, pp. 877–886, Sep. 2008, doi: 10.1016/j.cell.2008.07.041.

[91] S. Wakao *et al.*, "Multilineage-differentiating stress-enduring (Muse) cells are a primary source of induced pluripotent stem cells in human fibroblasts," *Proc. Natl. Acad. Sci.*, vol. 108, no. 24, pp. 9875–9880, Jun. 2011, doi: 10.1073/pnas.1100816108.

[92] S. Diecke *et al.*, "Novel codon-optimized mini-intronic plasmid for efficient, inexpensive and xeno-free induction of pluripotency," *Sci. Rep.*, vol. 5, no. 1, Art. no. 1, Jan. 2015, doi: 10.1038/srep08081.

[93] K. Okita *et al.*, "A more efficient method to generate integration-free human iPS cells," *Nat. Methods*, vol. 8, no. 5, pp. 409–412, May 2011, doi: 10.1038/nmeth.1591.

[94] L. Warren *et al.*, "Highly Efficient Reprogramming to Pluripotency and Directed Differentiation of Human Cells with Synthetic Modified mRNA," *Cell Stem Cell*, vol. 7, no. 5, pp. 618–630, Nov. 2010, doi: 10.1016/j.stem.2010.08.012.

[95] C. E. Murry and G. Keller, "Differentiation of Embryonic Stem Cells to Clinically Relevant Populations: Lessons from Embryonic Development," *Cell*, vol. 132, no. 4, pp. 661–680, Feb. 2008, doi: 10.1016/j.cell.2008.02.008.

[96] M. Zhang, K. Li, M. Xie, and S. Ding, "Chapter 4 - Chemical Approaches to Controlling Cell Fate," in *Principles of Developmental Genetics (Second Edition)*, S. A. Moody, Ed., Oxford: Academic Press, 2015, pp. 59–76. doi: 10.1016/B978-0-12-405945-0.00004-1.

[97] T. Xu, M. Zhang, T. Laurent, M. Xie, and S. Ding, "Concise Review: Chemical Approaches for Modulating Lineage-Specific Stem Cells and Progenitors," *STEM CELLS Transl. Med.*, vol. 2, no. 5, pp. 355–361, May 2013, doi: 10.5966/sctm.2012-0172.

[98] A. T. Naito *et al.*, "Developmental stage-specific biphasic roles of Wnt/β-catenin signaling in cardiomyogenesis and hematopoiesis," *Proc. Natl. Acad. Sci.*, vol. 103, no. 52, pp. 19812–19817, Dec. 2006, doi: 10.1073/pnas.0605768103.

[99] S. Ueno *et al.*, "Biphasic role for Wnt/β-catenin signaling in cardiac specification in zebrafish and embryonic stem cells," *Proc. Natl. Acad. Sci.*, vol. 104, no. 23, pp. 9685–9690, Jun. 2007, doi: 10.1073/pnas.0702859104.

[100] M. A. Laflamme *et al.*, "Cardiomyocytes derived from human embryonic stem cells in pro-survival factors enhance function of infarcted rat hearts," *Nat. Biotechnol.*, vol. 25, no. 9, pp. 1015–1024, Sep. 2007, doi: 10.1038/nbt1327.

[101] L. Yang *et al.*, "Human cardiovascular progenitor cells develop from a KDR+ embryonic-stem-cell-derived population," *Nature*, vol. 453, no. 7194, pp. 524–528, May 2008, doi: 10.1038/nature06894.

[102] A. Kubo *et al.*, "Development of definitive endoderm from embryonic stem cells in culture," *Dev. Camb. Engl.*, vol. 131, no. 7, pp. 1651–1662, Apr. 2004, doi: 10.1242/dev.01044.

[103] M. Yasunaga *et al.*, "Induction and monitoring of definitive and visceral endoderm differentiation of mouse ES cells," *Nat. Biotechnol.*, vol. 23, no. 12, pp. 1542–1550, Dec. 2005, doi: 10.1038/nbt1167.

[104] K. A. D'Amour, A. D. Agulnick, S. Eliazer, O. G. Kelly, E. Kroon, and E. E. Baetge, "Efficient differentiation of human embryonic stem cells to definitive endoderm," *Nat. Biotechnol.*, vol. 23, no. 12, pp. 1534–1541, Dec. 2005, doi: 10.1038/nbt1163.

[105] J. M. Wells and D. A. Melton, "Vertebrate Endoderm Development," *Annu. Rev. Cell Dev. Biol.*, vol. 15, no. Volume 15, 1999, pp. 393–410, Nov. 1999, doi: 10.1146/annurev.cellbio.15.1.393.

[106] Q.-L. Ying, M. Stavridis, D. Griffiths, M. Li, and A. Smith, "Conversion of embryonic stem cells into neuroectodermal precursors in adherent monoculture," *Nat. Biotechnol.*, vol. 21, no. 2, pp. 183–186, Feb. 2003, doi: 10.1038/nbt780.

[107] S. M. Chambers, C. A. Fasano, E. P. Papapetrou, M. Tomishima, M. Sadelain, and L. Studer, "Highly efficient neural conversion of human ES and iPS cells by dual inhibition of SMAD signaling," *Nat. Biotechnol.*, vol. 27, no. 3, Art. no. 3, Mar. 2009, doi: 10.1038/nbt.1529.

[108] K. Ogawa *et al.*, "Activin-Nodal signaling is involved in propagation of mouse embryonic stem cells," *J. Cell Sci.*, vol. 120, no. Pt 1, pp. 55–65, Jan. 2007, doi: 10.1242/jcs.03296.

[109] E. Stead *et al.*, "Pluripotent cell division cycles are driven by ectopic Cdk2, cyclin A/E and E2F activities," *Oncogene*, vol. 21, no. 54, pp. 8320–8333, Nov. 2002, doi: 10.1038/sj.onc.1206015.

[110] J. White and S. Dalton, "Cell cycle control of embryonic stem cells," *Stem Cell Rev.*, vol. 1, no. 2, pp. 131–138, 2005, doi: 10.1385/SCR:1:2:131.

[111] K. A. Becker *et al.*, "Self-renewal of human embryonic stem cells is supported by a shortened G1 cell cycle phase," *J. Cell. Physiol.*, vol. 209, no. 3, pp. 883–893, 2006, doi: 10.1002/jcp.20776.

[112] L. Liu *et al.*, "G1 cyclins link proliferation, pluripotency and differentiation of embryonic stem cells," *Nat. Cell Biol.*, vol. 19, no. 3, pp. 177–188, Mar. 2017, doi: 10.1038/ncb3474.

[113] K. N. Smith, A. M. Singh, and S. Dalton, "Myc represses primitive endoderm differentiation in pluripotent stem cells," *Cell Stem Cell*, vol. 7, no. 3, pp. 343–354, Sep. 2010, doi: 10.1016/j.stem.2010.06.023.

[114] V. S. Yang, S. A. Carter, S. J. Hyland, K. Tachibana-Konwalski, R. A. Laskey, and M. A. Gonzalez, "Geminin escapes degradation in G1 of mouse pluripotent cells and mediates the expression of Oct4, Sox2, and Nanog," *Curr. Biol. CB*, vol. 21, no. 8, pp. 692–699, Apr. 2011, doi: 10.1016/j.cub.2011.03.026.

[115] X. Zhang *et al.*, "A role for NANOG in G1 to S transition in human embryonic stem cells through direct binding of CDK6 and CDC25A," *J. Cell Biol.*, vol. 184, no. 1, pp. 67–82, Jan. 2009, doi: 10.1083/jcb.200801009.

[116] Y. Hong and P. J. Stambrook, "Restoration of an absent G1 arrest and protection from apoptosis in embryonic stem cells after ionizing radiation," *Proc. Natl. Acad. Sci.*, vol. 101, no. 40, pp. 14443–14448, Oct. 2004, doi: 10.1073/pnas.0401346101.

[117] C. Mantel and H. E. Broxmeyer, "Embryonic Stem Cells Bypass Numerous Cell Cycle Checkpoints; Not Just G1.," *Blood*, vol. 112, no. 11, p. 1331, Nov. 2008, doi: 10.1182/blood.V112.11.1331.1331.

[118] X. Chen, A. Hartman, and S. Guo, "Choosing Cell Fate Through a Dynamic Cell Cycle," *Curr. Stem Cell Rep.*, vol. 1, no. 3, pp. 129–138, 2015, doi: 10.1007/s40778-015-0018-0.

[119] S. Pauklin, R. A. Pedersen, and L. Vallier, "Mouse pluripotent stem cells at a glance," *J. Cell Sci.*, vol. 124, no. Pt 22, pp. 3727–3732, Nov. 2011, doi: 10.1242/jcs.074120.

[120] D. Coronado *et al.*, "A short G1 phase is an intrinsic determinant of naïve embryonic stem cell pluripotency," *Stem Cell Res.*, vol. 10, no. 1, pp. 118–131, Jan. 2013, doi: 10.1016/j.scr.2012.10.004.

[121] K. A. Becker, J. L. Stein, J. B. Lian, A. J. van Wijnen, and G. S. Stein, "Establishment of histone gene regulation and cell cycle checkpoint control in human embryonic stem cells," *J. Cell. Physiol.*, vol. 210, no. 2, pp. 517–526, 2007, doi: 10.1002/jcp.20903.

[122] I. Neganova, X. Zhang, S. Atkinson, and M. Lako, "Expression and functional analysis of G1 to S regulatory components reveals an important role for CDK2 in cell cycle regulation in human embryonic stem cells," *Oncogene*, vol. 28, no. 1, pp. 20–30, Jan. 2009, doi: 10.1038/onc.2008.358.

[123] S. Y. Lunt and M. G. Vander Heiden, "Aerobic glycolysis: meeting the metabolic requirements of cell proliferation," *Annu. Rev. Cell Dev. Biol.*, vol. 27, pp. 441–464, 2011, doi: 10.1146/annurev-cellbio-092910-154237.

[124] R. J. Burgess, M. Agathocleous, and S. J. Morrison, "Metabolic regulation of stem cell function," *J. Intern. Med.*, vol. 276, no. 1, pp. 12–24, 2014, doi: 10.1111/joim.12247.

[125] C. D. L. Folmes, P. P. Dzeja, T. J. Nelson, and A. Terzic, "Metabolic Plasticity in Stem Cell Homeostasis and Differentiation," *Cell Stem Cell*, vol. 11, no. 5, pp. 596–606, Nov. 2012, doi: 10.1016/j.stem.2012.10.002.

[126] K. Ito and T. Suda, "Metabolic requirements for the maintenance of self-renewing stem cells," *Nat. Rev. Mol. Cell Biol.*, vol. 15, no. 4, pp. 243–256, Apr. 2014, doi: 10.1038/nrm3772.

[127] V. A. Rafalski, E. Mancini, and A. Brunet, "Energy metabolism and energy-sensing pathways in mammalian embryonic and adult stem cell fate," *J. Cell Sci.*, vol. 125, no. 23, pp. 5597–5608, Dec. 2012, doi: 10.1242/jcs.114827.

[128] J. Zhang, E. Nuebel, G. Q. Daley, C. M. Koehler, and M. A. Teitell, "Metabolic Regulation in Pluripotent Stem Cells during Reprogramming and Self-Renewal," *Cell Stem Cell*, vol. 11, no. 5, pp. 589–595, Nov. 2012, doi: 10.1016/j.stem.2012.10.005.

[129] M. J. Birket *et al.*, "A reduction in ATP demand and mitochondrial activity with neural differentiation of human embryonic stem cells," *J. Cell Sci.*, vol. 124, no. Pt 3, pp. 348–358, Feb. 2011, doi: 10.1242/jcs.072272.

[130] C. D. L. Folmes *et al.*, "Somatic oxidative bioenergetics transitions into pluripotency-dependent glycolysis to facilitate nuclear reprogramming," *Cell Metab.*, vol. 14, no. 2, pp. 264–271, Aug. 2011, doi: 10.1016/j.cmet.2011.06.011.

[131] S. Chung, P. P. Dzeja, R. S. Faustino, C. Perez-Terzic, A. Behfar, and A. Terzic, "Mitochondrial oxidative metabolism is required for the cardiac differentiation of stem cells," *Nat. Clin. Pract. Cardiovasc. Med.*, vol. 4 Suppl 1, no. Suppl 1, pp. S60-67, Feb. 2007, doi: 10.1038/ncpcardio0766.

[132] W. Zhou *et al.*, "HIF1α induced switch from bivalent to exclusively glycolytic metabolism during ESC-to-EpiSC/hESC transition," *EMBO J.*, vol. 31, no. 9, pp. 2103–2116, May 2012, doi: 10.1038/emboj.2012.71.

[133] H. Kim *et al.*, "Core Pluripotency Factors Directly Regulate Metabolism in Embryonic Stem Cell to Maintain Pluripotency," *Stem Cells*, vol. 33, no. 9, pp. 2699–2711, Sep. 2015, doi: 10.1002/stem.2073.

[134] J. Zhang *et al.*, "UCP2 regulates energy metabolism and differentiation potential of human pluripotent stem cells," *EMBO J.*, vol. 30, no. 24, pp. 4860–4873, Nov. 2011, doi: 10.1038/emboj.2011.401.

[135] S. Zhu *et al.*, "Reprogramming of human primary somatic cells by OCT4 and chemical compounds," *Cell Stem Cell*, vol. 7, no. 6, pp. 651–655, Dec. 2010, doi: 10.1016/j.stem.2010.11.015.

[136] J. C. St John *et al.*, "The expression of mitochondrial DNA transcription factors during early cardiomyocyte in vitro differentiation from human embryonic stem cells," *Cloning Stem Cells*, vol. 7, no. 3, pp. 141–153, 2005, doi: 10.1089/clo.2005.7.141.

[137] E. M. Otis and R. Brent, "Equivalent ages in mouse and human embryos," *Anat. Rec.*, vol. 120, no. 1, pp. 33–63, 1954, doi: 10.1002/ar.1091200104.

[138] S. Easter, L. Ross, and A. Frankfurter, "Initial tract formation in the mouse brain," *J. Neurosci.*, vol. 13, no. 1, pp. 285–299, Jan. 1993, doi: 10.1523/JNEUROSCI.13-01-00285.1993.

[139] R. O'Rahilly and F. Müller, "Significant features in the early prenatal development of the human brain," *Ann. Anat. - Anat. Anz.*, vol. 190, no. 2, pp. 105–118, May 2008, doi: 10.1016/j.aanat.2008.01.001.

[140] R. G. Harrison, "Some Unexpected Results of the Heteroplastic Transplantation of Limbs," *Proc. Natl. Acad. Sci.*, vol. 10, no. 2, pp. 69–74, Feb. 1924, doi: 10.1073/pnas.10.2.69.

[141] V. C. Twitty and J. L. Schwind, "The growth of eyes and limbs transplanted heteroplastically between two species of Amblystoma," *J. Exp. Zool.*, vol. 59, no. 1, pp. 61–86, 1931, doi: 10.1002/jez.1400590105.

[142] P. Saiz-Lopez, K. Chinnaiya, V. M. Campa, I. Delgado, M. A. Ros, and M. Towers, "An intrinsic timer specifies distal structures of the vertebrate limb," *Nat. Commun.*, vol. 6, no. 1, pp. 1–9, Sep. 2015, doi: 10.1038/ncomms9108.

[143] J. Chen, C. Li, and S. Wang, "Periodic Heat Shock Accelerated the Chondrogenic Differentiation of Human Mesenchymal Stem Cells in Pellet Culture," *PLOS ONE*, vol. 9, no. 3, p. e91561, Mar. 2014, doi: 10.1371/journal.pone.0091561.

[144] F.-B. Gao, B. Durand, and M. Raff, "Oligodendrocyte precursor cells count time but not cell divisions before differentiation," *Curr. Biol.*, vol. 7, no. 2, pp. 152–155, Feb. 1997, doi: 10.1016/S0960-9822(06)00060-1.

[145] M. Raff, "Intracellular Developmental Timers," *Cold Spring Harb. Symp. Quant. Biol.*, vol. 72, pp. 431–435, Jan. 2007, doi: 10.1101/sqb.2007.72.007.

[146] D. G. Southwell *et al.*, "Intrinsically determined cell death of developing cortical interneurons," *Nature*, vol. 491, no. 7422, pp. 109–113, Nov. 2012, doi: 10.1038/nature11523.

[147] T. Watanabe and M. C. Raff, "Rod photoreceptor development in vitro: Intrinsic properties of proliferating neuroepithelial cells change as development proceeds in the rat retina," *Neuron*, vol. 4, no. 3, pp. 461–467, Mar. 1990, doi: 10.1016/0896-6273(90)90058-N.

[148] T. Rayon *et al.*, "Species-specific pace of development is associated with differences in protein stability," *Science*, vol. 369, no. 6510, p. eaba7667, Sep. 2020, doi: 10.1126/science.aba7667.

[149] I. Espuny-Camacho *et al.*, "Pyramidal Neurons Derived from Human Pluripotent Stem Cells Integrate Efficiently into Mouse Brain Circuits In Vivo," *Neuron*, vol. 77, no. 3, pp. 440–456, Feb. 2013, doi: 10.1016/j.neuron.2012.12.011.

[150] T. Otani, M. C. Marchetto, F. H. Gage, B. D. Simons, and F. J. Livesey, "2D and 3D Stem Cell Models of Primate Cortical Development Identify Species-Specific Differences in Progenitor Behavior Contributing to Brain Size," *Cell Stem Cell*, vol. 18, no. 4, pp. 467–480, Apr. 2016, doi: 10.1016/j.stem.2016.03.003.

[151] M. Schörnig *et al.*, "Comparison of induced neurons reveals slower structural and functional maturation in humans than in apes," *eLife*, vol. 10, p. e59323, Jan. 2021, doi: 10.7554/eLife.59323.

[152] G. La Manno *et al.*, "Molecular Diversity of Midbrain Development in Mouse, Human, and Stem Cells," *Cell*, vol. 167, no. 2, pp. 566-580.e19, Oct. 2016, doi: 10.1016/j.cell.2016.09.027.

[153] D. Linaro *et al.*, "Xenotransplanted Human Cortical Neurons Reveal Species-Specific Development and Functional Integration into Mouse Visual Circuits," *Neuron*, vol. 104, no. 5, pp. 972-986.e6, Dec. 2019, doi: 10.1016/j.neuron.2019.10.002.

[154] M. C. Marchetto *et al.*, "Species-specific maturation profiles of human, chimpanzee and bonobo neural cells," *eLife*, vol. 8, p. e37527, Feb. 2019, doi: 10.7554/eLife.37527.

[155] A. Dady, L. Davidson, P. A. Halley, and K. G. Storey, "Human spinal cord in vitro differentiation pace is initially maintained in heterologous embryonic environments," *eLife*, vol. 11, p. e67283, Feb. 2022, doi: 10.7554/eLife.67283.

[156] F. Mora-Bermúdez *et al.*, "Differences and similarities between human and chimpanzee neural progenitors during cerebral cortex development," *eLife*, vol. 5, p. e18683, Sep. 2016, doi: 10.7554/eLife.18683.

[157] C. Debès *et al.*, "Ageing-associated changes in transcriptional elongation influence longevity," *Nature*, vol. 616, no. 7958, pp. 814–821, Apr. 2023, doi: 10.1038/s41586-023-05922-y.

[158] K. Swovick *et al.*, "Interspecies Differences in Proteome Turnover Kinetics Are Correlated With Life Spans and Energetic Demands," *Mol. Cell. Proteomics*, vol. 20, Jan. 2021, doi: 10.1074/mcp.RA120.002301.

[159] A. A. Fushan *et al.*, "Gene expression defines natural changes in mammalian lifespan," *Aging Cell*, vol. 14, no. 3, pp. 352–365, 2015, doi: 10.1111/acel.12283.

[160] J. Lázaro *et al.*, "A stem cell zoo uncovers intracellular scaling of developmental tempo across mammals," *Cell Stem Cell*, vol. 30, no. 7, pp. 938-949.e7, Jul. 2023, doi: 10.1016/j.stem.2023.05.014.

[161] A. Bulut-Karslioglu *et al.*, "Inhibition of mTOR induces a paused pluripotent state," *Nature*, vol. 540, no. 7631, pp. 119–123, Dec. 2016, doi: 10.1038/nature20578.

[162] J. G. Ryall, T. Cliff, S. Dalton, and V. Sartorelli, "Metabolic Reprogramming of Stem Cell Epigenetics," *Cell Stem Cell*, vol. 17, no. 6, pp. 651–662, Dec. 2015, doi: 10.1016/j.stem.2015.11.012.

[163] M. Murakami *et al.*, "mTOR is essential for growth and proliferation in early mouse embryos and embryonic stem cells," *Mol. Cell. Biol.*, vol. 24, no. 15, pp. 6710–6718, Aug. 2004, doi: 10.1128/MCB.24.15.6710-6718.2004.

[164] G. B. West, J. H. Brown, and B. J. Enquist, "A general model for ontogenetic growth," *Nature*, vol. 413, no. 6856, pp. 628–631, Oct. 2001, doi: 10.1038/35098076.

[165] R. Iwata *et al.*, "Mitochondria metabolism sets the species-specific tempo of neuronal development," *Science*, vol. 379, no. 6632, p. eabn4705, Jan. 2023, doi: 10.1126/science.abn4705.

[166] L. Telley *et al.*, "Temporal patterning of apical progenitors and their daughter neurons in the developing neocortex," *Science*, vol. 364, no. 6440, p. eaav2522, May 2019, doi: 10.1126/science.aav2522.

[167] Q. Wu *et al.*, "Selective translation of epigenetic modifiers affects the temporal pattern and differentiation of neural stem cells," *Nat. Commun.*, vol. 13, no. 1, Art. no. 1, Jan. 2022, doi: 10.1038/s41467-022-28097-y.

[168] G. Ciceri *et al.*, "An epigenetic barrier sets the timing of human neuronal maturation." bioRxiv, p. 2022.06.02.490114, Jun. 03, 2022. doi: 10.1101/2022.06.02.490114.

[169] S. A. Baker and J. Rutter, "Metabolites as signalling molecules," *Nat. Rev. Mol. Cell Biol.*, vol. 24, no. 5, pp. 355–374, May 2023, doi: 10.1038/s41580-022-00572-w.

[170] Z. Dai, V. Ramesh, and J. W. Locasale, "The evolving metabolic landscape of chromatin biology and epigenetics," *Nat. Rev. Genet.*, vol. 21, no. 12, pp. 737–753, Dec. 2020, doi: 10.1038/s41576-020-0270-8.

[171] V. Ramesh, F. Liu, M. S. Minto, U. Chan, and A. E. West, "Bidirectional regulation of postmitotic H3K27me3 distributions underlie cerebellar granule neuron maturation dynamics," *eLife*, vol. 12, p. e86273, Apr. 2023, doi: 10.7554/eLife.86273.

[172] K. Mätlik, E.-E. Govek, M. R. Paul, C. D. Allis, and M. E. Hatten, "Histone bivalency regulates the timing of cerebellar granule cell development," *Genes Dev.*, vol. 37, no. 13–14, pp. 570–589, Jul. 2023, doi: 10.1101/gad.350594.123.

[173] B. W. Carey, L. W. S. Finley, J. R. Cross, C. D. Allis, and C. B. Thompson, "Intracellular α-ketoglutarate maintains the pluripotency of embryonic stem cells," *Nature*, vol. 518, no. 7539, pp. 413–416, Feb. 2015, doi: 10.1038/nature13981.

[174] J. Zhang *et al.*, "LIN28 Regulates Stem Cell Metabolism and Conversion to Primed Pluripotency," *Cell Stem Cell*, vol. 19, no. 1, pp. 66–80, Jul. 2016, doi: 10.1016/j.stem.2016.05.009.

[175] I.-Y. Hwang *et al.*, "Psat1-Dependent Fluctuations in α-Ketoglutarate Affect the Timing of ESC Differentiation," *Cell Metab.*, vol. 24, no. 3, pp. 494–501, Sep. 2016, doi: 10.1016/j.cmet.2016.06.014.

[176] T. TeSlaa *et al.*, "α-Ketoglutarate Accelerates the Initial Differentiation of Primed Human Pluripotent Stem Cells," *Cell Metab.*, vol. 24, no. 3, pp. 485–493, Sep. 2016, doi: 10.1016/j.cmet.2016.07.002.

[177] N. E. Lewis and J. Rossant, "Mechanism of size regulation in mouse embryo aggregates," *Development*, vol. 72, no. 1, pp. 169–181, Dec. 1982, doi: 10.1242/dev.72.1.169.

[178] M.-A. Power and P. P. L. Tam, "Onset of gastrulation, morphogenesis and somitogenesis in mouse embryos displaying compensatory growth," *Anat. Embryol. (Berl.)*, vol. 187, no. 5, May 1993, doi: 10.1007/BF00174425.

[179] T. Kobayashi *et al.*, "Generation of Rat Pancreas in Mouse by Interspecific Blastocyst Injection of Pluripotent Stem Cells," *Cell*, vol. 142, no. 5, pp. 787–799, Sep. 2010, doi: 10.1016/j.cell.2010.07.039.

[180] K. Bożyk, K. Gilecka, M. Humięcka, M. Szpila, A. Suwińska, and A. K. Tarkowski, "Mouse↔rat aggregation chimaeras can develop to adulthood," *Dev. Biol.*, vol. 427, no. 1, pp. 106–120, Jul. 2017, doi: 10.1016/j.ydbio.2017.05.002.

[181] J. Brown *et al.*, "Interspecies chimeric conditions affect the developmental rate of human pluripotent stem cells," *PLOS Comput. Biol.*, vol. 17, no. 3, p. e1008778, Mar. 2021, doi: 10.1371/journal.pcbi.1008778.

[182] A. Tanay and A. Regev, "Scaling single-cell genomics from phenomenology to mechanism," *Nature*, vol. 541, no. 7637, pp. 331–338, Jan. 2017, doi: 10.1038/nature21350.

[183] J. E. Rood, A. Maartens, A. Hupalowska, S. A. Teichmann, and A. Regev, "Impact of the Human Cell Atlas on medicine," *Nat. Med.*, vol. 28, no. 12, pp. 2486–2496, Dec. 2022, doi: 10.1038/s41591-022-02104-7.

[184] A. Wagner, A. Regev, and N. Yosef, "Revealing the vectors of cellular identity with single-cell genomics," *Nat. Biotechnol.*, vol. 34, no. 11, pp. 1145–1160, Nov. 2016, doi: 10.1038/nbt.3711.

[185] J. Cao *et al.*, "A human cell atlas of fetal gene expression," *Science*, vol. 370, no. 6518, p. eaba7721, Nov. 2020, doi: 10.1126/science.aba7721.

[186] Z. Miao, B. D. Humphreys, A. P. McMahon, and J. Kim, "Multi-omics integration in the age of million single-cell data," *Nat. Rev. Nephrol.*, vol. 17, no. 11, pp. 710–724, Nov. 2021, doi: 10.1038/s41581-021-00463-x.

[187] S. Ogbeide, F. Giannese, L. Mincarelli, and I. C. Macaulay, "Into the multiverse: advances in single-cell multiomic profiling," *Trends Genet.*, vol. 38, no. 8, pp. 831–843, Aug. 2022, doi: 10.1016/j.tig.2022.03.015.

[188] D. Arendt *et al.*, "The origin and evolution of cell types," *Nat. Rev. Genet.*, vol. 17, no. 12, pp. 744–757, Dec. 2016, doi: 10.1038/nrg.2016.127.

[189] S. A. Morris, "The evolving concept of cell identity in the single cell era," *Dev. Camb. Engl.*, vol. 146, no. 12, p. dev169748, Jun. 2019, doi: 10.1242/dev.169748.

[190] F. Tang *et al.*, "mRNA-Seq whole-transcriptome analysis of a single cell," *Nat. Methods*, vol. 6, no. 5, pp. 377–382, May 2009, doi: 10.1038/nmeth.1315.

[191] X. Tang, Y. Huang, J. Lei, H. Luo, and X. Zhu, "The single-cell sequencing: new developments and medical applications," *Cell Biosci.*, vol. 9, no. 1, p. 53, Jun. 2019, doi: 10.1186/s13578-019-0314-y.

[192] F. Ginhoux, A. Yalin, C. A. Dutertre, and I. Amit, "Single-cell immunology: Past, present, and future," *Immunity*, vol. 55, no. 3, pp. 393–404, Mar. 2022, doi: 10.1016/j.immuni.2022.02.006.

[193] J. Ding *et al.*, "Systematic comparison of single-cell and single-nucleus RNA-sequencing methods," *Nat. Biotechnol.*, vol. 38, no. 6, pp. 737–746, Jun. 2020, doi: 10.1038/s41587-020-0465-8.

[194] C. Ziegenhain *et al.*, "Comparative Analysis of Single-Cell RNA Sequencing Methods," *Mol. Cell*, vol. 65, no. 4, pp. 631-643.e4, Feb. 2017, doi: 10.1016/j.molcel.2017.01.023.

[195] F. C. Grandi, H. Modi, L. Kampman, and M. R. Corces, "Chromatin accessibility profiling by ATAC-seq," *Nat. Protoc.*, vol. 17, no. 6, pp. 1518–1552, Jun. 2022, doi: 10.1038/s41596-022-00692-9.

[196] M. J. Boland, K. L. Nazor, and J. F. Loring, "Epigenetic regulation of pluripotency and differentiation," *Circ. Res.*, vol. 115, no. 2, pp. 311–324, Jul. 2014, doi: 10.1161/CIRCRESAHA.115.301517.

[197] J. D. Buenrostro *et al.*, "Single-cell chromatin accessibility reveals principles of regulatory variation," *Nature*, vol. 523, no. 7561, pp. 486–490, Jul. 2015, doi: 10.1038/nature14590.

[198] M. Stauske *et al.*, "Non-Human Primate iPSC Generation, Cultivation, and Cardiac Differentiation under Chemically Defined Conditions," *Cells*, vol. 9, no. 6, Art. no. 6, Jun. 2020, doi: 10.3390/cells9061349.

[199] H. Heaton *et al.*, "Souporcell: robust clustering of single-cell RNA-seq data by genotype without reference genotypes," *Nat. Methods*, vol. 17, no. 6, Art. no. 6, Jun. 2020, doi: 10.1038/s41592-020-0820-1.

[200] S. L. Wolock, R. Lopez, and A. M. Klein, "Scrublet: Computational Identification of Cell Doublets in Single-Cell Transcriptomic Data," *Cell Syst.*, vol. 8, no. 4, pp. 281-291.e9, Apr. 2019, doi: 10.1016/j.cels.2018.11.005.

[201] A. T. L. Lun, K. Bach, and J. C. Marioni, "Pooling across cells to normalize single-cell RNA sequencing data with many zero counts," *Genome Biol.*, vol. 17, no. 1, Art. no. 1, Dec. 2016, doi: 10.1186/s13059-016-0947-7.

[202] A. T. Lun, D. J. McCarthy, and J. C. Marioni, "A step-by-step workflow for low-level analysis of single-cell RNA-seq data with Bioconductor.," 2016, Accessed: May 11, 2023. [Online]. Available: https://www.repository.cam.ac.uk/handle/1810/284686

[203] G. X. Y. Zheng *et al.*, "Massively parallel digital transcriptional profiling of single cells," *Nat. Commun.*, vol. 8, no. 1, Art. no. 1, Jan. 2017, doi: 10.1038/ncomms14049.

[204] L. McInnes, J. Healy, and J. Melville, "UMAP: Uniform Manifold Approximation and Projection for Dimension Reduction." arXiv, Sep. 17, 2020. doi: 10.48550/arXiv.1802.03426.

[205] E. Z. Macosko *et al.*, "Highly parallel genome-wide expression profiling of individual cells using nanoliter droplets," *Cell*, vol. 161, no. 5, pp. 1202–1214, May 2015, doi: 10.1016/j.cell.2015.05.002.

[206] I. Tirosh *et al.*, "Dissecting the multicellular ecosystem of metastatic melanoma by single-cell RNA-seq," *Science*, vol. 352, no. 6282, pp. 189–196, Apr. 2016, doi: 10.1126/science.aad0501.

[207] L. Heumos *et al.*, "Best practices for single-cell analysis across modalities," *Nat. Rev. Genet.*, vol. 24, no. 8, pp. 550–572, Aug. 2023, doi: 10.1038/s41576-023-00586-w.

[208] H. M. Amemiya, A. Kundaje, and A. P. Boyle, "The ENCODE Blacklist: Identification of Problematic Regions of the Genome," *Sci. Rep.*, vol. 9, no. 1, Art. no. 1, Jun. 2019, doi: 10.1038/s41598-019-45839-z.

[209] H. A. Pliner *et al.*, "Cicero Predicts cis-Regulatory DNA Interactions from Single-Cell Chromatin Accessibility Data," *Mol. Cell*, vol. 71, no. 5, pp. 858-871.e8, Sep. 2018, doi: 10.1016/j.molcel.2018.06.044.

[210] J. M. Granja *et al.*, "ArchR is a scalable software package for integrative single-cell chromatin accessibility analysis," *Nat. Genet.*, vol. 53, no. 3, pp. 403–411, Mar. 2021, doi: 10.1038/s41588-021-00790-6.

[211] K. Takahashi *et al.*, "Induction of Pluripotent Stem Cells from Adult Human Fibroblasts by Defined Factors," *Cell*, vol. 131, no. 5, pp. 861–872, Nov. 2007, doi: 10.1016/j.cell.2007.11.019.

[212] R. Tabuce *et al.*, "Early Tertiary mammals from North Africa reinforce the molecular Afrotheria clade," *Proc. R. Soc. B Biol. Sci.*, vol. 274, no. 1614, 2007, doi: 10.1098/rspb.2006.0229.

[213] I. Werneburg, A. C. Tzika, L. Hautier, R. J. Asher, M. C. Milinkovitch, and M. R. Sánchez-Villagra, "Development and embryonic staging in non-model organisms: the case of an afrotherian mammal," *J. Anat.*, vol. 222, no. 1, 2012, doi: 10.1111/j.1469-7580.2012.01509.x.

[214] M. D. Luecken and F. J. Theis, "Current best practices in single-cell RNA-seq analysis: a tutorial," *Mol. Syst. Biol.*, vol. 15, no. 6, p. e8746, Jun. 2019, doi: 10.15252/msb.20188746.

[215] M. D. Alonso, J. Lomako, W. M. Lomako, and W. J. Whelan, "A new look at the biogenesis of glycogen," *FASEB J.*, vol. 9, no. 12, pp. 1126–1137, 1995, doi: 10.1096/fasebj.9.12.7672505.

[216] K. Sandhoff, G. van Echten, M. Schröder, D. Schnabel, and K. Suzuki, "Metabolism of glycolipids: the role of glycolipid-binding proteins in the function and pathobiochemistry of lysosomes," *Biochem. Soc. Trans.*, vol. 20, no. 3, pp. 695–699, Aug. 1992, doi: 10.1042/bst0200695.

[217] E. Perenthaler *et al.*, "Loss of UGP2 in brain leads to a severe epileptic encephalopathy, emphasizing that bi-allelic isoform-specific start-loss mutations of essential genes can cause genetic diseases," *Acta Neuropathol. (Berl.)*, vol. 139, no. 3, pp. 415–442, Mar. 2020, doi: 10.1007/s00401-019-02109-6.

[218] L. Busby and B. Steventon, "Tissue tectonics and the multi-scale regulation of developmental timing," *Interface Focus*, vol. 11, no. 3, p. 20200057, Apr. 2021, doi: 10.1098/rsfs.2020.0057.

[219] H. Miyazawa and A. Aulehla, "Revisiting the role of metabolism during development," *Development*, vol. 145, no. 19, p. dev131110, Oct. 2018, doi: 10.1242/dev.131110.

[220] T. Nakamura *et al.*, "A developmental coordinate of pluripotency among mice, monkeys and humans," *Nature*, vol. 537, no. 7618, 2016, doi: 10.1038/nature19096.

[221] C. Y. Logan and R. Nusse, "THE WNT SIGNALING PATHWAY IN DEVELOPMENT AND DISEASE," *Annu. Rev. Cell Dev. Biol.*, vol. 20, no. Volume 20, 2004, pp. 781–810, Nov. 2004, doi: 10.1146/annurev.cellbio.20.010403.113126.

[222] D. Pan, "The Hippo Signaling Pathway in Development and Cancer," *Dev. Cell*, vol. 19, no. 4, pp. 491–505, Oct. 2010, doi: 10.1016/j.devcel.2010.09.011.

[223] B. Zhao, L. Li, and K.-L. Guan, "Hippo signaling at a glance," *J. Cell Sci.*, vol. 123, no. 23, pp. 4001–4006, Dec. 2010, doi: 10.1242/jcs.069070.

[224] X. Zhou, J. P. Chadarevian, B. Ruiz, and Q.-L. Ying, "Cytoplasmic and Nuclear TAZ Exert Distinct Functions in Regulating Primed Pluripotency," *Stem Cell Rep.*, vol. 9, no. 3, pp. 732–741, Sep. 2017, doi: 10.1016/j.stemcr.2017.07.019.

[225] E. Ugur *et al.*, "Comprehensive chromatin proteomics resolves functional phases of pluripotency and identifies changes in regulatory components," *Nucleic Acids Res.*, vol. 51, no. 6, pp. 2671–2690, Apr. 2023, doi: 10.1093/nar/gkad058.

[226] K. A. U. Gonzales and H.-H. Ng, "Choreographing pluripotency and cell fate with transcription factors," *Biochim. Biophys. Acta BBA - Gene Regul. Mech.*, vol. 1809, no. 7, pp. 337–349, Jul. 2011, doi: 10.1016/j.bbagrm.2011.06.009.

[227] R. Alberio, N. Croxall, and C. Allegrucci, "Pig Epiblast Stem Cells Depend on Activin/Nodal Signaling for Pluripotency and Self-Renewal," *Stem Cells Dev.*, vol. 19, no. 10, 2010, doi: 10.1089/scd.2010.0012.

[228] S. Erceg, M. Ronaghi, and M. Stojković, "Human Embryonic Stem Cell Differentiation Toward Regional Specific Neural Precursors," *Stem Cells*, vol. 27, no. 1, 2009, doi: 10.1634/stemcells.2008-0543.

[229] L. Vallier *et al.*, "Early Cell Fate Decisions of Human Embryonic Stem Cells and Mouse Epiblast Stem Cells Are Controlled by the Same Signalling Pathways," *PLOS ONE*, vol. 4, no. 6, p. e6082, Jun. 2009, doi: 10.1371/journal.pone.0006082.

[230] H. Shimada *et al.*, "Efficient Derivation of Multipotent Neural Stem/Progenitor Cells from Non-Human Primate Embryonic Stem Cells," *PLOS ONE*, vol. 7, no. 11, p. e49469, Nov. 2012, doi: 10.1371/journal.pone.0049469.

[231] N. Gaspard *et al.*, "An intrinsic mechanism of corticogenesis from embryonic stem cells," *Nature*, vol. 455, no. 7211, pp. 351–357, Sep. 2008, doi: 10.1038/nature07287.

[232] I. Kelava and M. A. Lancaster, "Stem Cell Models of Human Brain Development," *Cell Stem Cell*, vol. 18, no. 6, pp. 736–748, Jun. 2016, doi: 10.1016/j.stem.2016.05.022.

[233] A. M. Maroof *et al.*, "Directed Differentiation and Functional Maturation of Cortical Interneurons from Human Embryonic Stem Cells," *Cell Stem Cell*, vol. 12, no. 5, pp. 559–572, May 2013, doi: 10.1016/j.stem.2013.04.008.

[234] Y. Shi, P. Kirwan, and F. J. Livesey, "Directed differentiation of human pluripotent stem cells to cerebral cortex neurons and neural networks," *Nat. Protoc.*, vol. 7, no. 10, pp. 1836–1846, Oct. 2012, doi: 10.1038/nprot.2012.116.

[235] J. van de Leemput *et al.*, "CORTECON: A Temporal Transcriptome Analysis of In Vitro Human Cerebral Cortex Development from Human Embryonic Stem Cells," *Neuron*, vol. 83, no. 1, pp. 51–68, Jul. 2014, doi: 10.1016/j.neuron.2014.05.013.

[236] D. Shimojo *et al.*, "Rapid, efficient, and simple motor neuron differentiation from human pluripotent stem cells," *Mol. Brain*, vol. 8, no. 1, 2015, doi: 10.1186/s13041-015-0172-4.

[237] D. E. Buchholz, B. O. Pennington, R. H. Croze, C. R. Hinman, P. J. Coffey, and D. O. Clegg, "Rapid and Efficient Directed Differentiation of Human Pluripotent Stem Cells Into Retinal Pigmented Epithelium," *Stem Cells Transl. Med.*, vol. 2, no. 5, pp. 384–393, May 2013, doi: 10.5966/sctm.2012-0163.

[238] L. Y. Chan, W. R. Birch, E. K. F. Yim, and A. B. H. Choo, "Temporal application of topography to increase the rate of neural differentiation from human pluripotent stem cells," *Biomaterials*, vol. 34, no. 2, pp. 382–392, Jan. 2013, doi: 10.1016/j.biomaterials.2012.09.033.

[239] M. Gaur *et al.*, "Timed inhibition of p38MAPK directs accelerated differentiation of human embryonic stem cells into cardiomyocytes," *Cytotherapy*, vol. 12, no. 6, pp. 807–817, Oct. 2010, doi: 10.3109/14653249.2010.491821.

[240] R. J. Parchem *et al.*, "miR-302 Is Required for Timing of Neural Differentiation, Neural Tube Closure, and Embryonic Viability," *Cell Rep.*, vol. 12, no. 5, pp. 760–773, Aug. 2015, doi: 10.1016/j.celrep.2015.06.074.

[241] N. Sasaki *et al.*, "Chemical inhibition of sulfation accelerates neural differentiation of mouse embryonic stem cells and human induced pluripotent stem cells," *Biochem. Biophys. Res. Commun.*, vol. 401, no. 3, pp. 480–486, Oct. 2010, doi: 10.1016/j.bbrc.2010.09.085.

[242] Y. Zhu *et al.*, "Three-Dimensional Neuroepithelial Culture from Human Embryonic Stem Cells and Its Use for Quantitative Conversion to Retinal Pigment Epithelium," *PLOS ONE*, vol. 8, no. 1, p. e54552, Jan. 2013, doi: 10.1371/journal.pone.0054552.

[243] M. W. Amoroso *et al.*, "Accelerated High-Yield Generation of Limb-Innervating Motor Neurons from Human Stem Cells," *J. Neurosci.*, vol. 33, no. 2, pp. 574–586, Jan. 2013, doi: 10.1523/JNEUROSCI.0906-12.2013.

[244] S. M. Chambers *et al.*, "Combined small-molecule inhibition accelerates developmental timing and converts human pluripotent stem cells into nociceptors," *Nat. Biotechnol.*, vol. 30, no. 7, pp. 715–720, Jul. 2012, doi: 10.1038/nbt.2249.

[245] A. Ozeki, K. Suzuki, M. Suzuki, H. Ozawa, and S. Yamashita, "Acceleration of astrocytic differentiation in neural stem cells surviving X-irradiation," *NeuroReport*, vol. 23, no. 5, p. 290, Mar. 2012, doi: 10.1097/WNR.0b013e3283509a79.

[246] A. M. B. Tadeu *et al.*, "Transcriptional Profiling of Ectoderm Specification to Keratinocyte Fate in Human Embryonic Stem Cells," *PLOS ONE*, vol. 10, no. 4, p. e0122493, Apr. 2015, doi: 10.1371/journal.pone.0122493.

[247] Y. Mayshar *et al.*, "Time-aligned hourglass gastrulation models in rabbit and mouse," *Cell*, vol. 186, no. 12, pp. 2610-2627.e18, Jun. 2023, doi: 10.1016/j.cell.2023.04.037.

[248] M. Mittnenzweig *et al.*, "A single-embryo, single-cell time-resolved model for mouse gastrulation," *Cell*, vol. 184, no. 11, pp. 2825-2842.e22, May 2021, doi: 10.1016/j.cell.2021.04.004.

[249] B. Pijuan-Sala *et al.*, "A single-cell molecular map of mouse gastrulation and early organogenesis," *Nature*, vol. 566, no. 7745, pp. 490–495, Feb. 2019, doi: 10.1038/s41586-019-0933-9.

[250] L. Simpson *et al.*, "A single-cell atlas of pig gastrulation as a resource for comparative embryology." bioRxiv, p. 2023.08.31.555712, Sep. 02, 2023. doi: 10.1101/2023.08.31.555712.

[251] M.-L. N. Ton *et al.*, "An atlas of rabbit development as a model for single-cell comparative genomics," *Nat. Cell Biol.*, vol. 25, no. 7, pp. 1061–1072, Jul. 2023, doi: 10.1038/s41556-023-01174-0.

[252] R. C. V. Tyser, E. Mahammadov, S. Nakanoh, L. Vallier, A. Scialdone, and S. Srinivas, "Single-cell transcriptomic characterization of a gastrulating human embryo," *Nature*, vol. 600, no. 7888, pp. 285–289, Dec. 2021, doi: 10.1038/s41586-021-04158-y.

[253] J. Zhai *et al.*, "Primate gastrulation and early organogenesis at single-cell resolution," *Nature*, vol. 612, no. 7941, pp. 732–738, Dec. 2022, doi: 10.1038/s41586-022-05526-y.

[254] Q. Shen *et al.*, "The timing of cortical neurogenesis is encoded within lineages of individual progenitor cells," *Nat. Neurosci.*, vol. 9, no. 6, pp. 743–751, Jun. 2006, doi: 10.1038/nn1694.

[255] A. B. Alber, E. R. Paquet, M. Biserni, F. Naef, and D. M. Suter, "Single Live Cell Monitoring of Protein Turnover Reveals Intercellular Variability and Cell-Cycle Dependence of Degradation Rates," *Mol. Cell*, vol. 71, no. 6, pp. 1079-1091.e9, Sep. 2018, doi: 10.1016/j.molcel.2018.07.023.

[256] E. Appleton *et al.*, "Derivation of elephant induced pluripotent stem cells." bioRxiv, p. 2024.03.05.583606, Mar. 12, 2024. doi: 10.1101/2024.03.05.583606.

[257] J. V. Conrad *et al.*, "Efficient derivation of transgene-free porcine induced pluripotent stem cells enables in vitro modeling of species-specific developmental timing," *Stem Cell Rep.*, Nov. 2023, doi: 10.1016/j.stemcr.2023.10.009.

[258] T. Ezashi, Y. Yuan, and R. M. Roberts, "Pluripotent Stem Cells from Domesticated Mammals," *Annu. Rev. Anim. Biosci.*, vol. 4, no. Volume 4, 2016, pp. 223–253, Feb. 2016, doi: 10.1146/annurev-animal-021815-111202.

[259] S. Yoshimatsu *et al.*, "Non-viral Induction of Transgene-free iPSCs from Somatic Fibroblasts of Multiple Mammalian Species," *Stem Cell Rep.*, vol. 16, no. 4, pp. 754–770, Apr. 2021, doi: 10.1016/j.stemcr.2021.03.002.

[260] V. Zywitza *et al.*, "Induced pluripotent stem cells and cerebral organoids from the critically endangered Sumatran rhinoceros," *iScience*, vol. 25, no. 11, p. 105414, Nov. 2022, doi: 10.1016/j.isci.2022.105414.

[261] T. Burdon, A. Smith, and P. Savatier, "Signalling, cell cycle and pluripotency in embryonic stem cells," *Trends Cell Biol.*, vol. 12, no. 9, pp. 432–438, Sep. 2002, doi: 10.1016/S0962-8924(02)02352-8.

[262] M. A. Ciemerych and P. Sicinski, "Cell cycle in mouse development," *Oncogene*, vol. 24, no. 17, pp. 2877–2898, Apr. 2005, doi: 10.1038/sj.onc.1208608.

[263] A.-C. Fluckiger *et al.*, "Cell Cycle Features of Primate Embryonic Stem Cells," *Stem Cells*, vol. 24, no. 3, pp. 547–556, Mar. 2006, doi: 10.1634/stemcells.2005-0194.

[264] H. Fujii-Yamamoto, J. M. Kim, K. Arai, and H. Masai, "Cell Cycle and Developmental Regulations of Replication Factors in Mouse Embryonic Stem Cells *," *J. Biol. Chem.*, vol. 280, no. 13, pp. 12976–12987, Apr. 2005, doi: 10.1074/jbc.M412224200.

[265] C. Lange and F. Calegari, "Cdks and cyclins link G1 length and differentiation of embryonic, neural and hematopoietic stem cells," *Cell Cycle*, vol. 9, no. 10, pp. 1893–1900, May 2010, doi: 10.4161/cc.9.10.11598.

[266] A. Sakaue-Sawano *et al.*, "Visualizing Spatiotemporal Dynamics of Multicellular Cell-Cycle Progression," *Cell*, vol. 132, no. 3, pp. 487–498, Feb. 2008, doi: 10.1016/j.cell.2007.12.033.

[267] G. D. Grant, K. M. Kedziora, J. C. Limas, J. G. Cook, and J. E. Purvis, "Accurate delineation of cell cycle phase transitions in living cells with PIP-FUCCI," *Cell Cycle*, vol. 17, no. 21–22, pp. 2496–2516, Nov. 2018, doi: 10.1080/15384101.2018.1547001.

[268] M. Okamoto *et al.*, "Cell-cycle-independent transitions in temporal identity of mammalian neural progenitor cells," *Nat. Commun.*, vol. 7, no. 1, Art. no. 1, Apr. 2016, doi: 10.1038/ncomms11349.

[269] N. Shyh-Chang and H.-H. Ng, "The metabolic programming of stem cells," *Genes Dev.*, vol. 31, no. 4, pp. 336–346, Feb. 2017, doi: 10.1101/gad.293167.116.

[270] Y. V. Bukhman *et al.*, "Chromosome level genome assembly of the Etruscan shrew Suncus etruscus," *Sci. Data*, vol. 11, no. 1, pp. 1–11, Feb. 2024, doi: 10.1038/s41597-024-03011-x.

[271] H. Satam *et al.*, "Next-Generation Sequencing Technology: Current Trends and Advancements," *Biology*, vol. 12, no. 7, Art. no. 7, Jul. 2023, doi: 10.3390/biology12070997.

[272] C. Li, M. C. Virgilio, K. L. Collins, and J. D. Welch, "Multi-omic single-cell velocity models epigenome–transcriptome interactions and improves cell fate prediction," *Nat. Biotechnol.*, vol. 41, no. 3, Art. no. 3, Mar. 2023, doi: 10.1038/s41587-022-01476-y.

[273] M. R. Buchakjian and S. Kornbluth, “The engine driving the ship: metabolic steering of cell proliferation and death,” *Nat. Rev. Mol. Cell Biol.*, vol. 11, no. 10, pp. 715–727, Oct. 2010, doi: 10.1038/nrm2972.

[274] J. Kaplon, L. van Dam, and D. Peeper, “Two-way communication between the metabolic and cell cycle machineries: the molecular basis,” *Cell Cycle*, vol. 14, no. 13, pp. 2022–2032, Jul. 2015, doi: 10.1080/15384101.2015.1044172.

[275] D. A. Glauser and W. Schlegel, “The FoxO/Bcl-6/cyclin D2 pathway mediates metabolic and growth factor stimulation of proliferation in Min6 pancreatic β-cells,” *J. Recept. Signal Transduct.*, vol. 29, no. 6, pp. 293–298, Dec. 2009, doi: 10.3109/10799890903241824.

# Acknowledgments

*Over the past years, my journey as a PhD student has been an adventurous and transformative experience. This wild ride has been filled with challenges, discoveries, and growth, none of which would have been possible without the support and encouragement of the people who have surrounded me.*

*First and foremost, I would like to express my gratitude to my supervisor and mentor, Micha. Thank you for granting me the scientific freedom to explore my ideas independently. Your trust in my capabilities has been crucial in helping me develop into a confident scientist and navigate my PhD.*

*Furthermore, I would like to extend my gratitude to my thesis committee, Wolfgang Enard and Magdalena Götz. Our scientific discussions were instrumental in shaping my research, and your support, especially during the challenging early stages of my PhD, was immensely valuable.*

*Also, I would like to thank everyone I had the opportunity to collaborate with throughout my PhD journey. Especially, Christian Schröter and Carsten Marr, working with you has been and continues to be a great pleasure. Thank you for all the time you took to support me throughout this project and for every word of advice you've offered. Julia and Moritz, this project could not have succeeded without your help and contributions. Thank you for the fun times we had inside and outside the lab.*

*Further, I want to thank Enes Ugur and Heinrich Leonhardt for our collaboration. I am grateful I could contribute to your outstanding project.*

*To my dearest colleagues at the ISF, Ejona and Anna, thank you for all your help. I wouldn't have lasted a week without you two. Thank you for 'adopting' us PhD students and offering guidance at every step. I truly appreciate the dedication and knowledge you have shared.*

*Dolunay and Sebastian, thank you for every conversation, shared lunch and dinner, and your scientific (and emotional) support throughout these demanding times. Your friendship made the challenges manageable and enjoyable. And a special thanks goes to Markus: you introduced me to the fascinating world of stem cells during my internship seven years ago. Thanks for laying the foundation for this journey.*

*A big thank you goes out to all the people outside the lab who supported me all this time. Whether you were in Munich, Mannheim, Fort Lauderdale, or elsewhere, your friendship is irreplaceable. Whether through a quick chat, a weekend visit, or a much-needed holiday, you helped keep me sane through the ups and downs.*

*Mama, Papa, Bibi, and Calvin, I know what I do might sometimes be a riddle to you, but thank you for always being there for me, nonetheless. Your support and encouragement have shaped me into the person I am today and brought me this far. I know I can always count on you.*

*And to my favorite human, Philipp, thank you for being with me on this path for nearly twelve years, back when we were unknowing of where this would lead. Thank you for being by my side throughout it all (and for your patience with my nagging and my bad coding). I can't wait to see where this journey takes us next.*